Adsorption Separation of CO_2 from CO in Syngas: Improving the Conversion of the Reverse Water Gas Shift Reaction

By

Sean M. W. Wilson

Submitted to the School of Graduate Studies and Research

in partial fulfillment of requirements

for degree of M.A.Sc. in Chemical Engineering

Supervisor:

Dr. Handan Tezel

Department of Chemical and Biological Engineering

Faculty of Engineering

University of Ottawa

Ottawa, Canada

ABSTRACT

In this research project, adsorption is considered for the separation of CO_2 from CO for applications such as industrial syngas production and in particular to improve the conversion of the Reverse Water Gas Shift (RWGS) process. The use of adsorption technology for these applications requires an adsorbent that can effectively separate out CO_2 from a gas mixture containing CO_2, CO, and H_2. However, adsorption of H_2 is insignificant when compared to both CO_2 and CO, with only CO_2 and CO being the adsorbed species. The adsorption of CO_2 and CO was investigated in this work for four major types of industrial adsorbents which include: activated aluminas, activated carbons, silica gels, and zeolites. Zeolites, with their ability to be fine tuned many parameters which may affect adsorption, were investigated in terms of the effect of the cations present, SiO_2/Al_2O_3 ratios, and structure to determine how to optimize adsorption of CO_2 while decreasing adsorption of CO. This will help to determine a promising adsorbent for this separation with focus on maximizing the selective adsorption of CO_2 over CO.

To investigate this separation three scientific experimental methods were used; gravimetric adsorption isotherm analysis, volumetric adsorption isotherm analysis, and packed bed adsorption desorption breakthrough analysis. Gravimetric and volumetric methods allow for testing the adsorbent with the individual species of CO_2 and CO. This investigation will let us determine the pure component adsorption capacity, heats of adsorption, regenerability, and basic selectivity. Packed bed adsorption breakthrough experimentation was then carried out on promising adsorbents for the CO_2 separation from a mixture of CO_2, CO, and H_2. These experiments used a gas mixture that would be comparable to that produced from the RWGS reaction to determine the multicomponent gas mixture behaviour for adsorption. Temperature swing adsorption (TSA) with a purge gas stream of H_2 was then used to regenerate the adsorbent.

RÉSUMÉ

Dans ce projet de recherche, l'adsorption est considérée comme une manière de séparer le CO_2 du CO pour des applications telles que la production industrielle de gaz synthétique et en particulier l'amélioration de la conversion du processus de la réaction du gaz à l'eau inverse (RWGS). L'usage de la technologie de l'adsorption pour ces applications requiert un adsorbant qui peut séparer d'une manière efficace le CO_2 d'un mélange gazeux de CO_2, CO et H_2. Pourtant, l'adsorption du H_2 est insignifiant lorsqu'on la compare à l'adsorption du CO_2 et du CO, ces derniers étant les espèces chimiques adsorbées. L'adsorption du CO_2 et du CO a été investiguée dans ce projet pour quatre types majeurs d'adsorbents industriels y compris l'alumine activée. le charbon actif, les gels de silice, et les zéolites. Les zéolites, avec leur capacité d'affiner au poil plusieurs paramètres qui peuvent influencer l'adsorption, ont été étudiées par rapport aux cations présents, aux ratios entre le SiO_2 et l'Al_2O_3, et à leur structure afin de déterminer comment optimaliser l'adsorption du CO_2 et en même temps réduire l'adsorption du CO. Ceci aidera à déterminer un adsorbant efficace pour cette séparation, avec orientation sur la maximisation de l'adsorption sélective du CO_2 au lieu du CO.

Afin d'investiguer cette séparation, on a employé trois méthodes d'expérimentation scientifique: l'analyse gravimétrique des isothermes d'adsorption, l'analyse volumétrique des isothermes d'adsorption et l'analyse de la percée de l'adsorption et de la désorption avec tour de filtration. Les méthodes gravimétriques et volumétriques nous permettent de tester l'adsorbant avec les espèces chimiques individuelles (CO_2 et CO). Cette investigation nous permettra de déterminer la capicité maximum d'adsorption des composants, les chaleurs d'adsorption, la régénérabilité, et la sélectivité basique. On a ensuite fait des analyses de la percée de l'adsorption et de la désorption avec tour de filtration sur des adsorbants promettant la séparation du CO_2 d'un mélange de CO_2, CO et H_2. Ces expérimentations ont utilisé un mélange gazeux qui serait comparable à celui produit par le processus de la réaction du gaz à l'eau inverse (RWGS) pour ainsi déterminer le comportement du mélange gazeux à composants multiples en ce qui concerne l'adsorption. L'adsorption avec élan de température (TSA) avec un courant gazeux d'H_2 a ensuite été employé afin de régénérer l'adsorbant.

TABLE OF CONTENTS

I. LIST OF FIGURES

CHAPTER I

CHAPTER II

CHAPTER III

CHAPTER IV

II. LIST OF TABLES

CHAPTER I

CHAPTER II

CHAPTER III

CHAPTER IV

III. THESIS STRUCTURE

The current thesis structure is article based. The first chapter is a general introduction to the principles and concepts pertaining to the overall thesis. This includes a brief introduction into adsorption, information on the gas species tested, a review of 4 different types of industrial adsorbents used, a detailed discussion into the practical applications for this separation, and an overview of the experimental apparatus.

The preantepenultimate chapter pertains to a submitted paper to the Journal of Separation and Purification Technology titled "Equilibrium and Thermodynamic Analysis of CO_2 and CO Adsorption on ZSM-5 for Different SiO_2/Al_2O_3 Ratios". This article discusses pure component CO_2 and CO adsorption by MFI structured zeolites (ZSM-5 (30), ZSM-5 (50), ZSM-5 (280), and silicalite) and discusses the effect of SiO_2/Al_2O_3 ratio on the adsorption in zeolites using isotherms, vant Hoff plots, temperature dependant Toth (TD-Toth), and capacity ratio of CO_2/CO.

The antepenultamate chapter pertains to an article that has been submitted to the Journal of Microporous and Mesoporous Materials titled "Adsorbent Screening for CO_2/CO Separation". This article discusses four different types of industrial adsorbents for the separation and purification of syngas produced from the RWGS process and three industrial methods. This article reviews works that have been previously investigated into the matter and presents results obtained with 20 zeolites, 2 activated aluminas, 3 activated carbons, and 2 silica gels for adsorption isotherms and Henry's Law Constants to determine promising adsorbents to remove CO_2 from a gas mixture of CO_2, CO and H_2.

The penultimate chapter pertains to the article titled "Separation of H_2, CO_2, and CO Using Adsorbents for the Reverse Water Gas Shift Reaction" and will be submitted in the near future to a referred journal. This article investigates the potential use of three selected adsorbents (activated alumina AA-300, activated carbon BPL, and zeolite 4A) for the separation and recycle of CO_2 for the RWGS reaction. This study first determines the pure component isotherm data for the three adsorbents, and then investigates the breakthrough behaviour for the adsorption and desorption of a multicomponent mixture of CO_2, CO, and H_2 gases. This study uses cyclic steady state data to simulate an industrial separation of such a mixture.

Finally, the ultimate chapter discusses key conclusions from this thesis work for all three articles. With the aforementioned information, additional recommendations of further research will be recommended in order to peruse further understanding and knowledge on the subject matter.

IV. ACKNOWLEDGEMENTS

I would like to first thank my parents, without whom I would have never been inspired to becoming a chemical engineer. With their support and encouragement, I was able to overcome many obstacles, academic and otherwise, in order to be at this point in my life.

Secondly, I would like to thank my supervisor, Dr. F. Handan Tezel for giving me this opportunity and for all the hard work and understanding that goes along with it. With her help I was able to progress down this far into my research and to have completed my masters.

I would also like to thank Phoenix Canada Oil Company Ltd. for sponsoring a portion of this project and in particular Mr. Steve Aplin, for all his time and effort he put into helping with funding and talking about major issues with the project. His expertise, helped with many of the issues that were stumbled upon in the natural progress of science.

Lastly, I would like to thank all of the students that I have worked with and in particular; Dean Kennedy whose quid pro quos, long hours helping review papers, discussing research and charming personality helped me progress this far; Jeffrey Sims whose hands-on knowledge was of great help and importance as well as being an excellent roommate who I could go to for a good time and splendid conversation; and David Carter whose homemade brews and quick chats made every day feel a lot easier while being able to help trouble shoot problems.

V. CONTRIBUTIONS OF COLLABORATORS

I hereby declare that I am the sole and main author of this thesis. I performed all experiments, did every calculation, and wrote every word of this thesis, all under the supervision of Dr. F. Handan Tezel.

The lab scale experimentation was either previously built or constructed by myself or with the help of the technical support staff, Louis Tremblay, Gerard Nina and Franco Ziroldo. I performed all of the experiments for the pure gas adsorption isotherms as well as the breakthrough curve experimentation. Minor help was received from Y. Pan, A. El-Meligy, D. A. Kennedy during breakthrough experiment to open and close a GC valve every two and a half minutes.

With the help of Dean Kennedy and Dr. F. Handan Tezel, they made editorial comments and corrections on the work presented. Dr. F. Handan Tezel's week-to-week supervisions, discussions, and unrelenting support have produced and improved this written work.

Chapter I: Introduction

1.1 Preamble

Gas separation processes using adsorption technology are attractive to industry for their ability to achieve better economic efficiency and reliability when compared to using more conventional techniques such as cryogenic distillation, absorption, or membranes. This benefit is due to the less energy intensive nature of adsorption separation, which has continued expanding industrial applications due to the increase in environmental and quality requirements in industry. Currently, the industrial separation of CO_2 from CO is done using cryogenic distillation or absorption processes. Adsorption could offer significant economic benefits in comparison. However, there are challenges with respect to adsorption design and maximising purity and recovery of the final products. This design looks for the best adsorbent for the separation based on capacity, selectivity, regenerability, kinetics, and cost. Rarely however will there be an adsorbent that would be optimal for all of these criteria.

The separation of CO_2 from CO using adsorption technology would be beneficial to a variety of industries including syngas production from fossil fuels or biomass and the generation of CO using the reverse water gas shift (RWGS) process. Both of these processes have a mixture of CO_2, CO, and H_2 with the requirement for CO_2 separation. For syngas, the majority of processes require a combination of CO and H_2, therefore the presence of CO_2 is undesirable and is required to be removed. For the RWGS process, the feed contains CO_2. Therefore CO_2 is separated from the gas mixture of CO_2, CO and H_2 and recycled back into the reactor.

1.2 Application OF CO_2 Separation From CO Using Adsorbents

Currently in industry, CO_2 is being separated from CO and H_2 in applications involving syngas (also known as synthesis gas, synthetic gas, and producer gas) where the CO_2 acts as a major impurity and needs to be

removed before the syngas can be used to make valuable products. In order to achieve this separation, current industrial methods employ a combination of separation methods in order to get the syngas to meet application purity requirements. This study investigates CO_2 being separated using adsorbents from H_2 and CO which are the other two majority components for this separation.

Currently in industry, there are 3 main ways of producing syngas; partial oxidation (POX), steam reforming (SR), and autothermal reforming (ATR). However, a more carbon neutral way of producing syngas is becoming more attractive via the reverse water gas shift (RWGS) process. Each of these methods that produce syngas produces a different amount of CO_2, CO and H_2 with a variety of other gases as well which can be seen in Table 1.

Table 1 – The gas composition of syngas after being produced using different feedstocks: POX, SR, and ATR .

		Coal to Syngas POX [1]	Indirect Wood POX [2]	Natural Gas [3] SR	ATR
H_2	(Vol%)	25-30	15-45	70.3	62.6
CO	(Vol%)	30-60	20-45	14.1	27.2
CO_2	(Vol%)	5-15	10-25	7.6	4.7
CH_4	(Vol%)	0-5	8-17	6.3	3.3
N_2	(Vol%)	0.5-4	1-10	1.7	2.2
Other Impurities		H_2O, NH_4, H_2S, COS	C_2+, Benzene, NH_3, H_2S, H_2O	Ar	Ar

This unrefined syngas then needs to be purified in order to be used in applications including Fischer-Tropsch fuels, oxo-alcohols, methanol, ammonia, and a variety of other different applications. These applications requires the removal of all acid gas components, sulfur and nitrogen compounds, water, and a bulk separation of other components including N_2, CH_4, and CO_2 depending on the applications. Table 2 shows the required composition for four different applications.

Table 2 - The gas composition of syngas before being used for applications involving Fischer-Tropsch, oxo-alcohols, methanol, and ammonia [2].

Synthesis		Fischer-Tropche	Oxo-Alcohols	Methanol	Ammonia
H_2	(Vol%)	60	60	71	75
CO	(Vol%)	30	40	19	0-20ppm
CO_2	(Vol%)			4-8	0-20ppm
CH_4	(Vol%)	Low levels of all three inert gases	As low as possible		As low as possible
N_2	(Vol%)			As low as possible	25
Ar	(Vol%)				As low as possible

In this present study, only CO_2 separation from H_2 and CO will be investigated to determine its feasibility for applications involving syngas produced from a variety of industrial methods as well as from the RWGS process.

1.2.1 Partial Oxidation (POX)

POX involves the incomplete combustion of a hydrocarbon with less than stoichiometric quantities of oxygen. This exothermic reaction can be done with a wide variety of feedstock including natural gas, coal, petroleum coke, refinery off gas, LPG (Liquefied Petroleum Gas), naphtha, gas oil, vacuum residual fuel oil, shale oil, asphalt residual fuel oil, whole crude oil, as well as biomass. The POX reactions of natural gas and naphtha are presented in Equations 1 and 2, respectively. Since POX requires oxygen, the oxygen gas stream tends to be purified from air to minimize additional separation of the syngas. However, for production of syngas from biomass sources indirect partial oxidation can occur where no additional oxygen is required, since biomass contains oxygen within their hydrocarbons. The issue with partial oxidation is that they are extremely complex side reactions because of the thermal cracking at high temperatures produces low molecular weight hydrocarbon fragments which react with oxygen. The ratio of H_2/CO produced from POX is based upon the feed stock and is typically lower than other methods [4].

$$CH_4 + \frac{1}{2}O_2 \Leftrightarrow CO + 2H_2 \quad [1]$$

$$C_nH_{2n+2} + \frac{1}{2}nO_2 \Leftrightarrow nCO + (n+1)H_2 \quad [2]$$

1.2.2 Steam Reforming (SR)

SR is an endothermic reaction that occurs on a catalyst (ie. nickel) where methane (Equation 3) or naphtha (Equation 4) reacts with steam at high temperatures and pressures to produce carbon monoxide and hydrogen. These reactions produce a ratio of H_2/CO that is significantly higher than POX.

$$CH_4 + H_2O \Leftrightarrow CO + 3H_2 \quad [3]$$

$$C_nH_{2n+2} + nH_2O \Leftrightarrow nCO + (2n+1)H_2 \quad [4]$$

Since some applications only require H_2, SR is typically used in tandem with the water gas shift reaction in order to maximize the amount of H_2 in the mixture by reacting CO and H_2O into H_2 and CO_2 over a catalyst (Equation 5).

$$CO + H_2O \Leftrightarrow CO_2 + H_2 \quad [5]$$

Unlike POX, steam reforming cannot use such a large variety of feedstocks and is limited to light and middle distillates and alcohols. One of the major issues with steam reforming is catalytic poisoning from sulphur which is a major problem when selecting feedstocks [5].

1.2.3 Autothermal Reforming (ATR)

ATR is similar to POX except that the oxidation occurs on a catalyst where steam reforming can occur in tandem. This is done in order to control the CO/H_2 ratio of the syngas that is dependant based on the feedstock for partial oxidation.

1.2.4 Reverse Water Gas Shift (RWGS)

The RWGS reaction converts CO_2 and H_2 over a catalyst at high temperatures to produce CO and H_2O (Equation 6). This endothermic reaction, unlike POX, SR, and ATR, is considered carbon neutral. With carbon capture projects gaining interest, applications that use CO_2 can get reimbursed through the value of the carbon as a reactant making the whole process more economical.

$$CO_2 + H_2 \Leftrightarrow CO + H_2O \quad [6]$$

Currently, the RWGS reaction is not used in industry to make syngas but progress is underway especially with CO_2 becoming more of a political and environmental interest. The RWGS reaction was first investigated in industry by companies such as Sumitomo Metal Industries LTD [6] and Air Products LTD [7] for its beneficial low nitrous oxide fuels and for its rich CO stream but has since seen less interest from these industries. The U.S. Naval Research Laboratory however, has shown considerable interest in using the RWGS reaction from electrolysing sea water and capturing CO_2 from the atmosphere [8]. This reaction would use nuclear power produced on carriers for the reactions energy needs and would use the syngas to produce jet fuel grade petro [8]. Audi has also shown interest into using the RWGS reaction to produce renewable green diesel. Currently, Audi has a pilot plant producing 600L/day of diesel using this process in Dresden, Germany [9]. The space industry has investigated the RWGS technology [10] and has addressed the major problem with the low conversion inside the reactor.

The products that are produced from the RWGS process are CO, H_2, H_2O, and CO_2. Unlike the separation of CO_2 from syngas mixtures produced from industrial methods, the CO_2 that is separated is recycled back into the reactor. This recycle of CO_2 in the RWGS process then helps with the overall conversion of CO_2 for the overall process.

1.2.5 Cooling

Due to the nature of syngas production occurring at temperatures greater than 400^{O}C, cooling will be required in order to use adsorbents for the separation of CO_2 from a syngas mixture of CO_2, CO, and H_2. This in comparison to other current industrial methods for separation including, cryogenic distillation and absorption would require significantly less cooling making it more energy efficient if a feasible adsorbent were to be found.

1.3 ADSORPTION

Adsorption is the interaction of atoms or molecules with the surface of an object. The molecule that is adsorbed to the surface is known as the adsorbate and the solid is known as the adsorbent. This bond can

form via chemisorption or physisorption. Chemisorption relies on a chemical bond formed between adsorbent and adsorbate. Whereas physisorption relies on intermolecular forces such as the van der Waals force to bond the adsorbent and adsorbate together.

Adsorption of the adsorbate onto an adsorbent occurs in four main steps; external fluid film mass transfer, macropore transport, micropore transport, and sorption. External fluid film mass transfer refers to the movement of gases from the bulk gas phase into the outside fluid film surrounding the pellet [11]. The fluid is then transferred into the macropores of sizes >500Å. These channels are the space in-between crystals or are large pores formed during activation of the adsorbent. These macropores then connect into either mesopores (also known as transitional pores) of 20-500Å which are commonly found in activated carbons, or micropores of <20Å. After diffusion into the smallest pores which make up the majority of the adsorbents surface areas, the molecule adsorbs and forms a bond with the surface of the adsorbent.

Since the surface of the adsorbent interacts with the adsorbate, adsorbents that are used in industry tend to have very large areas. Such industrial adsorbents include activated carbons, silica gel, activated aluminas, and zeolites which have surface areas that are greater than 200m^2/g. Surface areas per gram of adsorbate are presented in Table 3.

Table 3 – Surface area of common industrial adsorbents [12]

Activated Aluminas	Activated Carbons	Silica Gels	Zeolites
200-500 m^2/g	300-4000 m^2/g	300-350 m^2/g 750-850 m^2/g	500-800 m^2/g

The separation using adsorbents is done using the affinity and selectivity of one gas over the other.. This is important such that the more affinity one adsorbate has over another, increases the purification and recovery of the adsorbate, making the overall process more economically viable.

This thesis investigates the four types of industrial adsorbents: activated aluminas, activated carbons, silica gels, and zeolites and determine their adsorption properties for the adsorbates; CO_2 and CO.

1.4 ADSORBATES

1.4.1 Carbon Monoxide

Carbon monoxide (CO) is a colorless, odourless, flammable, and very hazardous gas that is formed from the combination of a carbon atom and an oxygen atom bound by a covalent triple bond. Since the oxygen atom is significantly more electronegative than the carbon atom, carbon monoxide has dipole moment which is an unbalancing of charge inside the molecule.

CO is of interest due to its high chemical potential. This potential allows CO to be used as a production intermediary for organic compounds such as acetic acid, isocyanates, formic acid, Fischer-Tropsch fuels, and also certain polymers such as polycarbonates and polyketones.

1.4.2 Carbon Dioxide

Carbon dioxide (CO_2) is a colorless odourless gas that is a combination of two oxygen atoms covalently double bonded to a single carbon atom. Similar to CO, CO_2 oxygen atoms pull the electrons away from the carbon but unlike CO, this forms a strong quadrupole moment which can interact with the adsorbent.

Carbon dioxide is of interest because it is a greenhouse gas. Governments around the world have been pressuring industry to reduce the overall amount of CO_2 emitted into the atmosphere with major economies taking initiative such as China , the United States of America, and the European Union [13] [14] [15]. This has led to many industrial and academic projects investigating separating CO_2 from carbon point sources such as power plants and sequestering or utilizing the CO_2 [16] [17] [18]. One method that utilizes CO_2, instead of being sequestered into the ground, is through the RWGS process to produce chemically useful CO [19].

1.4.3 Properties

In order to understand the adsorption separation behaviour of CO_2 and CO, knowledge of the gas properties is needed in order to determine possible methods of separation. Table 4 shows the gas properties that are important for adsorption separation. For adsorption separation, the greater the difference between these properties, the easier the separation. For instance, if the kinetic diameter difference between two gases is

large enough, a molecular sieve with a pore that is in between the size of the two gas molecules could be used to separate out the two gases from each other. However, for CO_2 and CO gases, the molecular sizes are very similar and therefore molecular sieving is not possible. The quadruple moment for CO_2 is significantly larger than that of CO, by nine orders of magnitude, and the polarizability is also greater. This difference in adsorbate properties was noticed in literature with CO_2 having overall stronger adsorption properties than CO [11].

CO adsorption could also be favourable if the adsorbate interacts with its weak dipole moment. Also with the unique structure of CO, π-bonding can occur with adsorbents containing metals such as copper which are referred to as π-complexation sorbents [12]. For the enrichment of CO from syngas, Cu(I)Y was investigated and had a stronger adsorption of CO then other syngas components such as CO_2, N_2, H_2, and CH_4 [20]. However, this adsorbent requires re-reduction to Cu(I) using H_2. This is due to Cu(I) being oxidized to Cu(II) after regeneration.

Table 4 – Kinetic diameter, quadrupole moment, dipole moment, and polarizability of CO_2 and CO.

Adsorbate	Kinetic Diameter (Å)	Quadrupole Moment (C m^2)	Dipole Moment (D)	Polarizability (Å^3)
CO_2	3.3 [21]	4.6×10^{-31} [22]	-	2.24 [23]
CO	3.7 [21]	-8.36×10^{-40} [24]	0.122 [25]	1.84 [23]

1.5 ADSORBENTS

There are 4 major types of industrial adsorbents in the market; activated carbons, zeolites, silica gels and activated aluminas. Activated carbons and zeolites make up the majority of the adsorbent market with silica gels, and activated aluminas making up the minority which can be seen in Table 5. The different uses and applications of these adsorbents are numerous and have been identified in detail [12]. For this particular separation, a comprehensive report has yet to investigate which one of these industrial adsorbents would perform best for a CO_2 separation from a syngas mixture of CO_2, CO, and H_2 at moderate temperatures. A large selection of adsorbents was tested throughout this thesis due to there being a lack of knowledge weather they

would work or not. With so many different adsorbents out there, testing out a wide variety of adsorbents gained a more definitive result on which adsorbent would be the best for this separation.

Table 5 – Estimates of the worldwide sales of different common industrial adsorbents

	Activated Carbons	Zeolites	Silica Gel	Activated Alumina
1997 [26]	$1 billion	$100 million	$27 million	$26 million
2000 [12]	-	$1.07 billion	$71 million	$63 million

1.5.1 Activated Carbons

Activated carbons are the most widely used adsorbents, due to their cost and utility which comes from their large micropore and mesopore volumes as well as high surface areas. Activated carbons can also be manufactured to have defined pore sizes which are called carbon molecular sieves. Activated carbons are produced from raw carbon sources such as coconut shells, coal, coke, and other carbonous sources. The process of producing activated carbons from these sources is available in literature and is shown in Figure 1. The raw material is thermally decomposed via pyrolysis and activated using either physical or chemical methods. Common activation methods include using steam or CO_2 at high temperatures of around 700-1100^{0}C [11]. This activation process effectively opens the pores of the activated carbon by removing any tar like substances from the activated carbon.

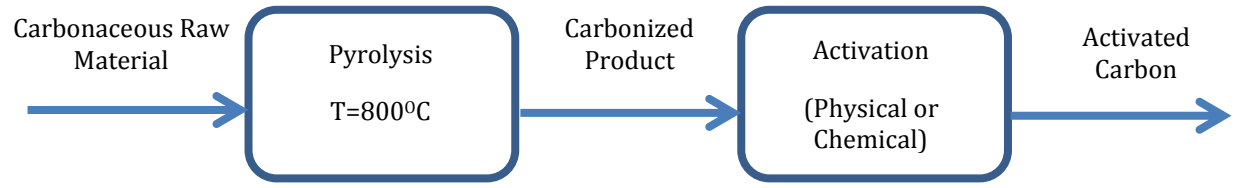

Figure 1 – Process of producing activated carbons from agricultural wastes from literature [27].

Activated carbons are popular adsorbents to be tested for separations because of their high surface areas and affordable costs.

1.5.2 Activated Aluminas

Activated aluminas are composed of amorphous porous hydrophobic aluminum oxide, and are commonly used in industry as desiccants, and for the removal of polar gases from hydrocarbons. Activated aluminas are synthesised from bauxite or monohydrate aluminum oxide by dehydration at controlled temperatures and then recrystallized. One of the main benefits of activated aluminas is their ability to have different pH's, from acidic to basic due to either brønsted acid sites and lewis acid sites within the alumina. With some gases forming acid base pairs upon adsorption, tuning these parameters allows for stronger adsorption for desired components compared to less desired components.

1.5.3 Silica Gels

Silica gels are composed of amorphous porous silica oxides, and are common desiccants at lower temperatures. Unlike activated aluminas, the properties of silica gels are harder to change during synthesis. There are two main types of silica gels, high density which have larger surface areas and low density which have smaller surface areas. These silica gels are typically manufactured from pure silica, that is naturally non polar, and dissolved in an acid solution to produce colloidal silicic acid. This solution is then dehydrated and neutralized and produces silica gel that is polar. Silica gels are promising adsorbents because they are relatively cheap compared to the cost of zeolites. Due to the oxidized structure of silica gel, silica gel can be modified using amine groups, which have been investigated for the adsorption of CO_2 [28].

1.5.4 Zeolites

Zeolites are composed of SiO_4 and AlO_4 tetrahedras that are joined together and are balanced out by metal cations. The framework of the zeolite can have many different structures (over 225 structures recognized by the International Zeolite Association) which are composed of smaller segments called building blocks. In a lab scale, some of these zeolite structures are synthesis by hydrothermal reaction with silica and alumina salts in autoclaves. The overall process of producing zeolites from literature is presented in Figure 2.

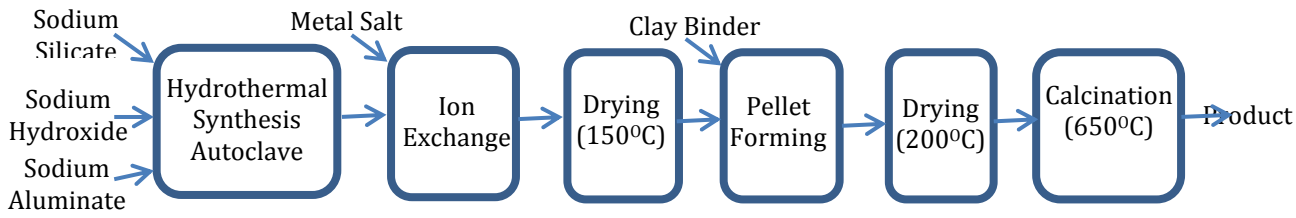

Figure 2 - Steps in lab scale production of pelletized zeolites from literature [11].

Even though there are over 225 structures of zeolites, only a limited number of zeolites are used as commercial adsorbents with many different applications discussed in detail in literature [12]. What makes zeolites interesting adsorbents is their ability to be fine-tuned for a particular application. Zeolite structures, the cation present, and the SiO_2/Al_2O_3 ratios all influence the adsorption selectivity and separation of gases in industry.

1.6 EXPERIMENTAL

In order to analyse adsorbents for a CO_2/CO separation, three experimental setups were used; volumetric adsorption isotherm analyser, micro gravimetric adsorption isotherm analyser, and packed bed adsorption breakthrough experiment. Using these three methods, adsorbents can be analysed to determine their adsorption capacities, kinetics, heats of adsorption, multicomponent mixture behaviour, and regenerability. Using these three experiments, preliminary research can be done to determine which adsorbents should and should not be tested in the pilot plant scale.

1.6.1 Volumetric Adsorption Isotherm Analyser

The volumetric adsorption isotherm analyser uses a known mass of adsorbent which is placed into the sample holder of a known volume. This sample is then regenerated using high temperatures and vacuum. Once the sample is regenerated, a fixed temperature is imposed by a heating element and the experiment can start. Two main steps must be taken to calculate an isotherm; determination of the skeletal volume of adsorbent that is placed into the sample holder, and the different equilibrium concentrations at known pressures to create the isotherm. An overall schematic of the volumetric system can be seen in Figure 3.

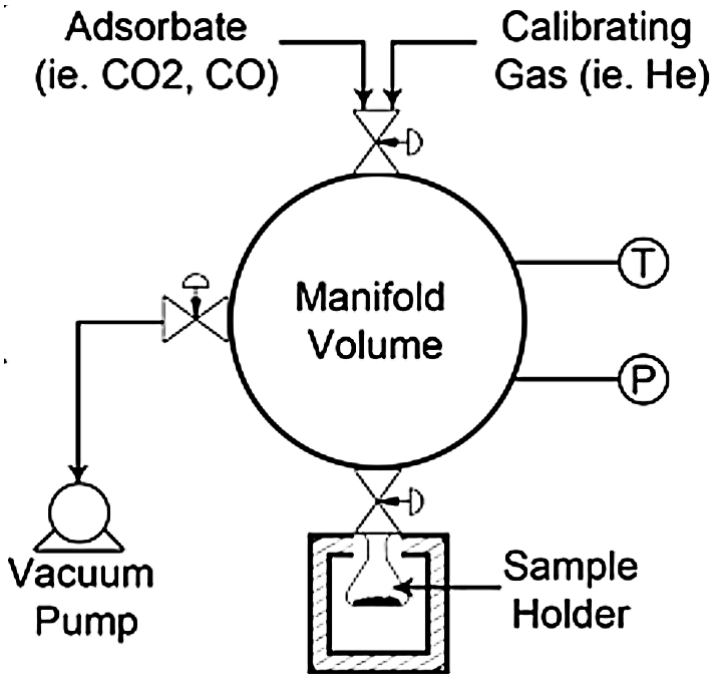

Figure 3 – Schematic diagram of the volumetric system.

The determination of the adsorbent skeletal volume (V_{AS}) is done using a helium dose from a known manifold volume (V_d) at a known pressure (P_1). This dose is then applied to the known sample volume (V_s) which was originally at vacuum, where the pressure will equilibrate (P_2) between the sample volume, manifold volume, and the adsorbent skeletal volume. This unaccounted additional pressure is due to the adsorbent skeletal volume which can be seen in Equation 7, where T_d and T_s is the temperature of the manifold and the sample cell, respectively.

$$\frac{P_1 V_d}{T_d} = \frac{P_2 V_d}{T_d} + \frac{P_2 (V_s - V_{AS})}{T_s} \quad [7]$$

Once the sample is regenerated after the adsorbent skeletal volume runs, the adsorption isotherms different equilibrium data points steps can begin. This is done by loading the manifold volume with a known amount of adsorbate. This adsorbate is then dosed into the sample volume (originally at vacuum) by opening the sample valve, the pressure decreases quickly due to the change in volume, and then decreases slowly due to the adsorption of the adsorbate onto the adsorbent. Once the adsorbate comes into equilibrium with the adsorbent, pressure (known as the equilibrium pressure) is recorded and the adsorbed concentration can be calculated. The step of dosing the reference volume with a known amount of adsorbate, and then releasing it

into the sample volume is repeated until there are many data points in the isotherm. A detailed description of the steps and calculation are available from Micrometrics [29].

1.6.2 Micro Gravimetric Adsorption Isotherm Analyser

The micro gravimetric isotherm analyser is another method used to measure single component adsorption isotherms. This is done by using the mass of the gas adsorbed which is measured by a microbalance. The mass of a solid adsorbent that is going to be tested is first placed into a bucket that hangs from a microbalance. This vessel is then regenerated using high temperatures and pressures, and a fixed temperature is imposed onto the sample cell. To create the adsorption isotherm at high pressures, a buoyancy/volume correction must also be performed using an inert gas. A schematic diagram of the micro gravimetric system can be seen in Figure 4.

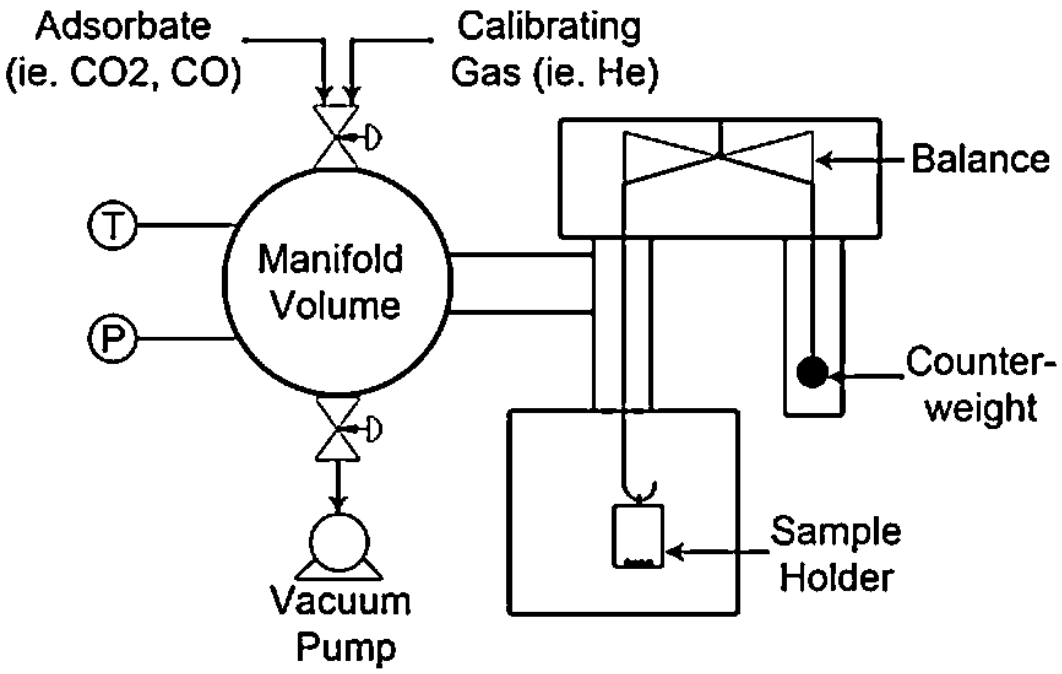

Figure 4 – Schematic diagram of the micro gravimetric system.

A buoyancy and volume correction of the adsorbent must be done when using the micro gravimetric system. This is because as the pressure of the gas increases inside the sample holder, the density of the gas increases. Increasing the gas density thusly increases the buoyancy force acting upon the adsorbents skeletal volume,

thus decreasing the weight of the sample. This buoyancy effect is presented in Figure 5, with the weight of the sample decreasing as pressure increases. In order to calculate this effect, a non-interacting species such as helium is dosed into the chamber at fixed pressures in order to calculate this buoyancy force on the skeletal volume of the adsorbent.

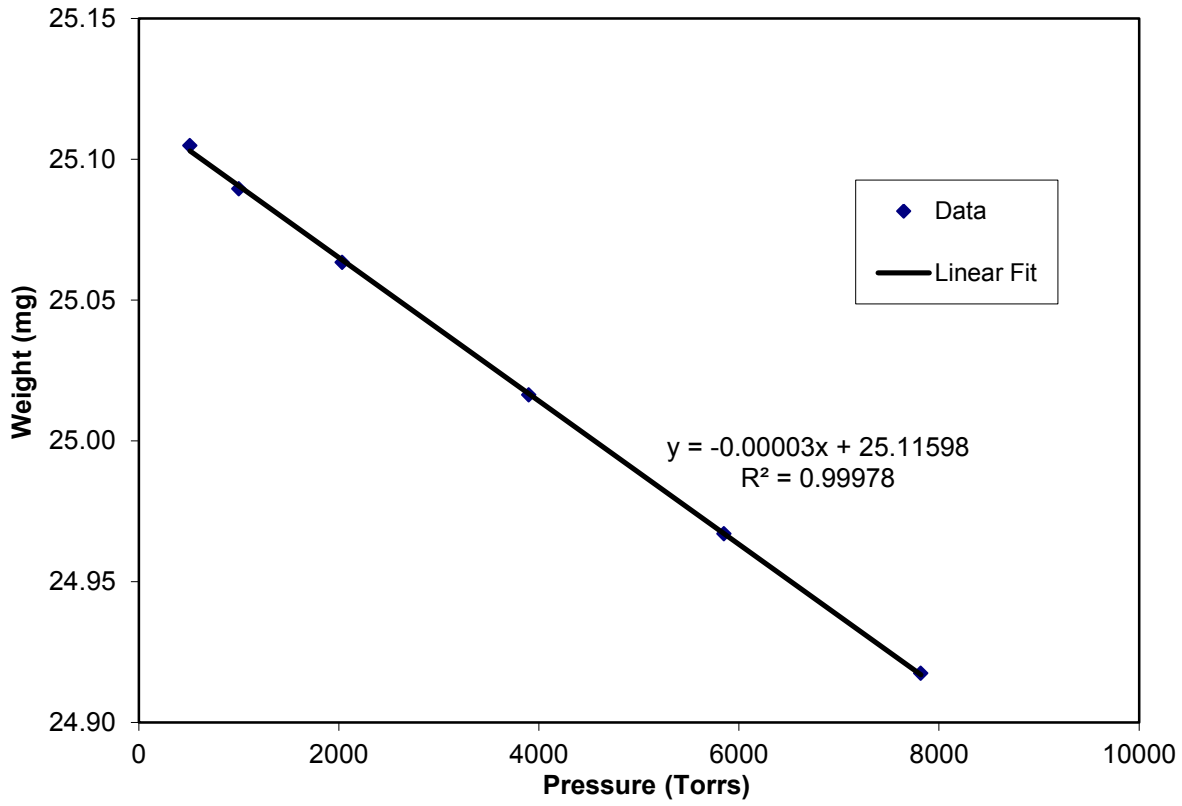

Figure 5 –Buoyancy effect as pressure increases in the micro gravimetric system during a He buoyancy/volume correction run.

After the buoyancy/volume correction, the adsorbent is regenerated again and the reference weight is taken at the imposed temperature at vacuum. The chamber is then dosed with a fixed pressure of adsorbate, and is left to reach equilibrium. Once the equilibrium is reached, data is recorded (exact weight, pressure, temperature) and the next fixed pressure is applied. This is then repeated until all data points are taken for the isotherm.

1.6.3 Advantages and Disadvantages of Gravimetric vs. Volumetric

Volumetric and gravimetric isotherm analysers both measure the adsorption isotherms for a particular adsorbent. Volumetric isotherm analysers are typically used at low pressures. This is because the volumetric method uses the change in pressure to determine the amount adsorbed, and when a small metered dose is applied, almost the entire dose is adsorbed. The gravimetric technique is more accurate at higher pressures because the difference in the reference weight and the adsorbed weight is greater than for lower pressures.

A major benefit of the gravimetric system over the volumetric system is the error. Error associated with the gravimetric technique is independent for each individual isotherm point. This due the fact that each isotherm point has an error that is associated with the difference in the reference weight and the adsorbed weight. For the volumetric technique however, each isotherm point is calculated from the previous, therefore, the error is cumulative and grows as there are more isotherm data points leading to a net associated cumulative error with the isotherm.

Another benefit to the gravimetric system is that each pressure for the data points can be fixed. This allows for simple programming of the experiment as well as benefits for calculation of kinetics of adsorption.

1.6.4 Packed Bed Adsorption-Desorption Breakthrough

A packed bed adsorption-desorption breakthrough experiment is performed in order to determine key adsorption parameters that would be involved with multicomponent gas flows which can be calculated and observed from the breakthrough curve. In order to obtain a breakthrough curve, a mass of solid adsorbent is packed into a column which is then mounted onto the experimental setup. Following desorption of the adsorbent using high temperature/purge gas or high temperature/vacuum pressure, the column is brought down to room temperature. A known gas flow rate and composition is then mixed together and enters the bottom of the column. The components of the gas stream then enter the bottom of the column where the mass transfer zone between the adsorbent and adsorbate travels up the column until the column is saturated and the gas composition breaks though. Set regeneration criteria (temperature, pressure, and purge gas) are

chosen to mirror industry conditions. Once regenerated using these criteria, breakthrough happens again until the breakthrough regeneration cycle reaches cyclic steady state.

The schematic diagram for the packed bed adsorption breakthrough experiment located at the University of Ottawa is presented in Figure 6. In this setup, CO_2, CO, and H_2 are first mixed together in a mixing column packed with glass beads under set flow rates for each gas controlled by individual mass flow controllers. This gas can then bypass the experiment, be directed towards the packed bed, or be hydrated and then sent to the packed bed. Once the gas preparation is complete, the gas is sent to the adsorption column where the pressure and temperature are monitored before entering the column. During the adsorption breakthrough, this column adsorbs a component of the gas stream while the temperature is being monitored on the outside of the column. The exiting concentration at the outlet of the column pressure and temperature are measured and then directed to either an IR spectroscope or a gas chromatograph to determine gas concentration with a thermal conductivity detector and a Porapak Q column.

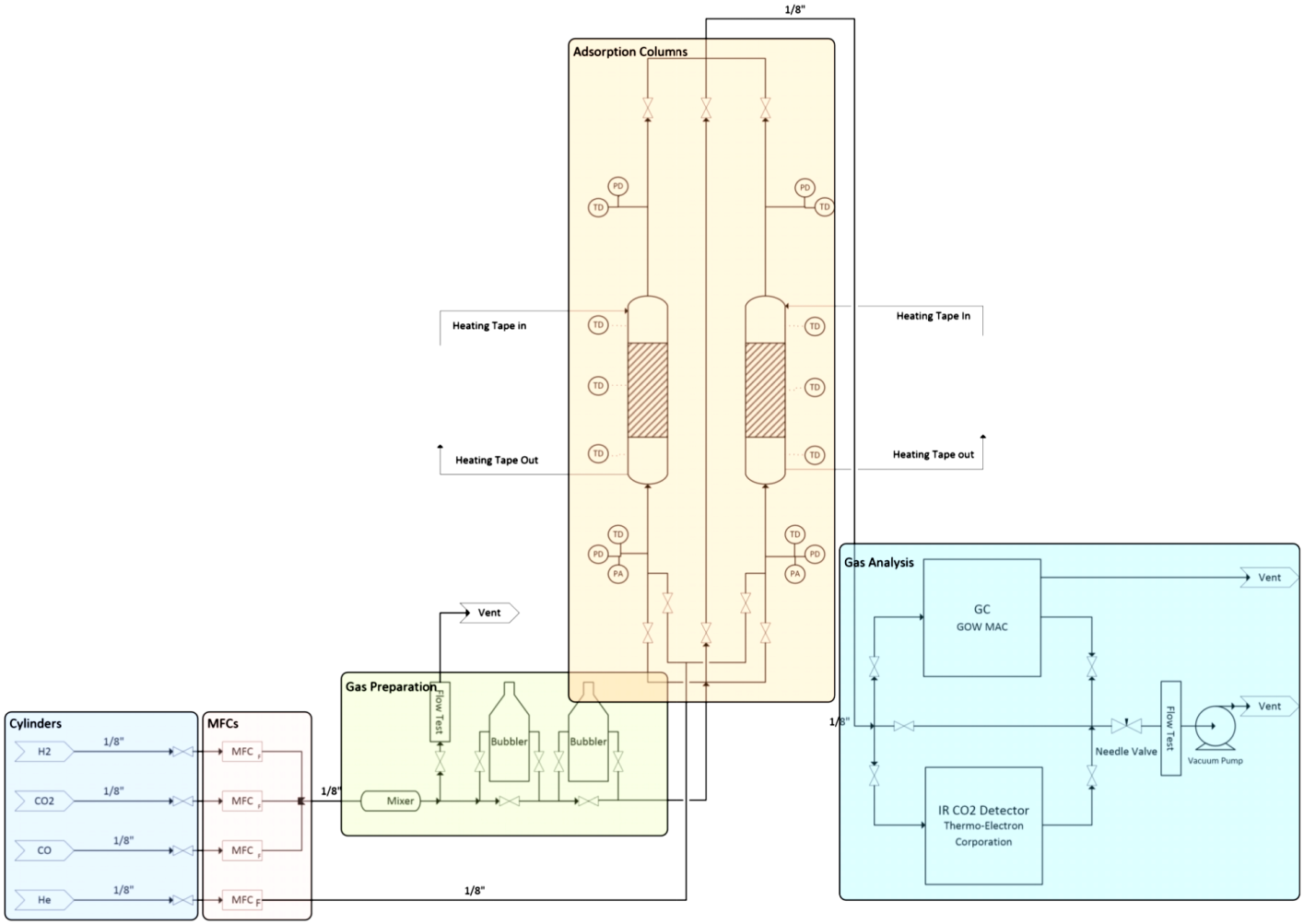

Figure 6 – P&ID of the fixed bed adsorption breakthrough experiment

1.7 OBJECTIVES

The purpose of this study was to investigate adsorbents that would be useful for the separation of CO_2 from CO in industrial syngas and in the RWGS process. Both applications will look into the performance of four major types of industrial adsorbents including: activated aluminas, activated carbons, silica gels, and zeolites.

Three main objectives of this thesis for the study of the adsorption separation of CO_2 from syngas were: the equilibrium and thermodynamic analysis for the effect of SiO_2/Al_2O_3 ratios on ZSM-5, the screening of promising adsorbents for the separation of CO_2 from CO for applications in syngas, and the ternary gas adsorption separation of CO_2, CO, and H_2 with the selected three adsorbents for the improvement of the overall conversion of the reverse water gas shift reaction.

In order to investigate these three main objectives, two main methods are used: pure gas adsorption isotherms, and multicomponent adsorption/desorption breakthrough runs. Using these two methods, possible adsorbents for these separations were investigated in order to determine those which are most promising for this separation.

1.8 NOMENCLATURE

P	Pressure (atm)
T	Temperature (K)
V_{AS}	Adsorbent skeletal volume (cm^3)
V_d	Manifold volume (cm^3)
V_s	Sample volume (cm^3)

1.9 LIST OF ABBREVIATIONS

ATR	Autothermal Reforming
POX	Partial Oxidation

RWGS	Reverse Water Gas Shift
SR	Steam Reforming

1.10 BIBLIOGRAPHY

1 National Energy Technology Labratory. Gasifier: Gasification Introduction. Syngas Composition [Internet]. 2015 May.

2 Boerrigter H, Rauch R. Handbook Biomass Gasification. Biomass Technology Group; 2005. p. Chapter 10.

3 Jenzer GA, Tio TH, Zuideveld PL, inventors. System and Process for Synthesis of Methanol. 2005. WO2005108336 A1.

4 Brown RC. Thermochemical Processing of Biomass: Conversion into Fuels, Chemicals and Power. Wiley; 2011.

5 Van Beurden P. On the Catalytic Aspects of Steam Methane Reforming. Technical Report. Energy Research Centre of the Netherlands (ECN); 2004. I-04-003.

6 LTD SMI, inventor. Gaseous Fuels with Low Nitrogen Oxides Formation by Carrying Out Reverse Water Gas Shift. 1975 April 25. JP50046702-A.

7 Wang S, Inc APaC, inventors. Carbon Monoxide mfr. - Using Steam-Methane Reforming and Reverse Water Gas Shift Reactions. 1988. EP291857-A ; JP63297209-A.

8 Parry D. Fueling the Fleet, Navy Looks to the Seas. U.S. Naval Research Labratory: Public Affairs & Media. 2012 Sep 24.

9 Time Fortune Editors. Audi Just Invented Fuel Made from CO2 and Water. Fortune. 2015 Apr 28:1.

10 Zubrin R, Clapp MB, Meyer T. New Approaches for Mars In-Situ Resource Utilization Based on the Reverse Water Gas Shift. In: 35th Aerospace Sciences Meeting and Exhibit; 1997; Reno, NV. p. AIAA-97-0895.

11 Ruthven DM. Principles of Adsorption & Adsorption Processes. John Wiley & Sons; 1984.

12 Yang RT. Adsorbents: Fundamentals and Applications. Hoboken (NJ): John Wiley & Sons Inc.; 2003.

13 Jiang B, Sun ZQ, Lui MQ. China's Energy Development Strategy Under the Low-Carbon Economy. Energy. 2010;35(11):4257-4264.

14 Fargione J, Fout T, Plasynski S, McIlvried H, Srivastava RD. Advances in CO_2 Capture Technology - The US Department of Energy's Carbon Sequestration Program. International Journal of Greenhouse Gas Control. 2008;2(1):9-20.

15 Hertwich EG, Peters GP. Carbon Footprint of Nations: A Global, Trade-Linked Analysis. Environmental Science & Technology. 2009;43(16):6414-6420.

16 Yang HQ, Xu ZH, Fan MH, Gupta R, Slimane RB, Bland AE, Wright I. Progress in Carbon Dioxide Separation and Capture: A Review. Journal of Environmental Sciences-China. 2008;20(1):14-27.

17 Song CS. Global Challenges and Strategies for Control, Conversion and Utilization of CO_2 for Sustainable Development Involving Energy, Catalysis, Adsorption and Chemical Processing. Catalysis Today. 2006;115(1-4):2-32.

18 Aaron D, Tsouris C. Separation of CO_2 from Flue Gas: A Reivew. Separation Science and Technology. 2005;40(1-3):321-348.

19 Mikkelsen M, Jorgensen M, Brebs FC. The Teraton Challenge: A Review of Fixation and Transformation of Carbon Dioxide. Energy & Environmental Science. 2010;3(1):43-81.

20 Li S, Huawei Y, Donghui Z. Enrichment of CO from Syngas with Cu(I)Y adsorbent by Five-Bed VPSA. Frontiers of Chemical Science and Engineering. 2013;7(4):472-481.

21 Beck DW. Zeolite Molecular Sieves. New York: Wiley & Sons; 1974.

22 Harries JE. The Quadrupole Moment of CO_2 Measured from the Far Infrared Spectrum. Journal of Physics B Atomic, Molecular, and Optical Physics. 1970;3(12):L150.

23 Cai WQ, Gough TE, Gu XJ, Isenor NR, Scoles G. Polarizability of CO_2 Studied in Molecular Beam Laser Stark Spectroscopy. Physical Review A. 1987;36(10):4722-4727.

24 Graham C, Imrie DA, Raab RE. Measurement of the Electric Quadrupole Moment of CO_2, CO, N_2, Cl_2, and BF_3. Molecular Physics. 1998;93(1):49-56.

25 Scuseria GE, Miller MD, Jensen F, Geertsen J. The Dipole Moment of Carbon Monoxide. Journal of Chemical Physics. 1991;94(10):6660-6663.

26 Humphrey JL, Keller GE. Separation Process Technology. McGraw-Hill; 1997.

27 Ioannidou O, Zabaniotou A. Agricultural Residues as a Precursors for Activated Carbon Production: A Review. Renewable and Sustainable Energy Reviews. 2007;11(9):1966-2005.

28 Leal O, Bolivar C, Ovalles C, Garcia JJ, Espidel Y. Reversible Adsorption of Carbon Dioxide on Amine Surface-Bonded Silica Gel. Inorganica Chimica Acta. 1995;240(1):183-189.

29 Micromeritics. Instruction Manual: Accusorb 2100 Surface Area Calculations Program v1.01. 1986.

Chapter II: Equilibrium and Thermodynamic Analysis of CO_2 and CO Adsorption on ZSM-5 for Different SiO_2/Al_2O_3 Ratios

Sean M.W. Wilson, F.H. Tezel

Department of Chemical and Biological Engineering, University of Ottawa, Ottawa ON. Canada

2.1 ABSTRACT

The adsorption of CO_2 and CO on MFI type zeolites with different SiO_2/Al_2O_3 ratios (ZSM-5 (30), ZSM-5 (50), ZSM-5 (280), and silicalite) were investigated in this study by a static gravimetric analyzer for pure isotherms at four different temperatures (30°C, 65°C, 100°C, and 135°C) over the pressure range of 0 – 10 atm. Adsorption capacity was higher for CO_2 than CO for all SiO_2/Al_2O_3 ratios, temperatures, and pressures. It was shown that the adsorption capacity of CO increases with decreasing SiO_2/Al_2O_3 ratios within ZSM-5. The adsorption of CO_2 for decreasing SiO_2/Al_2O_3 ratios, showed stronger adsorption at lower pressures; due to differences in adsorption surface area of the samples, at higher pressures the highest capacity varied from ZSM-5 (50) to ZSM-5 (30) at increasing temperature. Heats of adsorption at zero loading capacity were calculated using van't Hoff plots for CO_2 and CO for ZSM-5 samples. ZSM-5 (280) was found to have the highest selectivity for CO_2 within the widest range of pressures and temperatures tested. Optimal performance for CO and CO_2 separation is obtained at lower temperatures and pressures in this study at 30°C to increase the adsorption capacity of the adsorbent and to increase the selectivity of CO_2, compared to CO.

Keywords: Adsorption Separation of CO_2 and CO adsorption, ZSM-5, Silicalite, Reverse Water Gas Shift

2.2 INTRODUCTION:

The increasing amount of CO_2 in the atmosphere has led to global warming and more interest in carbon capture projects around the world. With many projects looking at just sequestering the CO_2, projects that utilize CO_2 get reimbursed through the value of the carbon. One method to recycle CO_2 is the Reverse Water Gas Shift (RWGS) reaction. This converts CO_2 and H_2 into CO and H_2O. After this equilibrium reaction takes place over a catalyst, the incomplete conversion of CO_2 to CO [1] requires a separation step in order to return the unused reactant back into the reactor to increase the overall conversion of the RWGS reaction. This requires purification of the CO product. This CO, with the combination of H_2, can then produce Fisher-Tropsch fuels, or be transformed into products such as urea, acetic acid, formic acid, and also certain polymers such as polycarbonates.

CO_2 and CO have been compared together in many papers for their adsorbent separation [2] [3] but the only MFI structured zeolites that have been studied are Ba-ZSM-5 [4] and Silicalite [5]. Thus MFI zeolites present an interesting area of investigation. ZSM-5 has been considered for other separations, including CO_2-N_2 [6], CO_2-CH_4 [7], CO-N_2 [8], and CO_2-CH_4-N_2 [9] [10] gas mixtures. The gas mixture of CO_2, C_2H_4, and C_3H_8 has been studied in the literature for Na-ZSM-5 with different SiO_2/Al_2O_3 ratios up to 0.9atm [11]. ZSM-5 is a zeolite from the pentasil family (MFI) with a structure that is composed of 5 and 6 member rings attached to each other. This creates pores that are 2 dimensional channels characterized by 10 membered oxygen rings with an aperture around 6Å [12]. Since the aperture is significantly larger than the kinetic diameter of CO_2 at 3.3Å and CO at 3.7Å the molecules will not be molecularly sieved [13]. ZSM-5 is composed of $[SiO_4]^0$ and $[AlO_4]^{-1}$ tetrahedrons which form the skeleton of the zeolite. Since $[AlO_4]^{-1}$ contains a negative charge; counter balancing cations are required to balance out the charges within the ZSM-5. In this paper we will be looking at $[NH_4]^{+1}$ ions to balance out the charges within the ZSM-5 at different SiO_2/Al_2O_3 ratios. As the SiO_2/Al_2O_3 ratio of ZSM-5 decreases, more ions are needed to balance out the charges of the $[AlO_4]^{-1}$ within the zeolite. When ZSM-5 almost has no Al_2O_3, it is called silicalite and contains almost no counter balancing cations. Due to the lack of ions, silicalite is hydrophobic and has been reported to have insignificant adsorption of water over other gases such as O_2 and n-hexane [14].

The adsorption of the adsorbate will be influenced by the quadruple moment, dipole moment, and the polarizability of the gaseous molecules. These values can be seen in Table 1 for the adsorbate gases used in this study. CO_2, a slightly smaller molecule, has no dipole moment but a significantly larger quadruple moment with similar polarizabilities than CO. These three factors interact with both the ZSM-5 structure and the concentration of ammonium ions which is also dependent on different SiO_2/Al_2O_3 ratios.

Table 1 - Quadruple, dipole moment, and polarizability of CO_2 and CO

Adsorbate	Quadruple Moment (C m^2)	Dipole Moment (D)	Polarizability (Å^3)
CO_2	4.6×10^{-31} [15]	0	2.24 [16]
CO	-8.37×10^{-40} [17]	0.122 [18]	1.84 [16]

In the present study, CO_2 and CO pure gas isotherms were analysed for the type of separation required for the RWGS reaction. H_2 adsorption will not be investigated due to its weak, uncompetitive adsorption relative to the adsorption of CO_2 and CO. This study aims to measure the adsorption of CO_2 and CO on NH_4-ZSM-5 with different SiO_2/Al_2O_3 ratios by determining its effect on the separation of these gases.

2.3 Materials and Methods:

2.3.1 Materials

CO_2 and CO gases have been obtained from Linde Canada (Burlington, Ontario) at purities of 99.99% and 99.7% respectively. The ammonium powder form of ZSM-5 was purchased from Zeolyst International (Conshokocken, Pennsylvania) with SiO_2/Al_2O_3 of 30, 50, and 280 ratios designated by ZSM-5 (30), ZSM-5 (50), and ZSM-5 (280), respectively. Silicalite (HISIV 3000) was purchased from Honeywell UOP (Calgary, Alberta). The chemical composition and surface areas of the ZSM-5 samples are presented in Table 2. The surface areas were analysed at the NRC (National Research Concil) using BET analysis. The compositions were calculated using information that the supplier provided about the adsorbent.

Table 2 – The chemical composition and surface areas of ZSM-5 (30), ZSM-5 (50), ZSM-5 (280), and silicalite. The specific surface areas for the ZSM-5 (50), ZSM-5 (280), and silicalite

	Composition of Anhydrous ZSM-5, wt%				BET surface area
Adsorbent	Na_2O	NH_3	Al_2O_3	SiO_2	(m^2/g)
ZSM-5 (30)	0.05	1.7292	5.2565	92.964	405**
ZSM-5 (50)	0.05	1.057	3.245	95.648	425**,373.57
ZSM-5 (280)	0.05	0.1733	0.6008	99.176	400**,385.57
Silicalite*	0.0515	--------	0.0847	99.864	317.83

*Silicalite's Si/Al ratio is greater than 1000
**Surface area were acquired from Zeolyst International

2.3.2 Experimental Details

Pure gas adsorption isotherms were determined using a gravimetric analysis done by a VTI Scientific Instruments GHP. The pure isotherms were performed on the gravimetric analyzer by regenerating the samples at 300°C under vacuum of around 10^{-8} atm. The samples were then evaluated at increasing pressures of up to 10atm. Desorption experiments were then performed briefly by decreasing the pressure to determine hysteresis. Buoyancy correction was done using helium at similar pressure and temperatures. Isotherms were conducted at temperatures of 30°C, 65°C, 100°C, and 135°C for both CO and CO_2 for ZSM-5 (30), ZSM-5 (50), ZSM-5 (280), and silicalite.

2.3.3 Model Equations

The adsorption data was then fit to Langmuir, Freundlich, Sips, and Toth model equations using the sum of least squares method. These isotherm models are given in Table 3. The model with the best fit for the coefficient of determination (R^2) was used to reflect the isotherm [19].

Table 3 - Langmuir, Freundlich, Sips, and Toth adsorption isotherm models

Langmuir Model	Freundlich Model	Sips Model	Toth Model
$\frac{q_e}{q_s} = \frac{\beta P}{1+\beta P}$	$q_e = k\,P^{\,1/n}$	$\frac{q_e}{q_s} = \frac{(\beta P)^n}{1+(\beta P)^n}$	$\frac{q_e}{q_s} = \frac{\beta P}{(1+(\beta P)^t)^{1/t}}$

In order to determine the adsorption equilibrium capacity over a wide range of temperatures, the empirical temperature dependent Toth (TD-Toth) model that gives temperature dependence to the individual

parameters q_s (Equation 1), β (Equations 2), and t (Equation 3) was used. This model correlates the q_s to q_{s0} and X, β to β_0 and Q, and t to t_0 and α. All these parameters are fitted to the adsorption equilibrium data for a T_0 of 303K.

$$q_s = q_{s0} exp\left[X(1 - \frac{T}{T_0})\right] \quad [1]$$

$$\beta = \beta_0 \exp\left[\frac{Q}{RT_0}(\frac{T_0}{T} - 1)\right] \quad [2]$$

$$t = t_0 + \alpha\left(1 - \frac{T_0}{T}\right) \quad [3]$$

The limiting heats of adsorption were determined using van't Hoff equation (Equation 4), knowing the Henrys law constant (K) from the adsorption isotherms at 30°C, 65°C, 100°C, and 135°C.

$$\frac{\delta lnK}{\delta T} = \frac{\Delta H_0}{RT^2} \quad [4]$$

Assuming ΔH_o is not a strong function of T, integrating Equation 4 gives Equation 5.

$$lnK = -\frac{\Delta H_0}{R}\frac{1}{T} + lnK_0 \quad [5]$$

When lnK versus $1/T$ is plotted, known as the van't Hoff plot, the slope of the line gives the ratio of the heat of adsorption at zero loading to the gas constant.

As mentioned before, since the H_2 gas adsorption is negligible compared to CO_2 and CO, the sorbent selection parameter will be the selectivity, which is defined as the adsorption equilibrium capacity for CO_2 over the adsorption equilibrium capacity for CO (Equation 6).

$$Selectivity = {}^{q_{e,CO2}}/_{q_{e,CO}} \quad [6]$$

2.4 Results and Discussion:

Figure 1 shows the adsorption equilibrium isotherms of CO_2 and CO for ZSM-5 (30), ZSM-5 (50), ZSM-5 (280), and silicalite at temperatures of 30°C, 65°C, 100°C, and 135°C obtained experimentally.

The increase in adsorption with decreasing temperature indicates that the adsorption is exothermic as expected for physical adsorption. It is clear that CO_2 has a higher capacity then CO for adsorption by ZSM-5 for all temperatures and all SiO_2/Al_2O_3 ratios. The adsorbent with the highest capacity for CO_2 is ZSM-5 (50) at 30°C with a capacity of 2.76 mmol/g at 10.5 atm. The adsorbent with the highest capacity for CO is ZSM-5 (30) at 30°C with a capacity of 1.41 mmol/g at 10.5 atm. The adsorption isotherms for CO_2 and CO follow Type I from Brunauer classification of isotherms. The adsorption isotherms for CO_2 at 30°C for all four samples are more rectangular and become less rectangular as temperature increases. This trend of changing shape of the isotherm also happens for CO adsorption but to a lesser effect than that for CO_2 for all SiO_2/Al_2O_3 due to temperature change.

2.4.1 Effect of SiO_2/Al_2O_3 Ratio on Capacity

In Figure 1, the graph of ZSM-5 (50) was found to have the highest adsorption capacity for CO_2 at 30°C at higher pressures of 10 atm compared with ZSM-5 (280), ZSM-5 (30), and silicalite in respectively decreasing order of adsorption capacities for CO_2. This is contrary to Calleja et al. [11] data within the pressure range of 0 to 0.9 atm that as the SiO_2/Al_2O_3 ratio decreases, CO_2 loading increases. This conclusion though holds true that at lower SiO_2/Al_2O_3 ratios, there is an increase in the amount of counter balancing ions and therefore an increase in attraction force between the adsorbent and the adsorbate, CO_2. This attraction is observed in Figure 1 by the increased adsorption capacity at lower pressures (low loading within the ZSM-5) making the isotherms most rectangular for ZSM-5(30), compared to ZSM-5(50), ZSM-5 (280) and silicalite having progressively less rectangular isotherms for the same temperatures. The factor that makes the ZSM-5 (50) have a higher adsorption capacity then ZSM-5 (30) at higher pressures is the larger surface area that ZSM-5 (50) has, compared to ZSM-5 (30). This difference in surface area between ZSM-5 (30) and ZSM-5 (50) is attributed to the increase in ammonium ions within ZSM-5 (30) which would sit and occupy surface area within the 10 member oxygen ring pore channels. This observation for the effect of SiO_2/Al_2O_3 ratio within the ZSM-5 was predicted using simulations by Newsome et al. [20] that lower SiO_2/Al_2O_3 ratios have substantially increased adsorption at lower pressure, but at higher pressures the effect of lower SiO_2/Al_2O_3 ratio would be minor due to all the NH_4^{+1} and AlO_4^{-1} sites are saturated with CO_2 molecules.

All isotherms have good fits for the Langmuir isotherm model compared to the Freundlich isotherm model. However, these two models contain only 2 fitting parameters and when compared to the Toth and Sips isotherm model which have 3 fitting parameters, the overall fit according to the coefficient of determination is less superior. In Figure 1, all CO_2 and CO isotherms are either Sips or Toth depending on their coefficient of determination (R^2).

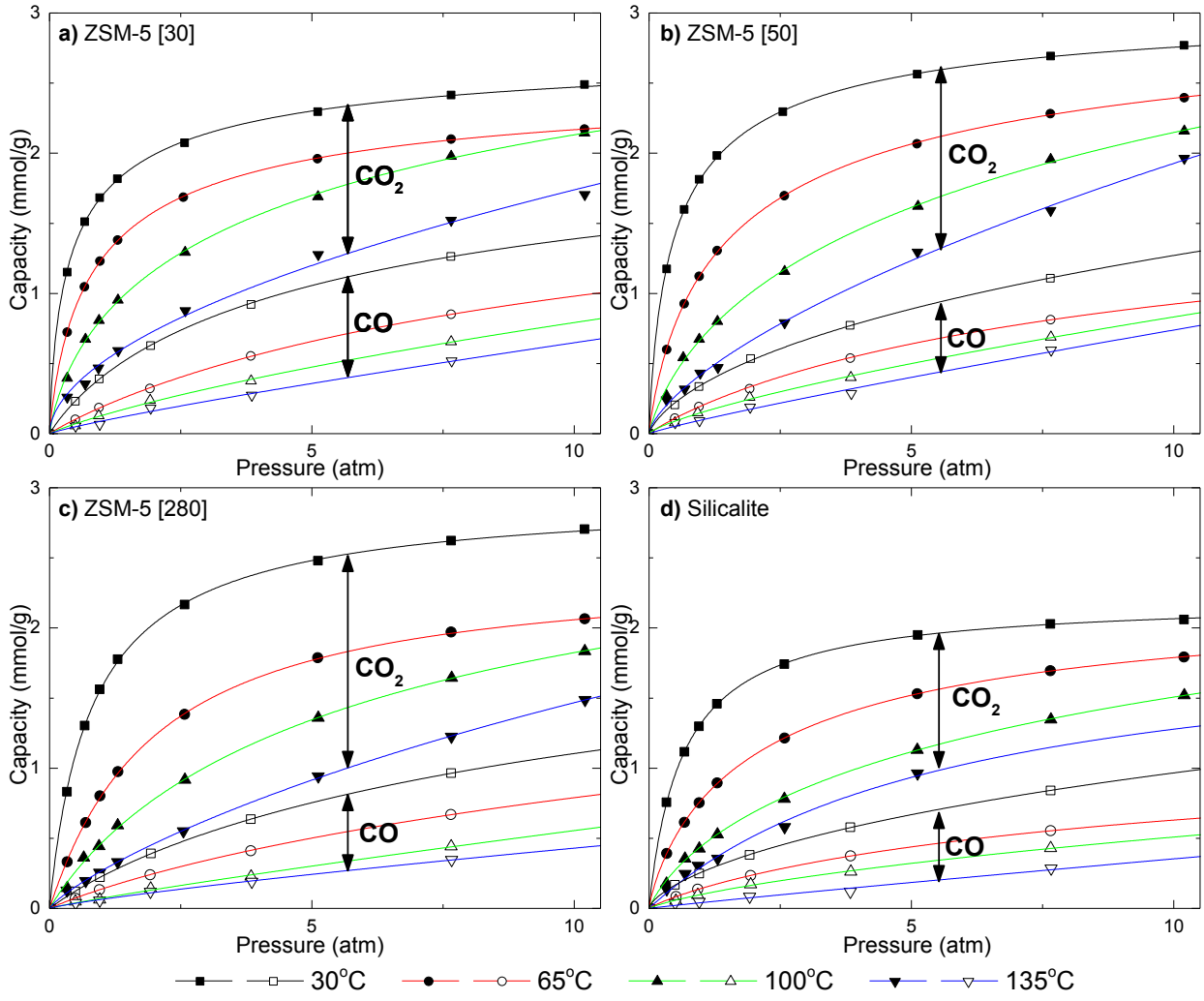

Figure 1 – CO_2 and CO pure adsorption isotherms at 30°C, 65°C, 100°C, and 135°C for a) ZSM-5 (30); b) ZSM-5 (50); c) ZSM-5 (280); and d) silicalite.

As temperature is increased, the effect of a larger surface area is less dominant than the attraction force of the ammonium ions to the adsorbate CO_2 for the overall capacity of the adsorbent. At higher temperatures of 135°C the isotherms of ZSM-5(30) has similar adsorption capacity over the 10.5 atm pressure range as ZSM-5

(50), compared to ZSM-5 (280), and silicalite in order of decreasing capacity for CO_2. The difference in capacity at 10.5 atm between the ZSM-5 with the highest capacity and silicalite has a maximum difference in CO_2 adsorption capacity of 0.70 mmol/g, 0.61 mmol/g, 0.652 mmol/g, and 0.60 mmol/g for temperatures of 30°C, 65°C, 100°C, and 135°C respectively.

For CO adsorption, ZSM-5 (30) has the highest adsorption capacity for all temperatures and pressures, with ZSM-5 (50), ZSM-5 (280), and silicalite following in order of decreasing capacities. This agrees with trends seen by Sethia et al. [8] at temperatures of 15°C and 30°C that as the SiO_2/Al_2O_3 ratio increase in ZSM-5, the adsorption capacity for CO decreases. As the SiO_2/Al_2O_3 ratio increases the amount of ammonium ions decreases, therefore decreasing the interaction between the ammonium ion and the dipole moment, quadruple moment, and polarizability of the adsorbate. This change in SiO_2/Al_2O_3 ratio at 10.5 atm has a difference in CO adsorption capacity between the ZSM-5 with the highest capacity and silicalite of 0.42 mmol/g, 0.36 mmol/g, 0.34 mmol/g, and 0.40 mmol/g at 30°C, 65°C, 100°C, and 135°C, respectively.

2.4.2 Effect of SiO_2/Al_2O_3 Ratio on Heats of Adsorption

The limiting heats of adsorption were calculated using the van't Hoff equation (Equation 5). The natural log of the Henrys law constant was plotted against the inverse of temperature in Figure 2. As can be seen from this figure, the overall trend is linear. The linear fits for CO_2 were better than CO using the coefficient of determination (R^2). The linear correlation for the CO_2 were very strong (R^2>=0.99) as well as for CO samples ZSM-5 (30) and ZSM-5 (50). ZSM-5 (280) and silicalite for CO adsorption has a lower linear correlation but still reasonable fits.

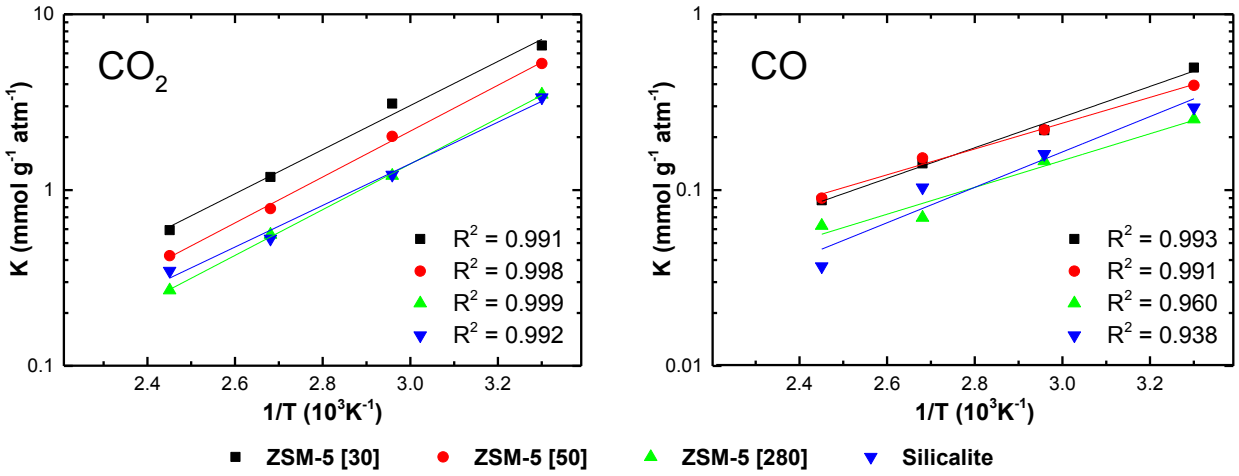

Figure 2 – Vant Hoff plot for CO_2 (left) and CO (right) for ZSM-5(30), ZSM-5(50), ZSM-5(280), and silicalite using calculated henrys law constants at temperatures of 30°C, 65°C, 100°C, and 135°C.

The calculated limiting heat of adsorption values are plotted in Figure 3. These values for carbon dioxide were found to be larger than those for carbon monoxide for all SiO_2/Al_2O_3 ratios as can be seen from this figure. This is expected since carbon dioxide adsorption is greater than carbon monoxide adsorption in Figure 1. This can also be seen in Table 4 where all heats of adsorption at zero loading from literature were found to be higher for CO_2 than for CO for similar samples.

The limiting heat of adsorption value in Figure 3 for CO_2 adsorption on ZSM-5 (30) was calculated to be 24.0 kJ/mol. This value increased slightly for ZSM-5 (50) to 25.0 kJ/mol then decreased slightly for ZSM-5 (280) to 24.9 kJ/mol. Silicalite heat of adsorption of CO_2 was lower than all other ZSM-5 samples at 22.7 kJ/mol. The effect of SiO_2/Al_2O_3 ratios in MFI type zeolites and in turn, the concentration of the ammonium ion, has a minimum effect on the heats of adsorption of CO_2 in the present study, as well as in the literature.

Table 4 – Heats of adsorption at zero loading for CO and CO_2 from literature for ZSM-5 samples with different SiO_2/Al_2O_3 ratios and silicalite. SiO_2/Al_2O_3 ratios are mentioned in brackets next to the adsorbent name.

Adsorbent	ΔH_{ads} for CO_2 (kJ/mol)	Source Reference	Adsorbent	ΔH_{ads} for CO (kJ/mol)	Source Reference
H-ZSM-5 (27)	28.8	[21]	Na-ZSM-5 (25)	33	[8]
H-ZSM-5 (30)	34.6	[9]	Na-ZSM-5 (28)	27	[22]
H-ZSM-5 (50)	33.1	[9]	Na-ZSM-5 (40)	30	[8]
H-ZSM-5 (62)	26.1	[23]	Na-ZSM-5 (100)	28	[8]
H-ZSM-5 (80)	32.6	[9]	Na-ZSM-5 (400)	25	[8]
H-ZSM-5 (280)	32.3	[9]	Na-ZSM-5 (900)	23	[8]
Na-ZSM-5 (23)	46.3	[21]	Silicalite	16.6	[5]
Na-ZSM-5 (62)	42	[23]			
Silicalite	24.1	[5]			
Silicalite	33.4	[9]			
Silicalite	21.7	[23]			
Silicalite	23.4	[21]			

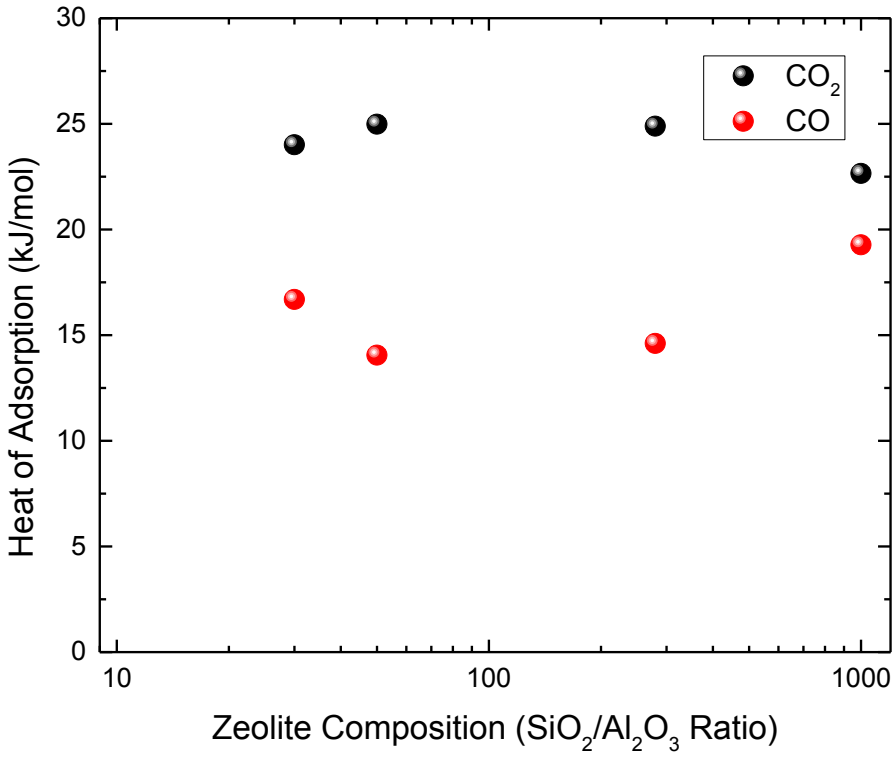

Figure 3 – Heat of adsorption at zero loading of CO_2 and CO for ZSM-5 (30), ZSM-5 (50), ZSM-5 (280), and silicalite. Silicalite is represented by a SiO_2/Al_2O_3 ratio of 1000 on this graph for simplistic purposes.

When comparing values from literature, differences in the type of cation in the MFI structure significantly changes the heats of adsorption, particularly with the increase in strength of the sodium ion. This was shown by Yamazaki et al. [21] in ZSM-5 samples with the same SiO_2/Al_2O_3 ratios that the heat of adsorption changes based on the ion, $[Li]^{+1}>[Na]^{+1}>[K]^{+1}>[Rb]^{+1}>[Cs]^{+1}>H^{+}$ [21]. Silicalite was found to have the lowest heats of adsorption for CO_2 out of the entire ion exchanged ZSM-5 samples by Yamazaki et al. [21]. This agrees with the calculated heats of adsorption with silicalite which has a lower heat of adsorption compared to the other ZSM-5 samples in this study.

Adsorption of CO on ZSM-5 produced a significantly lower heat of adsorption data than CO_2 data. ZSM-5 (30) limiting heats of adsorption were 16.7 kJ/mol for CO compared to 24.0 kJ/mol for CO_2. There is a decrease in the heat of adsorption for CO as the SiO_2/Al_2O_3 ratio is increased to ZSM-5 (50) at 14.0 kJ/mol. There is then minimum change for ZSM-5 (280) at 14.6 kJ/mol. Sethia, et al. [8] reported a noticeable increasing trend in the heats of adsorption for sodium ZSM-5 samples, as the SiO_2/Al_2O_3 ratio decreases [8]. This trend was attributed to the increase in the amount of counter balancing sodium ions interacting with the adsorbate within the ZSM-5 samples as the SiO_2/Al_2O_3 ratio decrease. Since there is only a slightest difference between ZSM-5 (30) and ZSM-5 (50), differences in heats of adsorption are within experimental error and the NH_4^{+1} ions have significantly less influence in the adsorption of CO, particularly compared to Na^{+1} ions.

2.4.3 Effect of SiO_2/Al_2O_3 Ratio on Selectivity

The adsorption equilibrium isotherm of CO_2 and CO for ZSM-5 (30), ZSM-5 (50), ZSM-5 (280), and silicalite at temperatures of 30°C, 65°C, 100°C, and 135°C were fit to the TD-Toth model and the values for q_{s0}, X, β_0, Q, t_0, and α for a T_o of 30°C can be seen in Table 5.

Table 5 –The fitted parameters for the TD-Toth model for ZSM-5 (30), ZSM-5 (50), ZSM-5 (280), and silicalite for carbon monoxide and carbon dioxide adsorption.

Toth	ZSM-5 (30)		ZSM-5 (50)		ZSM-5 (280)		Silicalite	
Parameters	CO_2	CO	CO_2	CO	CO_2	CO	CO_2	CO
q_{so} (mmol/g)	2.879	8.786	3.041	10.824	2.842	2.370	2.266	10.578
$b_{o\,(}atm^{-1})$	6.247	0.1585	2.598	0.132	1.112	0.121	1.667	0.114
Q (kJ/mol)	31.212	51.717	26.643	43.272	20.574	27.475	21.884	28.825
t_o	0.563	0.342	0.749	0.303	1.040	0.807	0.885	0.281
α	0.492	-0.311	-0.034	-0.085	0.127	-1.303	-0.466	0.195
χ	-0.192	-9.050	-0.368	-6.869	0.758	-4.101	0.0914	-1.088

As the SiO_2/Al_2O_3 ratio increases, the capacity of the adsorbent tends to decrease for both CO and CO_2. This effect is not equal though for these adsorbents. Figure 4 shows the selectivity of CO_2 over CO calculated from the pure isotherm data which was computed using the TD-Toth equation (Equations 1-3). For ZSM-5 (30), ZSM-5 (50), ZSM-5 (280), and silicalite the selectivity starts out higher at low pressures and then decreases as pressure increases. This decrease is because of the rectangular shape of the CO_2 isotherms compared to the more linear shape of the CO isotherms. Since the CO_2 adsorption is the largest at low pressures compared to CO adsorption, it is best to utilize low pressures to separate these two gases.

ZSM-5 (280) has the highest selectivity for CO_2 over CO within the widest range of pressures and temperatures tested and would offer the best performance for the CO_2 separation from CO due to this difference in selectivity. This excludes the regions for ZSM-5 (30) of pressures below 0.5atm and above temperatures of 60°C and silicalite for temperatures above 125°C over the entire range of pressures which have the best performance. The lowest selectivity was found for ZSM-5 (30) at temperatures of below 45°C and above 7 atm where the selectivity dropped below 2. Overall ZSM-5 (30) and ZSM-5 (50) were found to have the lowest selectivities for CO_2 with ZSM-5 (30) is having the lowest performance for temperatures below 85°C and ZSM-5 (50) having the lowest performance above temperatures of 85°C.

Even though ZSM-5 (50) had the highest capacity for CO_2, it did not have the highest selectivity. This is because ZSM-5 (50) has high capacities for CO_2 as well as CO which reduces the overall selectivity for CO_2.

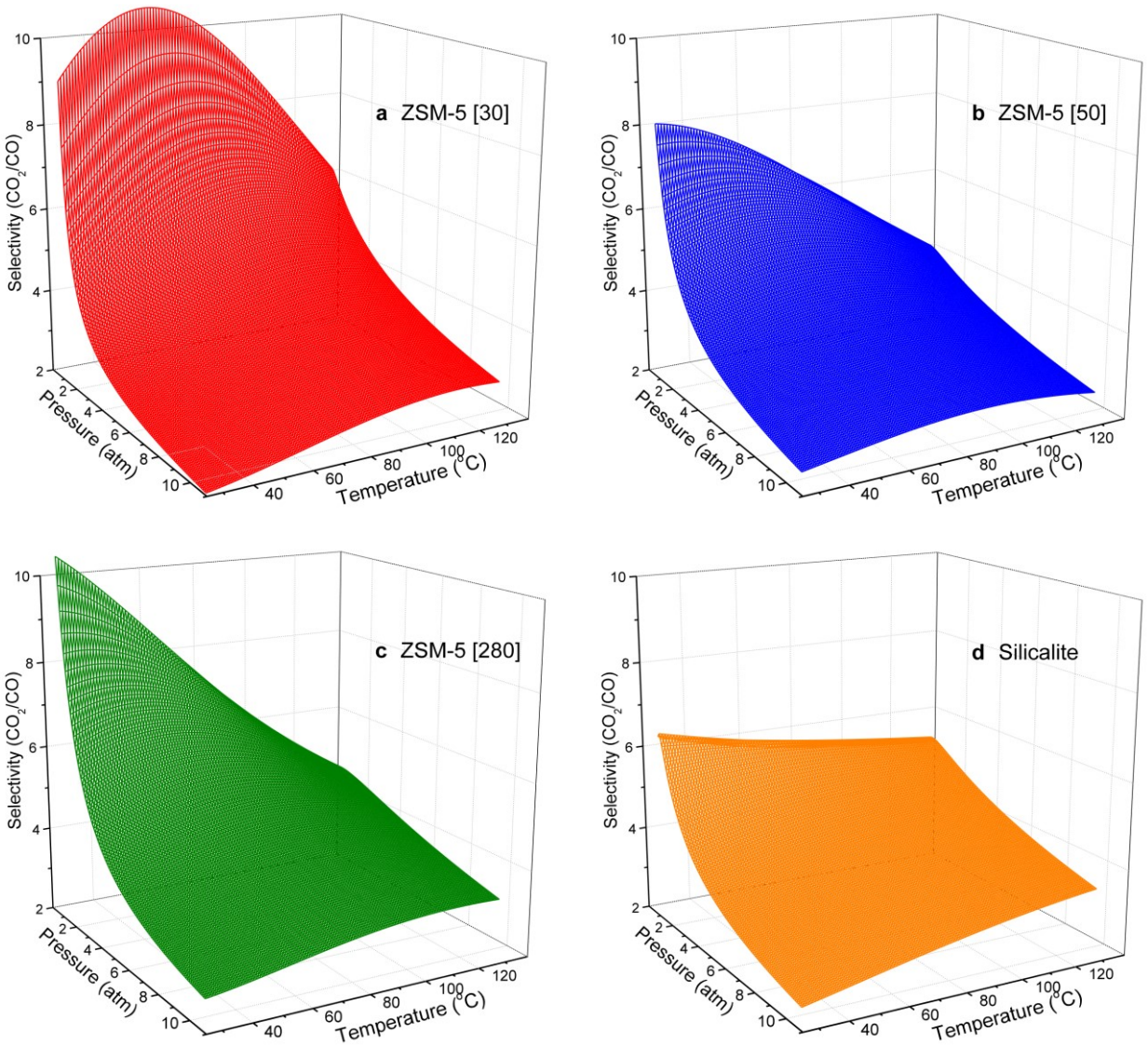

Figure 4 - Selectivity ratio of CO_2 over CO for a) ZSM-5 [30], b) ZSM-5 [50], c) ZSM-5 [280], and d) silicalite for temperatures of 30°C to 135°C and pressures of 0 to 10.5atm.

2.5 CONCLUSIONS:

In conclusion, CO_2 had higher adsorption capacities than CO for ZSM-5 (30), ZSM-5 (50), ZSM-5 (280), and silicalite for temperatures of 30°C to 135°C and pressures of 0 to 10.5atm. The effect of increasing the SiO_2/Al_2O_3 ratio within ZSM-5 decreased the adsorption capacity for CO. However, the effect of increasing the SiO_2/Al_2O_3 ratio within the ZSM-5 for CO_2 capacity only showed increased capacity at lower pressures but due

to the differences in adsorption surface areas of the different samples, at higher pressures the highest capacity varied from ZSM-5 (50) to ZSM-5 (30) at increasing temperature.

Henry's law constants were calculated from the pure gas adsorption isotherms and heats of adsorption at zero loading capacity were calculated using van't Hoff plots after using the adsorption isotherms determined at different temperatures. CO_2 had higher heats of adsorption compared to CO for all samples. The effect of changing the SiO_2/Al_2O_3 ratio within the ZSM-5 had a small effect on the heats of adsorption for CO and CO_2. For silicalite however, there was a noticeable difference between its heat of adsorption and the other ZSM-5 samples.

With small differences in heats of adsorption and uneven change between CO_2 and CO capacities for different SiO_2/Al_2O_3 ratios, ZSM-5 (280) had the highest selectivity for CO_2 within the widest range of pressures and temperatures tested. Operating an adsorption separation system with ZSM-5 (280) composed of CO_2 and CO gases would perform the best at lower temperatures to increase the adsorption capacity of the adsorbent; and lower pressures which have favourable adsorption capacities for CO_2, compared to CO.

2.6 NOMENCLATURE

H_0	Heat of adsorption (kJ/mol)
k	Freundlich parameter (mmol g^{-1} atm^{-1})
K	Henrys law constant (mmol g^{-1} atm^{-1})
n	Freundlich parameter (dimensionless)
P	Pressure (atm)
q_e	Equilibrium adsorption capacity (mmol/g)
q_s	Monolayer or saturated adsorption capacity (mmol/g)
q_{s0}	Empirically TD-Toth (mmol/g)
Q	Empirically TD-Toth Heat of adsorption (kJ/mol)
R	Gas constant (kJ K^{-1} mol^{-1})
R^2	Coefficient of determination
t	Toth parameter (dimensionless)
t_0	Empirically TD-Toth reference parameter (dimensionless)
T	Temperature (K)

T_0	Empirically TD-Toth reference temperature (K)
α	Empirically TD-Toth parameter (dimensionless)
β	Langmuir parameter (atm^{-1})
β_0	Empirically TD-Toth reference parameter (atm^{-1})
χ	Empirically TD-Toth constant (dimensionless)

2.7 List of Abbreviations

MFI	Pentasil
RWGS	Reverse Water Gas Shift
TD-Toth	Temperature Dependant Toth

2.8 Bibliography

1 Holladay, J. D., Brooks, K. P., Wegeng, R., Hu, J., Sanders, J., and Baird, S. Microreactor Development for Martian in Situ Propellant Production. *Catalysis Today*, 120, 1 (2007), 35-44.

2 Pakseresht, S., Kazemeini, M., and Akbarnejad, M. M. Equilibrium Isotherms for CO, CO_2, CH_4, and C_2H_4 on the 5A Molecular Sieve by a Simple Volumetric Apparatus. *Separation and Purification Technology*, 28, 1 (2002), 53-60.

3 Triebe, R. W. and Tezel, F. H. Adsorption of Nitrogen, Carbon Monoxide, Carbon Dioxide and Nitric Oxide on Molecular Sieves. *Gas Separation & Purification*, 9, 4 (1995), 223-230.

4 Wirawan, S. K. and Creaser, D. Multicomponent H_2/CO/CO_2 adsorption on Ba-ZSM-5. *Separation and Purification Technology*, 52, 2 (2006), 224-231.

5 Golden, T. C. and Sircar, S. Gas Adsorption on Silicalite. *Journal of Colloid and Interface Science*, 162 (1994), 182-188.

6 Katoh, M., Yoshikawa, T., Tomonari, T., Katayama, K., and Tomida, T. Adsorption Characteristics of Ion-Exchanged ZSM-5 Zeolite for CO_2/N_2 Mixtures. *Journal of Colloid and Interface Science*, 226, 1 (2000), 145–150.

7 Li, P. and Tezel, F. H. Pure and Binary Adsorption Equilibria of Methane and Carbon Dioxide on Silicalite. *Separation Science and Technology*, 42, 14 (2007), 3131-3153.

8 Sethia, G., Dangi, G. P., Jetwani, A. L, Somani, R. S., Bajaj, H. C., and Jasra, R. V. Equilibrium and Dynamic Adsorption of Carbon Monoxide and Nitrogen on ZSM-5 with Different SiO_2/Al_2O_3 Ratio. *Separation Science and Technology*, 45, 3 (2010), 413–420.

9 Harlick, P. J. E. and Tezel, F. H. Adsorption of Carbon Dioxide, Methane, and Nitrogen: Pure and Binary Mixture Adsorption by ZSM-5 with SiO_2/Al_2O_3 Ratio of 30. *Separation Science and Technology*, 37, 1 (2002), 33-60.

10 Harlick, P. J. E. and Tezel, F. H. Adsorption of Carbon Dioxide, Methane, and Nitrogen: Pure and Binary Mixture Adsorption for ZSM-5 with SiO_2/Al_2O_3 ratio of 280. *Separation and Purification Technology*, 33, 2 (2003), 199-210.

11 Calleja, G., Pau, J., and Calles, J. A. Pure and Multicomponent Adsorption Equilibrium of Carbon Dioxide, Ethylene, and Propane on ZSM-5 Zeolites with Different Si/Al Ratios. *Journal of Chemical and Engineering Data*, 43, 6 (1998), 994-1003.

12 Ruthven, D. M. *Principles of Adsorption & Adsorption Processes*. John Wiley & Sons, 1984.

13 Beck, D. W. *Zeolite Molecular Sieves*. Wiley & Sons, New York, 1974.

14 Flanigen, E. M., Bannett, J. M., Grose, R. W., Cohen, J. P., Patton, R. L., Kirchner, R. M., and Smith, J. V. Silicalite, a New Hydrophobic Crystalline Silica Molecular Sieve. *Nature*, 271 (1978), 512-516.

15 Harries, J. E. The Quadrupole Moment of CO_2 Measured from the Far Infrared Spectrum. *Journal of Physics B Atomic, Molecular and Optical Physics*, 3, 12 (1970), L150.

16 Cai, W. Q., Gough, T. E., Gu, X. J., Isenor, N. R., and Scoles, G. Polarizability of CO_2 Studied in Molecular-Beam Laser Stark Spectroscopy. *Physical Review A*, 36, 10 (1987), 4722–4727.

17 Graham, C., Imrie, D. A., and Raab, R. E. Measurement of the Electric Quadrupole Moment of CO_2, CO, N_2, CL_2, and BF_3. *Molecular Physics*, 93, 1 (1998), 49-56.

18 Scuseria, G. E., Miller, M. D., Jensen, F., and Geertsen, J. The Dipole Moment of Carbon Monoxide. *Journal of Chemical Physics*, 94, 10 (1991), 6660-6663.

19 Foo, K. Y. and Hameed, B. H. Insights into the Modeling of Adsorption Isotherm Systems. *Chemical Engineering Journal*, 156, 1 (2010), 2-10.

20 Newsome, D., Gunawan, S., Baron, G., Denayer, J., and Coppens, M. Adsorption of CO_2 and N_2 in Na-ZSM-5: Effects of Na+ and Al Content Studied by Grand Canonical Monte Carlo Simulations and Experiments. *Adsorption*, 20, 1 (2014), 157-171.

21 Yamazaki, T., Katoh, M., Ozawa, S., and Ogino, Y. Adsorption of CO_2 over Univalent Cation Exchanged ZSM-5 Zeolites. *Molecular Physics*, 80, 2 (1993), 313-324.

22 Gerrone, E., Fubini, B., Bonelli, B., Onida, B., and Arean, C. O. Thermodynamics of CO Adsorption on the Zeolite Na-ZSM-5: A Combined Microcalorimetric and FTIR Spectroscopic Study. *Physical Chemistry Chemical Physics*, 1, 4 (1999), 513-518.

23 Choudhary, V. R. and Mayadevi, S. Adsorption of Methane, Ethane, Ethylene, and Carbon Dioxide on High Silica Pentasil Zeolites and Zeolite-Like Materials Using Gas Chromatography Pulse Technique. *Separation Science and Technology*, 28, 1 (1993), 2197-2209.

Chapter III: Adsorbent Screening for CO_2/CO Separation

Sean M.W. Wilson, Dean A. Kennedy, F.H. Tezel,
Department of Chemical and Biological Engineering, University of Ottawa, Ottawa ON. Canada

3.1 ABSTRACT

Single gas carbon dioxide (CO_2) and carbon monoxide (CO) adsorption is investigated in detail for the potential separation of syngas. In this study, 20 zeolites, 2 activated aluminas, 3 activated carbons, and 2 silica gels were studied for pure gas isotherms of CO_2 and CO at 30^oC and compared to literature to determine which adsorbents would be the most promising for CO_2 separation from syngas. Since CO_2 concentrations vary in syngas based on the method of production, different separations from purification to bulk separation would be required.

The individual adsorption capacities of CO_2 and CO are analysed separately using a gravimetric system and then compared for all of the adsorbents studied. CO_2 is shown to be more favourably adsorbed compared to CO, with CO_2 having higher adsorption capacities and heats of adsorption. This leads to CO_2 being favourably adsorbed over CO which was seen in literature from adsorbents such as Ba-ZSM-5 [1], 5A [2], Na-X [3], and activated carbon [4].

High-density silica gel and H-Y were found to be promising adsorbents for bulk separation of CO_2 from syngas using a PSA cycle with the highest adsorption capacity ratios for CO_2 over CO. For a purification of CO_2 from syngas, Na^+ exchanged FAU structured zeolites with their strong adsorption capacity at low pressures, and activated alumina for its strong adsorption of CO_2, were found to be promising adsorbents.

Keywords: CO_2, CO, Syngas, Reverse-Water-Gas-Shift (RWGS) Reaction, Separation

3.2 INTRODUCTION

Adsorption of carbon dioxide (CO_2) and carbon monoxide (CO) have been investigated in detail separately for many applications but few studies have investigated the separation of the two from each other. Existing literature studies that investigate the adsorbent separation of CO_2 and CO determine their separation for applications that involve syngas production (also known as synthesis gas, synthetic gas or producer gas) a gas mixture primarily containing CO and H_2, but also major impurities such as CO_2 as well as some CH_4 and N_2 [3] [4] [2] [1] [5]. Although these studies address the bulk separation of CO_2 from CO, they are limited in the scope and variety of adsorbents tested.

The purpose of this study is to determine the most promising commercially available adsorbent that could be utilized to separate CO_2 from a syngas mixture of CO_2, CO, and H_2. A promising adsorbent for CO_2 separation from syngas will have to be selective towards CO_2, be easily regenerable, have a high loading capacity, as well as be inexpensive [6].

Currently, industrial syngas production relies on the conversion of fossil fuels or biomass sources by several reaction pathways. These pathways include steam reforming (SR), partial oxidation (POX), and autothermal reforming (ATR). Syngas mixture composition is heavily dependent on the method of production, with different methods using different feed stocks and reaction pathways. The variability of syngas compositions is outlined in Table 1 [7] [8] [9].

Table 1 – The gas composition of syngas after being produced using POX, SR, and ATR using different feedstock's.

		Coal to Syngas POX [7]	Indirect Wood POX [8]	Natural Gas [9] SR	Natural Gas [9] ATR
H_2	(Vol%)	25-30	15-45	70.3	62.6
CO	(Vol%)	30-60	20-45	14.1	27.2
CO_2	(Vol%)	5-15	10-25	7.6	4.7
CH_4	(Vol%)	0-5	8-17	6.3	3.3
N_2	(Vol%)	0.5-4	1-10	1.7	2.2
Other Impurities		H_2O, NH_4, H_2S, COS	C_2+, Benzene, NH_3, H_2S, H_2O	Ar	Ar

SR processes typically react a light hydrocarbon with water vapour to produce CO and H_2 at high temperatures and pressures over a catalyst (Equation 1). This syngas composition is primarily composed of H_2 as can be seen in Table 1. POX involves the incomplete combustion of a hydrocarbon with less than stoichiometric quantities of O_2 to produce a syngas mixture (Equation 2). The benefit of this reaction pathway is that a wide variety of feed stocks from simple hydrocarbons to very large complex hydrocarbons such as bitumen and biomass may be used. However, this advantage comes at the expense of complex chemistry, difficult to control CO/H_2 ratios, and undesirable side reactions. Since POX CO/H_2 ratios are dependent on the feedstock, ATR was developed to fix this by oxidizing the hydrocarbon on a catalyst. ATR catalytic oxidation works by simultaneously allowing POX and SR to occur at the same time. Regardless of the method of syngas production, the bulk production of gas requires a separation step for by-products CO_2 and H_2O, as well as undesirable products/impurities.

$$C_nH_{2n+2} + nH_2O \longleftrightarrow nCO + (2n+1)H_2 \quad [1]$$

$$C_nH_{2n+2} + {}^1/_2\, nO \longleftrightarrow nCO + (n+1)H_2 \quad [2]$$

An additional potential method of producing syngas is through the Reverse Water Gas Shift (RWGS) reaction (Equation 3). This endothermic equilibrium reaction converts CO_2 and H_2, into CO and H_2O at high temperatures over a catalyst which results in a mixture of CO_2, CO, H_2O, and H_2. This method is gaining interest with the development of carbon capture projects. Projects that utilize CO_2 instead of sequestering it in the ground essentially get reimbursed through the value of the carbon as a useful product.

$$CO_2 + H_2 \longleftrightarrow CO + H_2O \quad [3]$$

The RWGS reaction was first investigated in industry by companies such as Sumitomo Metal Industries LTD [10] and Air Products LTD [11] with current interest from the U.S. Naval Research Laboratory [12] and Audi [13] for producing jet grade petrol and diesel, respectively. The space industry has also investigated RWGS technologies and determined several solutions to improve the overall conversion inside the reactor [14].

1. Increase the molar stoichiometric ratio of H_2 over CO_2 entering the reactor to drive the reaction towards CO and to force almost complete consumption of CO_2. The leftover reactants would then be separated and recycled back into the reactor.
2. Overload the reactor with CO_2 to drive the reaction towards CO and have almost complete consumption of H_2. This would also require the separation and recycle of reactants back into the reactor.
3. Using a desiccant to remove water as soon as it is produced in the reactor to drive the equilibrium reaction towards CO.

These methods or a combination of two of them, would improve the overall reactor conversion efficiencies. However, for syngas production, choosing to use stoichiometric excesses of H_2 would produce a product gas mixture that would require less CO_2 to be removed while also producing a mixture of H_2 and CO as the desired final components.

For the majority of industrial processes that require syngas, the presence of CO_2 is not desired and its removal is required. This separation of CO_2 from CO and H_2 in industry involves applications in syngas production, which currently utilizes multiple separation methods including absorption, adsorption, cryogenic distillation, and membranes. For instance, Air Liquide POX of coal produces a syngas mixture that first goes through an absorption column to remove the majority of CO_2 and any additional acid gases, with an adsorption column to purify the syngas of any remaining CO_2 [15].

Separation using only adsorption for syngas can have many benefits compared to absorption and cryogenic distillation. Both cryogenic distillation and solvent absorption processes such as the Rectisol process require large amounts of cooling and compression which is highly energy intensive. An adsorption process however, only requires moderate temperatures and pressures in comparison.

This study examines pure gas adsorption isotherms for CO_2 and CO adsorption for 27 different commercially available adsorbents and compares them to results from literature to identify promising adsorbents for this separation. Since hydrogen adsorption is insignificant when compared to CO_2 and CO, it will not be the focus

of this article [4] [1]. This article will cover commercially available adsorbents including activated aluminas, activated carbons, silica gels, and zeolites.

3.3 MATERIALS & METHODS

3.3.1 Materials

High purity CO_2 and CO gases were obtained from Linde Canada Ltd at purities of 99.99% and 99.7% respectively. The adsorbents that were tested included activated aluminas, activated carbons, and silica gels as well as a large selection of zeolites. The details of these adsorbents are given in Table 2 and Table 3.

Table 2 – Zeolite samples with their respective manufacturer, trademark name, structure and cation. N/A are parameters not provided by the company.

Manufacturer	Name	Structure	Ion	SiO_2/Al_2O_3	Pellet/Powder
CECA Arkema Group	Nitroxy 5	FAU	Na	<4	Pellet (20×30)
CECA Arkema Group	Nitroxy SXSDM	FAU	Li	<4	Pellet (20×30)
CECA Arkema Group	Na-LSX	FAU	Na	2	Pellet (12×18)
Honeywell UOP	APG-III	FAU	Na	<4	Pellet (6×8)
Honeywell UOP	Na-Y	FAU	Na	N/A	Pellet (8×12)
Zeochem	Ca-X	FAU	Ca	<4	Pellet (8×12)
Zeolyst International	H-Y	FAU	H	30	Powder
Zeolyst International	H-Y	FAU	H	50	Powder
Zeolyst International	H-Y	FAU	H	80	Powder
Honeywell UOP	HiSiv3000	MFI	Na	>1000	Pellet (6×8)
Zeolyst International	ZSM-5	MFI	NH_4	30	Powder
Zeolyst International	ZSM-5	MFI	NH_4	50	Powder
Zeolyst International	ZSM-5	MFI	NH_4	280	Powder
Union Carbide	4A	LTA	Na	2	Pellet (10×16)
Union Carbide	5A	LTA	Ca	2	Pellet (6×8)
Zeolyst International	H-β	BEA	H	300	Powder
	SAPO-5	AFI	-	N/A	Powder
	SAPO-11	AEL	-	N/A	Powder
GSA Resources	Casorb-Na	CHA	Na	N/A	Pellet (20×60)
The PQ Corporation	Zeolon 900H	MOR	H	N/A	Pellet (20×60)

Table 3 - Activated alumina, activated carbon, and silica gel samples with their respective manufacture and trademark name.

Manufacturer	Name	Pellet/Powder
Alcan	AA-300	Pellet (8×14)
Selecto Scientific	Super I Alumina A	Pellet (100×230)
Calgon Carbon	BPL	Pellet (4×10)
Calgon Carbon	Xtrusorb A754	Pellet (4×10)
Calgon Carbon	Xtrusorb HP115	Pellet (4×10)
Selecto Scientific	Silica Gel	Pellet (70×230)
Strem Chemicals	Silica Gel	Pellet (63×200)

3.3.2 Methods

Pure gas adsorption isotherms were taken using a gravimetric analysis done by a VTI Scientific Instruments GHP. The pure isotherms were performed on the gravimetric analyzer by regenerating the samples at 300^{O}C temperatures (360^{O}C for activated aluminas) under vacuum pressure of approximately 10^{-8} atm. The samples were then evaluated at increasing pressures of up to 10 atm. Desorption experiments were then performed briefly by decreasing the pressure to determine hysteresis. Buoyancy correction was performed using helium at similar pressure and temperatures. Isotherms were conducted at temperatures of 30^{o}C for both CO and CO_2 for the adsorbents.

The experimental adsorption data was then fit to Langmuir, Freundlich, Sips, and Toth model equations using the sum of least squares method. The isotherm model with the highest coefficient of determination (R^2) was used to reflect the isotherm. The equations for these models are presented in Table 4. ΔH_{ads} for this study were acquired from literature.

Table 4 - Langmuir, Freundlich, Sips, and Toth adsorption isotherm models

Langmuir Model	Freundlich Model	Sips Model	Toth Model
$\frac{q_e}{q_s} = \frac{\beta P}{1+\beta P}$	$q_e = k\,P^{\,1/n}$	$\frac{q_e}{q_s} = \frac{(\beta P)^n}{1+(\beta P)^n}$	$\frac{q_e}{q_s} = \frac{\beta P}{(1+(\beta P)^t)^{1/t}}$

3.4 RESULTS & DISCUSSION

A promising adsorbent for CO_2 separation from syngas will be selective towards its desired component, be easily regenerable, have a high loading capacity, as well as be inexpensive. Kinetics is generally secondary in importance [6]. In this study, 20 zeolites, 2 activated aluminas, 3 activated carbons, and 2 silica gels pure gas isotherms were analysed for CO_2 and CO adsorption at 30^{O}C to determine which adsorbents would be the most promising. Each of these adsorbents tested at 30^{O}C follow a Type I from Braunaur classification for isotherms which is also known as a favourable isotherm. Since the concentration of CO_2 in syngas can vary from requiring bulk separation to purification, adsorbents with isotherms that are rectangular are more suited for vacuum pressure swing adsorption (VPSA) for purification, and more linear isotherms are more suited for pressure swing adsorption (PSA) for bulk separation.

3.4.1 Activated Alumina

Composed of crystalline Al_2O_3, activated alumina is a hydrophilic amorphous adsorbent that is commonly used in industry as a desiccant. Activated alumina can be acidic, basic, or neutral due to tuneable Lewis and Brønsted acid sites present in the alumina during synthesis. To test the performance of activated alumina for the syngas separation, experimental adsorption isotherms were performed on two samples at 30^{O}C; AA-300 from Alcan (Currently Axens), and Super I Alumina A from Selecto Scientific which can be seen in Figure 1.

The magnitude in difference for CO_2 adsorption capacity over CO adsorption capacity is significant for activated alumina samples tested and concurs with existing literature [16] [17] [18]. For CO_2, adsorption capacity was observed to be 20 times higher than CO for pressures below 0.5atm and levelling out to 6 times higher than CO for higher pressures for AA-300 sample. Alumina A has approximately 5 times the capacity for CO_2 than CO for all pressures. This difference in adsorption capacity concurs with literature with CO_2 adsorption capacity over 15 times that at low pressures for γ-alumina samples [16]. Heats of adsorption reported in literature can be seen in Table 5 and shows a large variation with CO_2 heats of adsorption ranging from slightly larger to significantly larger than CO heats of adsorption. This deviation can occur from the preparation of diaspore during the synthesis step of producing α-alumina, by either grounding up the

diaspore or preparing it with ungrounded diaspore. With grounded samples heat of adsorption for CO_2 and CO being similar, and ungrounded samples heats of adsorption having a large difference [17]. This study confirms with literature that pure CO_2 adsorption capacity is greater than pure CO adsorption capacity, which is indicative of preferential CO_2 adsorption in competitive CO_2/CO systems.

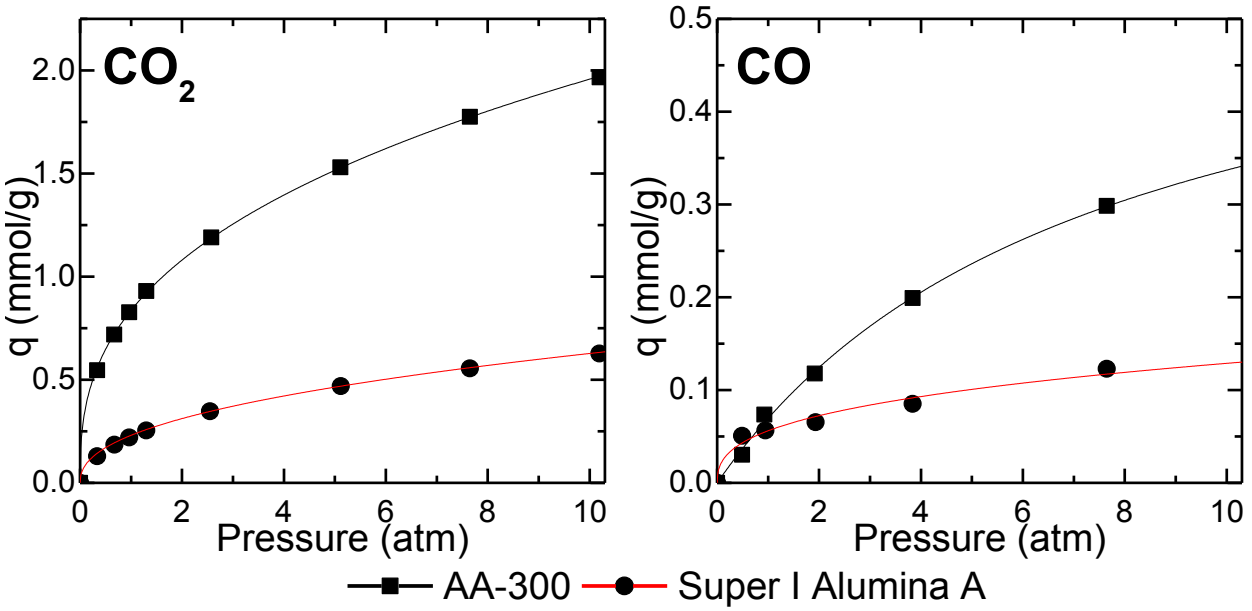

Figure 1 – CO_2 and CO pure adsorption isotherms at 30°C for AA-300 from Alcan and Super I Alumina A from Selecto Scientific.

Table 5 - Heat of adsorption at zero loading for CO_2 and CO adsorption on different alumina samples from literature

Alumina Sample	$-\Delta H_{ads}$ (kJ/mol)		Source
	CO_2	CO	
γ-Al_2O_3	130/50	64	[16]
Grounded α-Al_2O_3	67	64.5	[17]
Ungrounded α-Al_2O_3	89.6	25.5	[17]

The loading of CO_2 and CO on activated alumina varies significantly between AA-300 sample and the Super I Alumina A samples. AA-300 had a higher adsorption capacity for both CO_2 and CO compared to Super I Alumina A above ambient pressures. This difference in adsorption capacity is due to the surface area and acidity of the samples. The surface area of AA-300 (350-380 m^2/g [19]) is greater than Super I Alumina A (200 m^2/g) and where AA-300 is considered neutral, the pH of Super I Alumina A is 4.5. Due to CO_2 being an acid

gas [20], the higher the basicity of the activated alumina, the more CO_2 it can adsorb, which has also been observed in zeolites [21]. This effect of acidity also effects adsorption of CO with the magnitude of adsorption being greater for the more acidic Super I Alumina A than the AA-300 at pressures below ambient pressures.

AA-300 and Super I Alumina A samples have noticeable hysteresis upon degassing for CO_2 adsorption but only AA-300 had significant hysteresis for CO adsorption. The CO_2 hysteresis can be explained due to chemisorption of CO_2 that has been seen in literature, with chemisorption happening due to the formation of bicarbonates, bidentate and monodentate carbonate, and bridging carbonate groups with the metal oxides that are present on the surface of the adsorbent [17]. CO hysteresis however, is not as common on activated alumina with studies reporting only reversible adsorption [17] and other studies reporting small amounts of irreversible adsorption [16]. This difference between reversible and irreversible adsorption is due to the type of bond that forms on the activated alumina with the CO adsorbate; with a weak surface carbonyl bond being reversible and the chemical formation of a formate bond being irreversible [16]. AA-300 has a combination of these two types of bonding sites with the majority of the sites being reversible. Super I Alumina A only has one noticeable site for CO adsorption which is completely reversible. This hysteresis upon degassing with literature reporting irreversible adsorption shows that a more energy intensive desorption cycle, such as a combination temperature and pressure swing adsorption, would be required to fully regenerate an activated alumina sample.

Activated alumina, particularly AA-300, with its high adsorption capacity for CO_2 compared to CO makes it a desirable candidate for CO_2 syngas separation. However, the adsorption capacity of activated aluminas is small compared to faujasite structured zeolites, and due to the high heat of adsorption along with chemisorption of CO_2, regeneration could be cumbersome. If AA-300 was used for this separation with the shape of the isotherm having a sharp Henry's law region and continuously increasing capacity as pressure increases, a VPSA cycle or PSA cycle could be utilized in order to separate the CO_2 from the syngas.

3.4.2 Activated Carbon

Primarily composed of carbon, activated carbon is a hydrophobic adsorbent that can have amorphous or structured pores (such as carbon molecular sieves), with large micropore and mesopore volumes, and large surface areas, which are good for adsorption and make it attractive for a CO_2/CO separation. Activated carbons' most interesting parameter as an adsorbent is its wide ability to change its adsorption behaviour due to the raw starting carbonaceous material, low-temperature carbonization, and its activation manufacturing steps. For instance, the degree of activated carbons hydrophobicity is dependent on its ash content, level of surface oxidation, and other molecular species on the surface.

Activated carbons are the most industrially used adsorbents [20] and many studies looked into CO_2 andCO adsorption behaviour for a wide variety of different types of activated carbon [4] [2] [22] [23] [24] [25] [26] [27]. In this present study, three activated carbons; BPL, Xtrusorb A754, and Xtrusorb HP115, were acquired from Calgon Carbon to test their performance for pure adsorption isotherms of CO_2 and CO at 30^0C. These isotherms are given in Figure 2. The adsorption capacity was found to be the largest for Xtrusorb A754 for both CO_2 and CO adsorption, with BPL and Xtrusorb HP115 having similar adsorption capacities. The CO_2 adsorption capacity of all three activated carbon samples was observed to be greater than CO, which confirms the results from literature for similar activated carbons [4] [23] [26] [22] [24]. This difference in adsorption capacity is greater than 5 times at pressures above 1 atm and plateaus to 3 times at 10 atm for all activated carbon samples in this work. The adsorption capacity of CO_2 and CO on activated carbons in literature however, can vary greatly with different samples. This difference in adsorption capacity can be attributed to differences in surface areas, with the ash content and level of surface oxidation as lesser influences on the capacity.

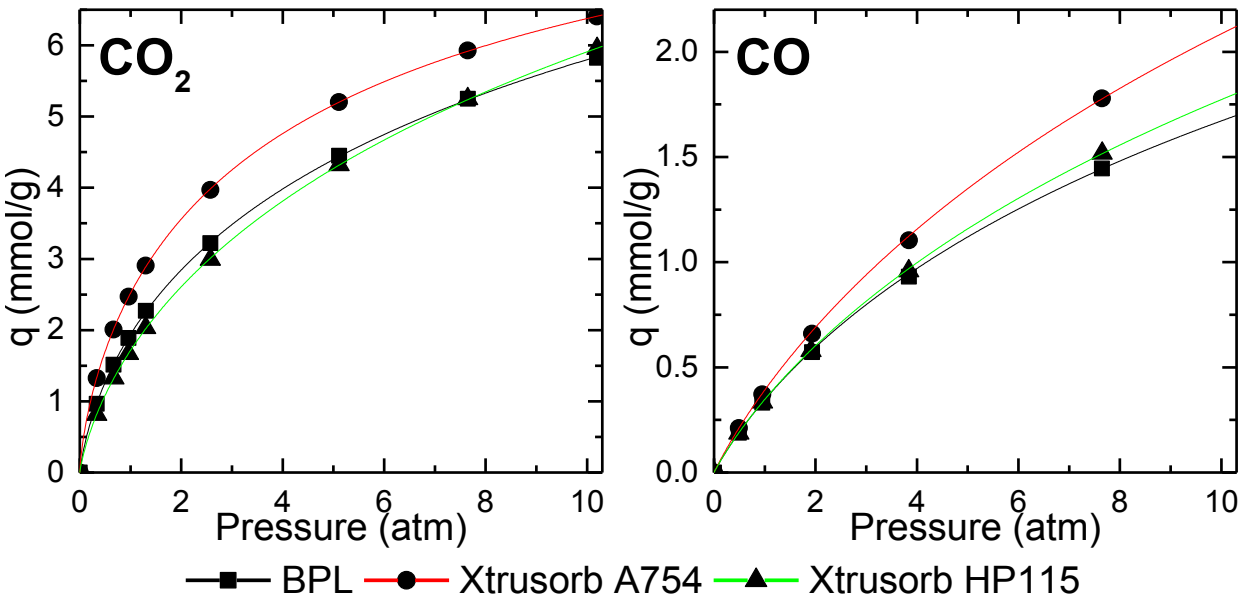

Figure 2 - CO_2 and CO pure adsorption isotherms at 30°C for BPL, Xtrusorb HP115, and Xtrusorb A754 from Calgon Carbon.

The adsorption of CO_2 is also stronger than that of CO is presented in Table 6 with limiting heats of adsorption of different activated carbon samples from literature. The average limiting heats of adsorption is approximately 29 kJ/mol for CO_2 and 18 kJ/mol for CO. However, there is deviation with the CO_2 heat of adsorption, with coal derived activated carbon being noticeably higher compared to other samples [24]. With CO_2 having higher adsorption capacities and heats of adsorption, CO_2 is favourably adsorbed compared to CO. This concurs with literature with multicomponent breakthrough data showing adsorption of CO_2 is more favourable than CO, with CO first breaking through the column and then being displaced by CO_2 for adsorption sites and exiting above feed conditions [22].

Table 6 - Heat of adsorption at zero loading for CO_2 and CO adsorption on different activated carbon samples from literature.

Activated Carbon Sample	$-\Delta H_{ads}$ (kJ/mol)		Source
	CO_2	CO	
Supelio Activated Carbon	28.1	17.6	[23]
Air Products CMS A	28.4	19.9	[25]
Coal Derived Activated Carbon	35	18	[24]
Degussa F30-470 Activated Carbon	25	17	[2]
Activated Carbon	27.9	19.1	[4]

Activated carbons being relatively inexpensive compared to other adsorbents, are always investigated for separations. For a CO_2 syngas separation, as long as the pressure swing is large enough, activated carbons will have the largest CO_2 loading of all the adsorbents, and are easy to regenerate with no hysteresis and low heat of adsorption making them ideal for a bulk separation using PSA, which concurs with literature [22]. However, compared to other adsorbents tested, the affinity for CO_2 over CO is significantly less which would lead to poorer recoveries and purities in turn.

3.4.3 Silica Gel

Composed of silicon dioxide, silica gel is a hydrophilic amorphous adsorbent commonly used in industry as a desiccant due to its large capacity for water. The pores of silica gel vary in size but the majority of the surface area comes from mesopores larger than 20 Å. Two common forms of silica gels can be proposed for the separation of a syngas mixture of CO_2/CO; high-density silica gel, and low density silica gel. High-density silica gels have an average pore diameter between 22-26 Å with surface areas between 750-850 m^2/g and low-density silica gels have an average pore diameter between 100-150 Å with surface areas between 300-350 m^2/g [20]. Since adsorption is a surface phenomenon, only high-density silica gel will be investigated.

To determine the performance of silica gel for a syngas mixture, two high density silica gel samples (one from Selecto Scientific, and another from Strem Chemicals) were investigated. The CO_2 and CO adsorption isotherms were determined at 30°C and are presented in Figure 3. Both silica gel samples have significantly larger capacities for CO_2 than for CO. This difference in adsorption capacities are greater than 14 times at pressures below 1 atm and slowly decreases to 6 times at pressures of 10 atm for both samples. The adsorption capacity for Strem Chemicals silica gel is larger than that of the sample from Selecto Scientific for both CO_2 and CO adsorption. This difference in adsorption capacity is due to the higher surface area of Strem Chemicals (SA ≈ 835 m^2/g) silica compared to Selecto Scientifics (SA ≈ 550 m^2/g). Since the surface area of the silica gel sample from Strem Chemicals is in the upper range of high-density silica gel, surface modification can be performed to increase the adsorption capacity. Previous literature studies have investigated the effect of the addition of nitrogen containing compounds to the surface of silica gel which

increase the adsorption capacity of CO_2. However, these studies did not look into the effect of carbon monoxide [28].

This significantly greater adsorption of CO_2 was found to also be competitive, with preferential adsorption of CO_2 in binary mixtures on silica gel at temperatures of 0^oC and 100^oC for pressures up to 1 atm [29]. In literature, gas chromatography columns filled with silica gel is commonly used to separate CO_2 from CO, with CO_2 having a significantly stronger interaction with silica gel when compared to CO [30].

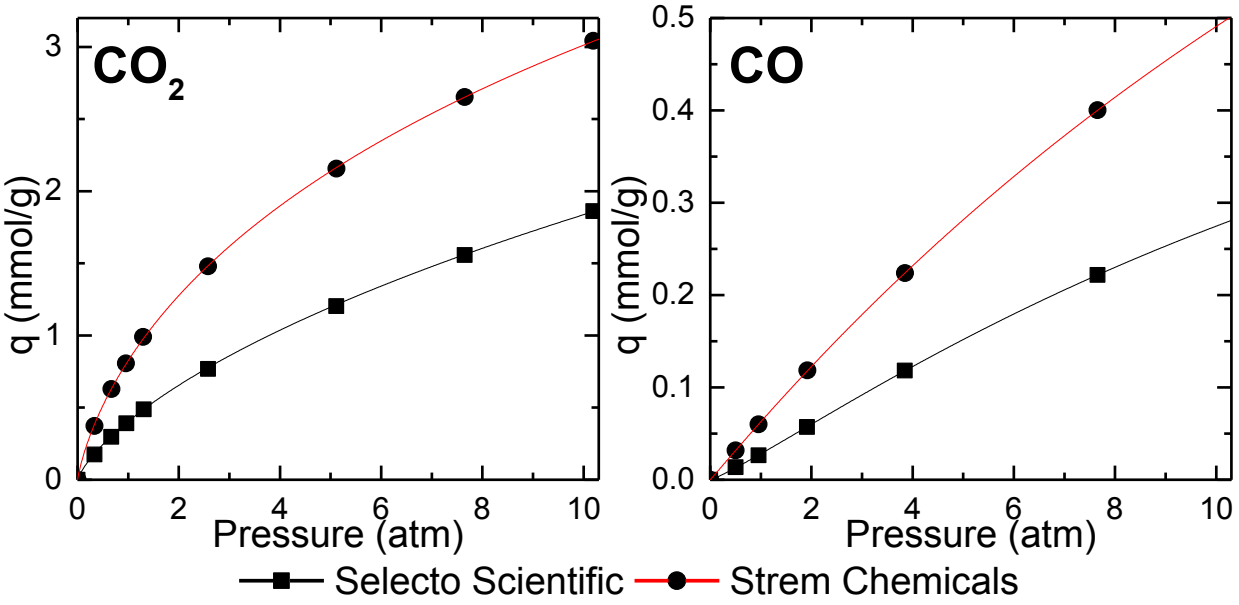

Figure 3 - CO_2 and CO pure adsorption isotherms at 30^oC for silica gel from Selecto Scientific and Strem Chemicals.

The regenerability of silica gel has yet to be investigated in literature but with this study, no hysteresis upon degassing was found for either CO_2 and CO adsorption indicating only physical adsorption was present.

For the syngas separation of CO_2 from a syngas mixture, high density silica gel is one of the best candidates with adsorption significantly favouring CO_2 over CO, no evidence of any regeneration problems, and the low cost of silica gel compared to other adsorbents. This concurs with industry with companies such as BASF marketing Sorbead LE-32, a type of silica gel, for a CO_2/CO separation. The adsorption process that would best utilize silica gel would be a PSA system which would operate over a wide range of pressures due to the linearity of the isotherm.

3.4.4 Zeolites

Composed of crystalline aluminum oxide and silicon oxide, zeolite adsorbents are calcinated in order to remove their waters of hydration. This leaves well defined pores and cage structure that is balanced out with cations to produce an adsorbent with a high surface area that makes them prospective adsorbents for syngas separation of CO_2 from CO. Zeolites are commonly referred to as molecular sieves due to their defined pore size. For this particular separation, CO_2 (3.3 Å) and CO (3.7 Å) pore size are so similar that molecular sieving is unlikely. Zeolites in industry are used for gas and liquid separations due to their robustness, durability, regenerability, and tuneability. Zeolites can be tuned by changing the structure (with over 225 structures recognized by the International Zeolite Association), augmenting their SiO_2/Al_2O_3 ratios, and changing their counter balancing cation. Changing these three parameters can have a very large impact on the overall adsorption potential.

To determine the feasibility of zeolites for a syngas CO_2 separation, 20 different zeolites pure gas adsorption isotherms were analyzed to determine their performance at 30^oC. This includes commonly used zeolites in industry including faujasite (FAU), Linde Type A (LTA), pentasil (MFI), mordenite (MOR), and chabazite (CHA), along with less commonly used zeolites including beta polymorph A (BEA), SAPO-5 (AFI), and SAPO-11 (AEL).

FAU structured zeolites are one of the most common zeolites in industry. Due to their large 7.4 Å pores and their 3 dimensional channel system, FAU structure zeolites have some of the highest adsorption capacities compared to other zeolites. 13X has received considerable interest in particular for greenhouse gas separation of CO_2 from other post combustion gases. In this study, 9 different FAU zeolites were analysed for CO_2 and CO pure adsorption isotherms at 30^oC including; APG-III, a type of 13X and Na-Y from Honeywell UOP; Ca-X from Zeochem; H-Y with three different SiO_2/Al_2O_3 ratios (denoted in the brackets as 5.1, 30, and 80) from Zeolyst International; Na-LSX from CECA Arkema Group; and Nitroxy 5 and Nitroxy SXSDM, a FAU with sodium and lithium cations, respectively, from CECA Arkema Group. Figure 4 shows CO_2 and CO isotherms for a variety of FAU zeolites at 30^oC and Figure 5 shows the effect of SiO_2/Al_2O_3 ratio on H-Y.

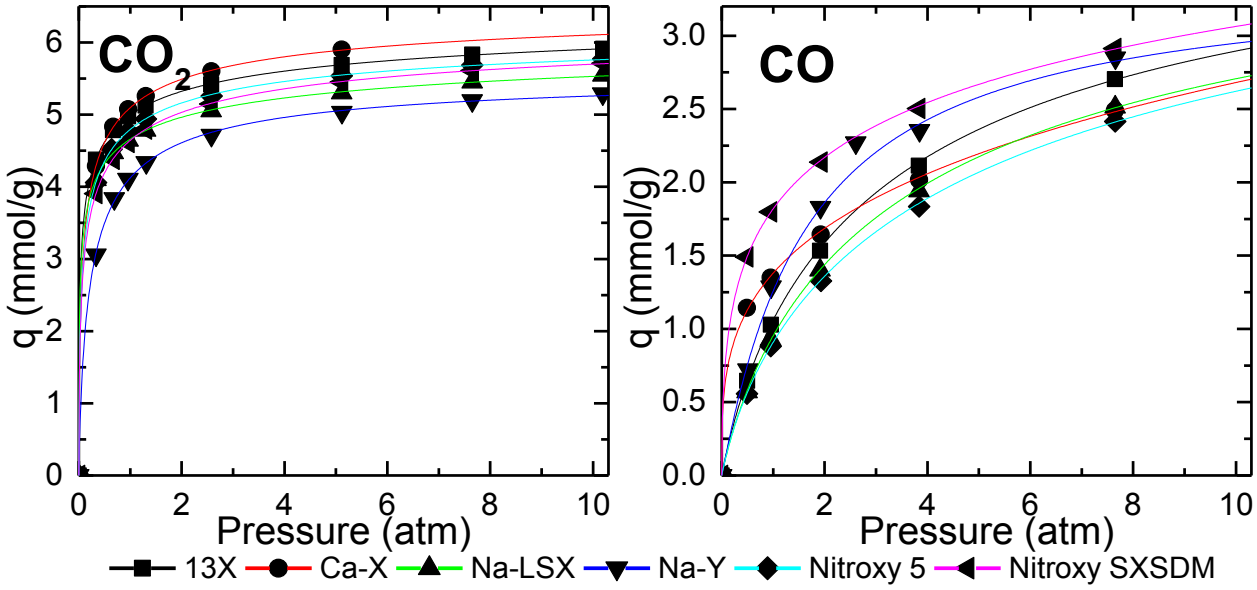

Figure 4 - CO_2 and CO pure adsorption isotherms at 30°C for faujasite structured zeolites including APG-III from Honeywell UOP, Ca-X from Zeochem, Na-LSX from CECA Arkema Group, Na-Y from Honeywell UOP, and Nitroxy 5 and Nitroxy SXSDM from CECA Arkema Group.

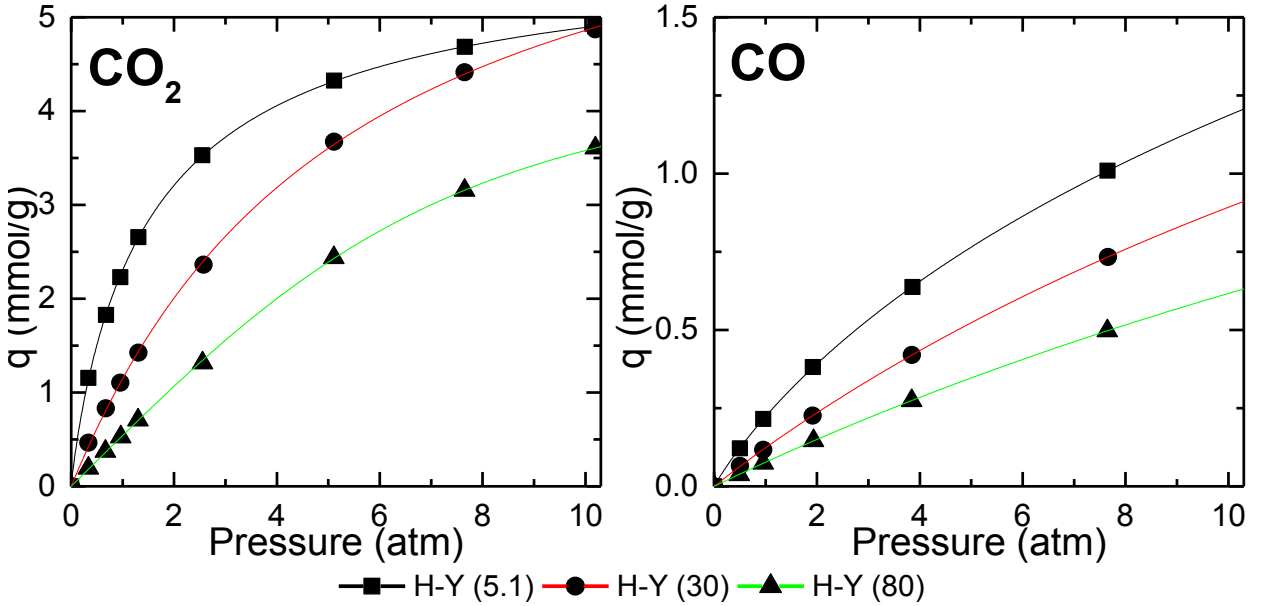

Figure 5 - CO_2 and CO pure adsorption isotherms at 30°C for H-Y (5.1), H-Y (30), and H-Y (80) from Zeolyst International.

The adsorption of CO_2 and CO is both heavily influenced by the type and amount of cations present in the zeolite. This is apparent for FAU zeolites with the capacities of both CO_2 and CO varying depending on the type and amount of cation present in the zeolite. For CO_2 adsorption, in literature it was found that the CO_2 adsorption strength increases in the order $H^+<Li^+<Na^+<K^+<Rb^+<Cs^+$ cations due to the increase in strength of their basic sites [21]. This effect was also observed with the slope of the isotherm in the Henry's law region which can be seen in Table 7. This shows two things, that as more cations are present in zeolites with lower SiO_2/Al_2O_3 ratios, the CO_2 isotherms are sharper in the Henry's Law region which can be seen in the H-Y samples. This agrees with literature with SiO_2/Al_2O_3 ratios in Na-ZSM-5 where CO_2 adsorption increased due to the increase of the counter balancing cations present in the structure [31]. Secondly, it confirms that adsorption strength follows the order of $Na^+>Li^+>H^+$ for zeolites with similar SiO_2/Al_2O_3 ratios which was seen in the literature [21]. It was also found that Ca-X had similar Henry's Law constants to that of Na-X further extending the trend to $Na^+\approx Ca^+>Li^+>H^+$.

Table 7 – Henry law constants at zero loading calculated using the Langmuir model for faujasite structured zeolites.

	Henry Law Constant	
	CO_2 (mmol g^{-1} atm^{-1})	CO (mmol g^{-1} atm^{-1})
13X	43.8	1.48
Ca-X	42.5	3.09
Na-LSX	41.7	1.30
Na-Y	19.9	1.97
Nitroxy 5	35.8	1.21
Nitroxy SXSDM	31.4	5.03
H-Y (5.1)	3.96	0.24
H-Y (30)	1.36	0.13
H-Y (80)	0.60	0.08

For CO adsorption, strength increases with the presence of more ions. This can be seen in the H-Y samples where the Henry's Law constant decreases from 0.24 mmol g^{-1} atm^{-1} to 0.13 mmol g^{-1} atm^{-1} to 0.08 mmol g^{-1} atm^{-1} as the SiO_2/Al_2O_3 ratios increase from 5.1 to 30 to 80, respectively. With the cation present however, studies have found that ions that effect π-bonding increases CO adsorption capacity with adsorption of Li^+ exchanged Na-X increasing with increasing Li^+ ions amount compared to Na^+ [32]. This is also seen in this work with adsorption being strongest in the Henrys Law region for Li^+ cations exchanged Nitroxy SXSDM. The Ca^+

cation was also found to have a stronger interaction when compared to Na^+ and H^+ for CO adsorption. This was also found in literature with Ca^+ chabazite having a uniquely strong interaction with CO [33].

The heat of adsorption for zeolites can be seen in Table 8 with the heats of adsorption on zeolites being greater for CO_2 than CO. The heat of adsorption was found to be the highest for Li-LSX for both CO_2 and CO adsorption. The data also shows that CO_2 adsorption increases with decreasing SiO_2/Al_2O_3 ratios which can be seen in the H-Y samples decreasing from 33.1 kJ/mol to 25.3 kJ/mol at SiO_2/Al_2O_3 ratios of 5.1 and 80, respectively. This trend is also apparent with Na-Y samples decreasing from 36.1 kJ/mol to 34.9 kJ/mol at SiO_2/Al_2O_3 ratios of 5.1 and 20, respectively. This trend of increasing heats of adsorption with decreasing SiO_2/Al_2O_3 ratio in the zeolite is also noted for other structured zeolites such as MFI structured zeolites which also show that zeolites that contain almost no cations having the lowest heats of adsorption [34]. For the cation present in zeolites, Na^+ zeolites have higher CO_2 heats of adsorption compared to H^+ cations which agrees with D. Barthomeuf [21] data. However, D. Barthomeuf data contradicts Y. Park et al [24], with CO_2 heats of adsorption being significantly higher than other Na^+ FAU zeolites. For CO heat of adsorption, Li^+ cation zeolites have the strongest adsorption with Na^+, and Ca^+ in decreasing order capacity.

CO_2/CO breakthrough data has been investigated with CO_2 on Na-X adsorbing and displacing CO inside the column; effectively separating the gases [3]. This present study shows that CO_2 is preferentially adsorbed over CO, and that there is effective separation. However previous studies do not mention the selection of the cations or the SiO_2/Al_2O_3 ratio within the zeolite used for the separation.

Table 8 - Heat of adsorption at zero loading for CO_2 and CO for different zeolite samples from literature. The contents within the brackets next to the zeolite name indicates the SiO_2/Al_2O_3 ratio if indicated by the source.

Zeolite Sample	Structure	$-\Delta H_{ads}$ (kJ/mol)		Source
		CO_2	CO	
H-Y (5.1)	FAU	33.1	-	[35]
H-Y (30)	FAU	23.7	-	[35]
H-Y (80)	FAU	25.3	-	[35]
Zeochem Z10-05-03 ~ Li-LSX	FAU	69	43	[24]
LiNa-X	FAU	-	37.7	[32]
Na-X	FAU	31	20	[3]
Na-X	FAU	-	28.9	[32]
13X	FAU	42.5	-	[35]
Na-Y (5.1)	FAU	36.1	-	[35]
Na-Y (10)	FAU	35.9	-	[35]
Na-Y (20)	FAU	34.9	-	[35]
Bayer KEL200 ~ 5A	LTA	64	35	[2]
5A	LTA	-	32.7	[23]
5A	LTA	47.1	-	[35]
4A	LTA	-	27.6	[23]
H-ZSM-5 (30)	MFI	34.6	-	[35]
H-ZSM-5 (50)	MFI	33.1	-	[35]
H-ZSM-5 (80)	MFI	32.6	-	[35]
H-ZSM-5 (280)	MFI	32.3	-	[35]
Silicalite	MFI	33.4	-	[35]
Silicalite	MFI	24.1	16.7	[36]
Clinoptilolite	HEU	-	48.6	[23]
H-Mordenite	MOR	-	23.5	[23]

The effect of different cations is presented in Figure 6 with adsorption capacity ratios of CO_2 over CO changing between the seven FAU type zeolites studied in this work. Na-LSX, APG-III, and Nitroxy 5 are all low SiO_2/Al_2O_3 ratio FAU zeolites with Na^+ cations, which have the high adsorption for CO_2 and the least adsorption for CO at vacuum pressures. This difference in adsorption capacity between CO_2 over 20 times that of CO when the pressure is close to vacuum. However as there becomes less Na^+ cations present, as with Na-X to Na-Y, this adsorption capacity ratio decreases significantly. This indicates that Na^+ cations benefit CO_2 adsorption more than the CO adsorption. Even though Ca-X had the highest adsorption capacity for CO_2, the presence of the Ca^{2+} was also significantly beneficial to CO adsorption, making the difference in adsorption capacity between negligible. However, the Li^+ cation that is present in Nitroxy SXSDM has the lowest adsorption capacity ratio. This low adsorption capacity ratio is due to the Li^+ cation increasing π-bonding and therefore adsorption of CO in the zeolite while not being very beneficial for CO_2 adsorption. The best cation is

H^+ for a bulk CO_2/CO separation, with the adsorption capacity for CO_2 being significantly higher than that of CO for pressures within the PSA range when compared to the other cations of FAU structure.

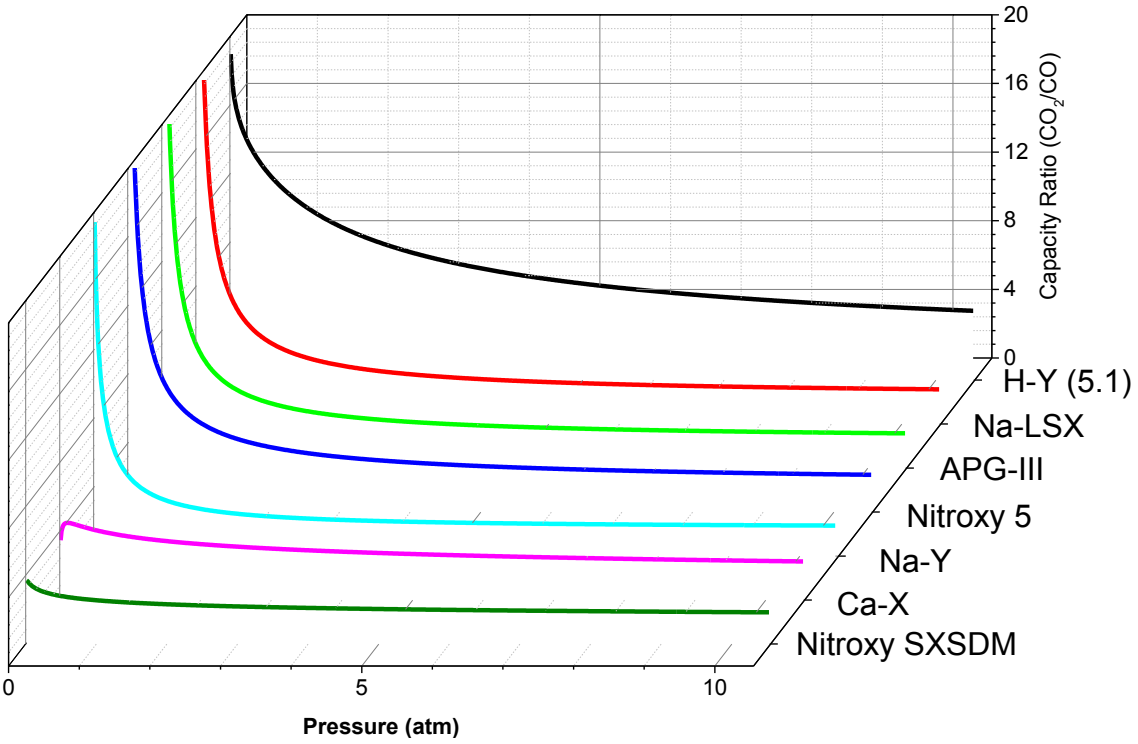

Figure 6 - Adsorption capacity ratios of faujasite structured zeolites including APG-III, Ca-X, Na-LSX, Na-Y, Nitroxy 5, and Nitroxy SXSDM at 30°C.

The effects of SiO_2/Al_2O_3 ratios obtained in this study are presented in Figure 7 with the H-Y samples with SiO_2/Al_2O_3 ratios of 5.1, 30, and 80, respectively. As the SiO_2/Al_2O_3 ratios decrease in H-Y, there is an increase in the adsorption capacity for both CO_2 and CO in Figure 5. However, the CO_2/CO capacity ratio is favourable in the VPSA range for H-Y samples of low SiO_2/Al_2O_3 ratios, and is favourable in the PSA range for H-Y samples of high SiO_2/Al_2O_3 ratio at high pressures.

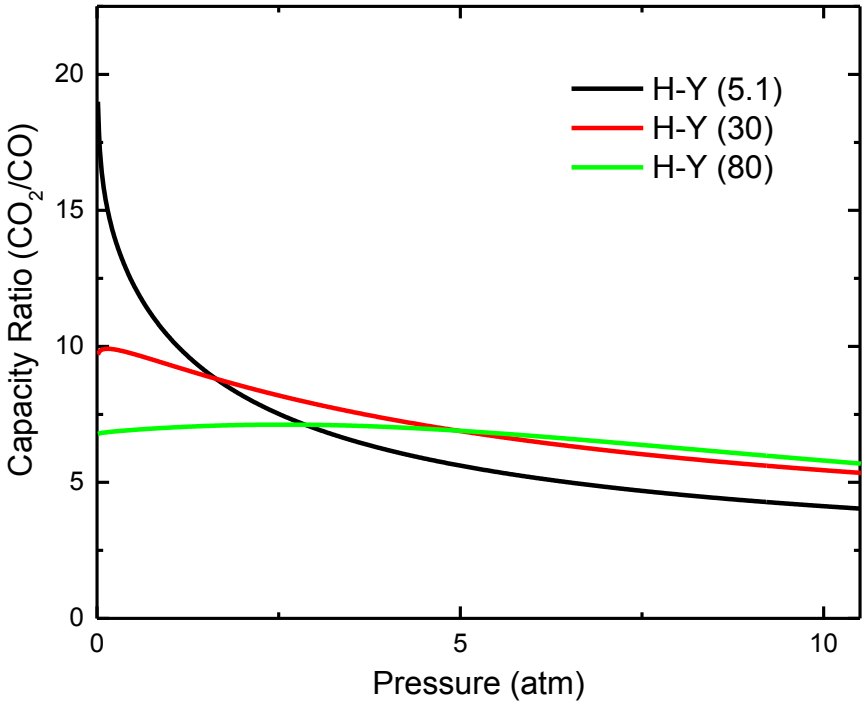

Figure 7 - Adsorption capacity ratios of CO_2 over CO of faujasite structured zeolites including H-Y (5.1), H-Y (30), and H-Y (80) at 30^{O}C.

Other common industrial zeolites present are LTA structured zeolites which have tunable pore sizes according to the presence of different cations. The pores with 3A containing K^+ cations, 4A containing Na^+ cations, and 5A containing Ca^{2+} cations have pore sizes of approximately 3 Å, 3.8 Å, and 4.4 Å, respectively [6]. In this study, 2 different LTA structured zeolites pure gas adsorption isotherms were analysed to determine their performance for a syngas separation of CO_2 including 4A and 5A procured from Union Carbide (currently known as the Dow Chemical Company). The pure gas adsorption isotherms for CO_2 and CO at 30^{O}C can are presented in Figure 8.

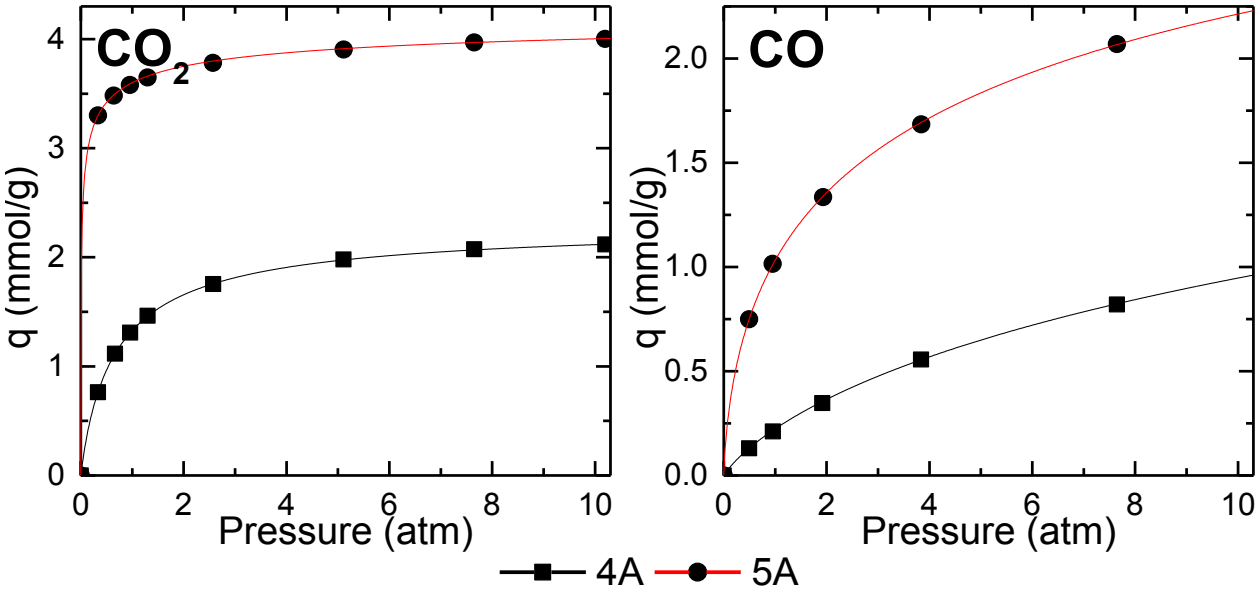

Figure 8 - CO_2 and CO pure adsorption isotherms at 30°C for LTA structure zeolites including 4A and 5A from Union Carbide.

The adsorption capacity of CO_2 and CO differs between 4A and 5A, with 5A having a higher adsorption capacity for both CO_2 and CO. This is due to the amount of cations present within the zeolite, and their location within the LTA structure. Ca^{2+} compared to Na^{+}, requires half as many cations to balance out the negative charge within the zeolite. This difference in amount of cations has found that Ca^{2+} cations occupy only type I sites in the zeolite which do not interfere with the aperture into the cage of the zeolite. However, Na^{+} cations occupy type I, type II, and type III sites within the LTA structure, with type II and type III sites restricting the aperture [6]. Due to the strong adsorption of CO_2 on Na^{+}, type II and type III sites cause pore plugging into the rest of the 4A zeolite. This pore plugging therefor causes an overall decrease in the adsorption capacity of 4A with respects to 5A.

The binary adsorption of CO_2 over CO has been investigated on 5A with CO_2 adsorbing competitively onto the zeolite [2]. This adsorption is noticeable at even low CO_2 partial pressures where CO_2 adsorption is still significant. This is expected with CO_2 adsorption capacity being significantly larger than CO at low pressures as well as CO_2 having higher heats of adsorption than CO.

LTA zeolties have lesser adsorption capacities compared to FAU zeolites, but 5A with its CO_2 adsorption capacities being significantly larger than that of CO at low pressures as well as having higher heats of adsorption when compared to Na^+ FAU zeolites could be more suited to VPSA for purification separation. 3A zeolite was initially considered for this separation; however, due to the small pore size of 3 Å, adsorption of CO_2 and CO took a distended period of time with CO_2 data points equilibrating over several days and CO showing no significant adsorption. This shows that 3A is able to molecularly sieve CO_2 but has poor kinetics.

MFI structure zeolites are commonly used in industry with channel like pores of around 6 Å in size. In this study, 4 different MFI structured zeolites CO_2 and CO pure gas adsorption isotherms were analysed to determine their performance for a CO_2 syngas separation. This can be seen in Figure 9 with three different SiO_2/Al_2O_3 ratio ZSM-5 samples from Zeolyst International and Silicalite from Honeywell UOP.

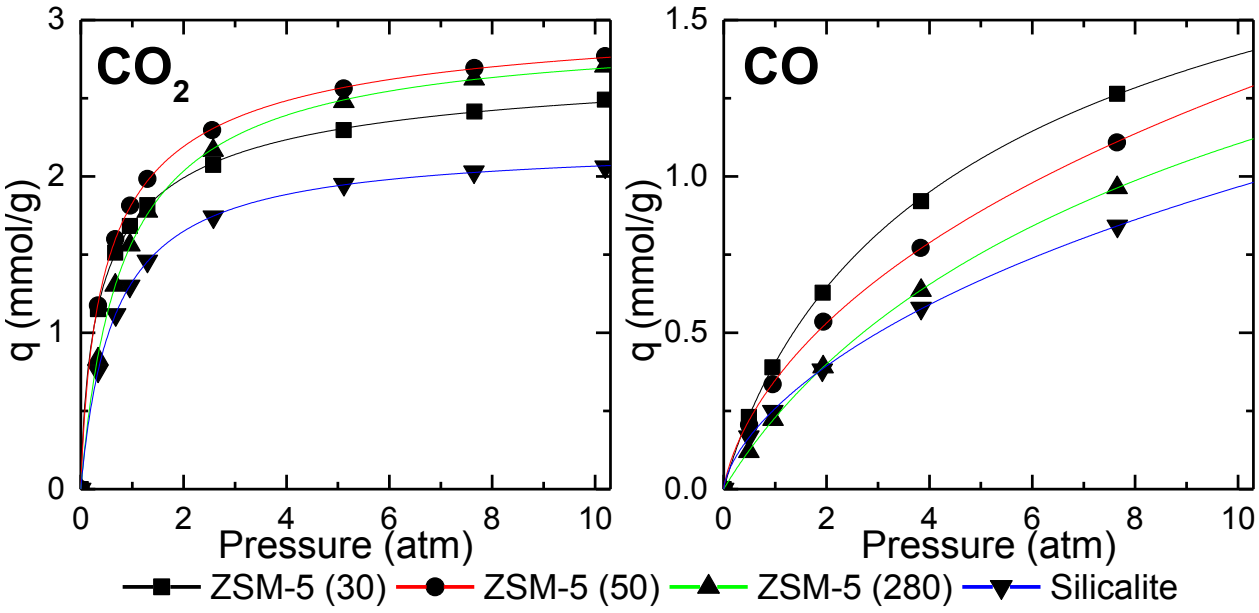

Figure 9 - CO_2 and CO pure adsorption isotherms at 30°C for MFI structure zeolites including ZSM-3 (30), ZSM-5 (50), and ZSM-5 (280) from Zeolyst International, and HISIV 3000, a type of silicalite from Honeywell UOP.

MFI structured zeolites show similar trends for SiO_2/Al_2O_3 ratios that were observed for H-Y samples. Samples with low SiO_2/Al_2O_3 ratios show higher CO adsorption capacities at all pressures. CO_2 adsorption capacity at low loading has a similar trend, however at higher loading the ZSM-5 (50), ZSM-5 (280), ZSM-5

(30), and silicalite in order of decreasing capacity, does not follow the same trend. This is due to the effect of cations on the surface areas of the adsorbents which is discussed in literature with cations taking up pore space decreasing the surface area of the adsorbents [34].

Pure gas adsorption isotherm and breakthrough data was reported for Ba-ZSM-5 in the literature [1]. This data showed that Ba-ZSM-5 can be used for this separation with CO breaking through the column first then being displaced by CO_2. This study also indicated that a small amount of CO_2 chemisorption occurred due to the presence of barium. However, no hysteresis was observed in this study for all MFI type zeolite samples. The ratio of CO_2 capacity over CO capacity in the MFI zeolites was greater at lower pressures and decreased as pressure increased. Overall, the adsorption capacity ratio of CO_2 over CO in MFI zeolites is significantly less when compared to FAU zeolites, particularly the H-Y samples.

The performance using MFI zeolites for a CO_2 syngas separation would not be as effective as LTA and FAU zeolites. This is because FAU zeolites have higher capacities for CO_2 than MFI, and 5A has stronger adsorption of CO_2 at low pressures than MFI.

Other common zeolites in industry include natural zeolites. These natural zeolites are mined rather than synthesised, and are significantly lower priced than their synthesised counterparts. Natural zeolites, due to being formed over a very long time, have much larger crystal sizes when compared to synthetic zeolites which can be beneficial to adsorption. However, where synthetic zeolites are produced from known ingredients, natural ones contain additional impurities. Two natural zeolites were tested in this study including Casorb-Na (CHA) from GSA resources, and Zeolon 900H (MOR) from the PQ Corporation. Pure gas adsorption isotherms of CO_2 and CO at 30^0C for these zeolites are presented in Figure 10 with 3 other zeolites including H-Beta (BEA), SAPO-5 (AFI), and SAPO-11 (AEL). SAPO-5 and SAPO-11, are zeolites that contain PO_4^+ in addition to AlO_4^- and SiO_4, thus eliminating the need for cations and creating brønsted acid sites.

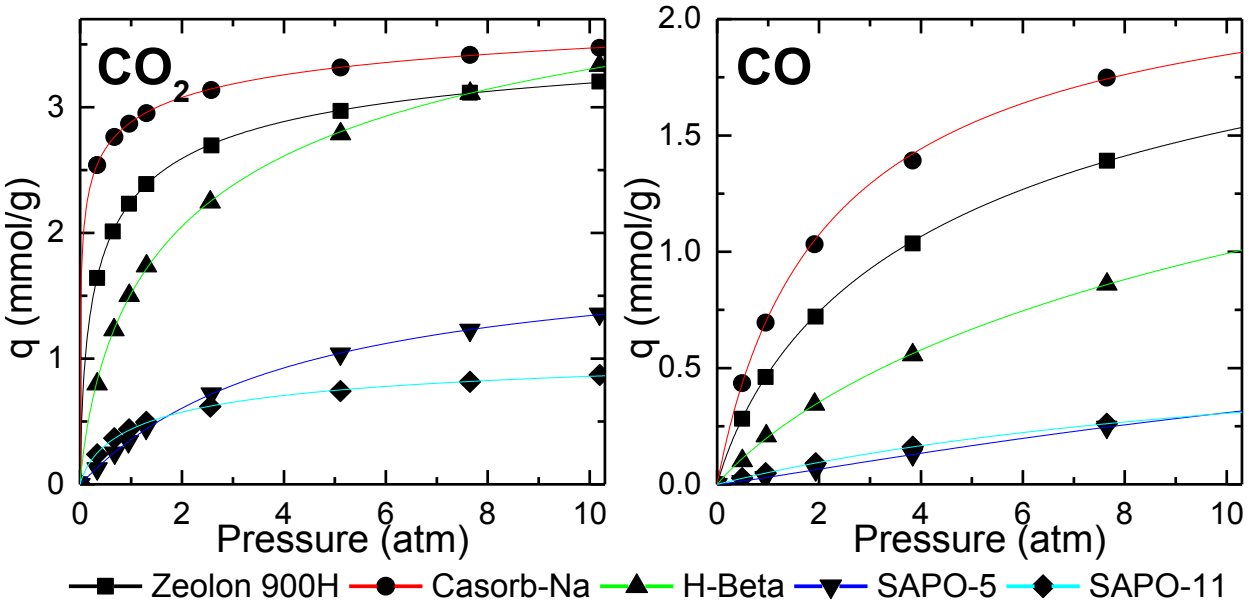

Figure 10 - CO_2 and CO pure adsorption isotherms at 30°C for H-Mordenite (MOR), Chabazite (CHA), H-Beta (BEA), SAPO-5 (AFI), and SAPO-11 (AEL).

None of these 5 adsorbents have any data into the separation of CO_2 from CO available from literature, with only pure equilibrium data for H-mordenite [23].

Some conclusions can be drawn from the present study for these adsorbents. Cabsorb-Na which has similar shape for CO_2 and CO isotherm but with lesser capacity of that of FAU structure could possibly be feasible to separate out CO_2 from CO at 30°C at low pressures, this at the fraction of the cost of synthetic zeolites. The two SAPO samples show significantly less adsorption of CO_2 and CO compared to other zeolites, but have staggeringly larger CO_2 adsorption capacities compared to CO adsorption capacities as can be seen from Figure 10. This difference in adsorption capacities indicates SAPO-5 and SAPO-11 has the potential to be used for syngas separation if adsorption capacities were increased. H-Beta has only modest adsorption capacities of CO_2 and CO making less viable compared to other adsorbents.

Overall for zeolites, CO_2 adsorption capacity was higher compared to CO. This trend extends further with the literature data showing that the heat of adsorption being more exothermic for CO_2 than for CO. While degassing, no significant hysteresis was observed for CO_2 and CO adsorption for all zeolite samples.

To increase the adsorption of CO_2 in a zeolite, augmenting the structure, cation, and SiO_2/Al_2O_3 ratio were found to have major impacts as can be seen in Table 9. To maximise this adsorption of CO_2, FAU structure with more basic cations having the most and strongest adsorption. Also the more heterogeneous the surface of the adsorbent is due to cations were within the zeolite due to low SiO_2/Al_2O_3 ratio, the greater the adsorption.

Table 9 – The effect of the structure, cation, and low SiO_2/Al_2O_3 ratio of the zeolite on the adsorption of CO_2.

	Effect on CO_2 Adsorption
Structure	FAU > LTA > CHA ≈ BEA ≈ MOR ≈ MFI > AFI ≈ AEL
Cation	$Cs^+ > Rb^+ > K^+ > Na^+ \approx Ca^{2+} > Li^+ > H^+$
SiO_2/Al_2O_3 ratio	As SiO_2/Al_2O_3 ratio decreases, CO_2 adsorption increases

The adsorption of CO is also affected by the structure, cation, and SiO_2/Al_2O_3 ratio which are presented in Table 10. To maximize the adsorption of CO, FAU structure has the highest adsorption capacities, Li^+ cation increased the adsorption of CO significantly, and lower SiO_2/Al_2O_3 ratios in the zeolite showed increased strengths and capacity of adsorption.

Table 10 - The effect of the structure, cation, and low SiO_2/Al_2O_3 ratio of the zeolite on the adsorption of CO.

	Effect on CO Adsorption
Structure	FAU > LTA > CHA > MOR > MFI ≈ BEA > AFI ≈ AEL
Cation	$Li^+ > Ca^{2+} > Na^+ > H^+$
SiO_2/Al_2O_3 ratio	As SiO_2/Al_2O_3 ratio decreases, CO_2 adsorption increases

In order to do a CO_2/CO separation, the adsorption of CO_2 over CO must be maximized. This was found at low pressures in the VPSA range for Na^+ FAU zeolites with low SiO_2/Al_2O_3 ratios. In order to maximize the adsorption of CO_2 over CO in the PSA range, H^+ FAU zeolites were found to be the best candidate. SAPO-5 also had a good adsorption capacity ratio but did not have very good adsorption capacities relative to FAU zeolites.

3.5 CONCLUSIONS

For the syngas produced from either industrial methods or from the RWGS process, CO_2 must be removed before it can be used for being synthesized into useful products. From previous studies, adsorbents such as Ba-ZSM-5, 5A, Na-X, and activated carbon were investigated to determine their separation for syngas mixtures and were found to effectively separate CO_2 from a gas mixture of CO_2 and CO.

After investigating activated alumina, activated carbon, silica gel, and zeolites in this study; high-density silica gel and H-Y were found to be the best adsorbents for syngas bulk separation using a PSA cycle with the highest adsorption capacities ratios for CO_2 over CO. For a purification of syngas however, Na^+ exchanged FAU structured zeolites with their strong adsorption capacity at low pressures, and activated alumina for its extremely strong adsorption of CO_2, would be able to purify the syngas mixture from CO_2. This purification separation would be effective using a VPSA for Na^+ FAU zeolite. However, activated alumina would require additional investigation in order to determine if VPSA would be alone appropriate for regeneration.

3.6 ACKNOWLEDGEMENTS

The authors would like to thank NSERC, Phoenix Canada Oil Company and NRCan for funding received throughout this study.

3.7 NOMENCLATURE

k	Freundlich parameter (mmol g^{-1} atm^{-1})
K	Henrys law constant (mmol g^{-1} atm^{-1})
n	Freundlich parameter (dimensionless)
P	Pressure (atm)
q_e	Equilibrium adsorption capacity (mmol/g)
q_s	Monolayer or saturated adsorption capacity (mmol/g)
R^2	Coefficient of Determination (dimensionless)
t	Toth parameter (dimensionless)

β	Langmuir parameter (atm^{-1})
ΔH_{ads}	Heat of Adsorption at zero loading (kJ/mol)

3.8 List of Abbreviations

AEL	SAPO-11
AFI	SAPO-5
ATR	Autothermal Reforming
BEA	Beta Polymorph A
CHA	Chabazite
FAU	Faujasite
LTA	Linde Type A
MFI	Pentasil
MOR	Mordenite
POX	Partial Oxidation
PSA	Pressure Swing Adsorption
RWGS	Reverse Water Gas Shift
SR	Steam Reforming
VPSA	Vacuum Pressure Swing Adsorption

3.9 Bibliography

1 Wirawan SK, Creaser D. Multicomponent $H_2/CO/CO_2$ Adsorption on BaZSM-5 Zeolite. Separation & Purification Technology. 2006;52(2):224-231.

2 Sievers W, Mersmann A. Single and Multicomponent Adsorption Equilibria of Carbon Dioxide, Nitrogen, Carbon Monoxide and Methane in Hydrogen Purification Processes. Chemical Engineering Technology. 1994;17(5):325-337.

3 Belmabkhout Y, Pirngruber G, Jolimaitre E, Methivier A. A Complete Experimental Approach for Synthetic Gas Separation Studies Using Static Gravimetric and Column Breakthrough Experiments. Adsorption. 2007;13(3-4):341-349.

4 Grande CA, Lopes FVS, Ribeiro AM, Loureiro JM, Rodrigues AE. Adsorption of Off-Gases from Steam Methane Reforming (H_2, CO_2, CH_4, CO, and N_2) on Activated Carbon. Separation Science and Technology. 2008;43(6):1338-1364.

5 Krishna R. Adsorptive Separation of $CO_2/CH_4/CO$ Gas Mixtures at High Pressures. Microporous and

Mesoporous Materials. 2012;156(1):217-223.

6 Ruthven DM. Principles of Adsorption & Adsorption Processes. John Wiley & Sons; 1984.

7 National Energy Technology Labratory. Gasifier: Gasification Introduction. Syngas Composition [Internet]. 2015 May.

8 Boerrigter H, Rauch R. Handbook Biomass Gasification. Biomass Technology Group; 2005. p. Chapter 10.

9 Jenzer GA, Tio TH, Zuideveld PL, inventors. System and Process for Synthesis of Methanol. 2005. WO2005108336 A1.

10 LTD SMI, inventor. Gaseous Fuels with Low Nitrogen Oxides Formation by Carrying Out Reverse Water Gas Shift. 1975 April 25. JP50046702-A.

11 Wang S, Inc APaC, inventors. Carbon Monoxide mfr. - Using Steam-Methane Reforming and Reverse Water Gas Shift Reactions. 1988. EP291857-A ; JP63297209-A.

12 Parry D. Fueling the Fleet, Navy Looks to the Seas. U.S. Naval Research Labratory: Public Affairs & Media. 2012 Sep 24.

13 Time Fortune Editors. Audi Just Invented Fuel Made from CO_2 and Water. Fortune. 2015 Apr 28:1.

14 Zubrin R, Clapp MB, Meyer T. New Approaches for Mars In-Situ Resource Utilization Based on the Reverse Water Gas Shift. In: 35th Aerospace Sciences Meeting and Exhibit; 1997; Reno, NV. p. AIAA-97-0895.

15 Air Liquide. Syngas Purification Units: From Gasification to Chemicals. [Internet]. [cited 2014 November 11]. Available from: www.airliquide.com.

16 Manchado MC, Guil JM, P. MA, Paniego AR, Menayo JM. Adsorption of H_2, O_2, CO, and CO_2 on a Gamma-Alumina: Volumetric and Calorimetric Studies. Langmuir. 1994;10(3):685-691.

17 Mao CF, Vannice MA. High Surface Area Alpha-Alumina. I. Adsorption Properties and Heats of Adsorption of Carbon Monoxide, Carbon Dioxide, and Ethylene. Applied Catalyst. A, General. 1994;111(2):151-173.

18 Dewaele O, Froment GF. TAP Study of the Sorption of CO and CO_2 on Gamma-Al_2O_3. Applied Catalysis A: General. 1999;185(2):203-210.

19 Arsenic Research Partnership. Adsorbent Treatment for Arsenic Removal. American Water Works Research Foundation; 2005.

20 Yang RT. Adsorbents: Fundamentals and Applications. John Wiley & Sons; 2003.

21 Barthomeuf D. Conjugate Acid-Base Pairs in Zeolites. Physical Chemistry. 1984;88(1):42-45.

22 Hwang KS, Lee WK. The Adsorption and Desorption Breakthrough Behavior of Carbon Monoxide and Carbon Dioxide on Activated Carbon. Effect of Total Pressure and Pressure-Dependent Mass Transfer Coefficients. Separation Science and Technology. 1994;29(14):1857-1891.

23 Triebe RW, Tezel FH. Adsorption of Nitrogen, Carbon Monoxide, Carbon Dioxide and Nitric Oxide on Molecular Sieves. Gas Separation & Purification. 1995;9(4):223-230.

24 Park Y, Moon DK, Kim YH, Ahn H, Lee CH. Adsorption Isotherms of CO_2, CO, N_2, CH_4, Ar, and H_2 on Activated Carbon and Zeolite LiX up to 1.0MPa. Adsorption. 2014;20(4):631-647.

25 Reid CR, Thomas KM. Adsorption of Gases on a Carbon Molecular Sieve Used for Air Separation: Linear Adsorptives as Probes for Kinetic Selectivity. Langmuir. 1999;15(1):3206-3218.

26 Bae YS, Lee CH. Sorption Kinetics of Eight Gases on a Carbon Molecular Sieve at Elevated Pressure. Carbon. 2005;43(1):96-107.

27 Lithoxoos GP, Peristeras LD, Boulougouris GC, Economou IG. Monte Carlo Simulation of Carbon Monoxide, Carbon Dioxide and Methane Adsorption on Activated Carbon. Molecular Physics. 2012;110(11-12):1153-1160.

28 Vansant EF, Voort VD, Vrancken KC. Characterization and Chemical Modification of the Silica Surface. Wilrijk: Elsevier; 1995.

29 Markham EC, Benton AF. The Adsorption of Gas Mixtures by Silica. Journal fo the American Chemical Society. 1931;53(2):497-507.

30 Greene SA, Pust H. Use of Silica Gel and Alumina in Gas-Adsorption Chromatography. Analytical Chemistry. 1957;29(7):1055-1055.

31 Gerrone E, Fubini B, Bonelli B, Onida B, Arean CO. Thermodynamics of CO Adsorption on the Zeolite Na-ZSM-5: A Combined Microcalorimetric and FTIR Spectroscopic Study. Physical Chemistry Chemical Physics. 1999;4(1):513-518.

32 Tsitsishvili GV, Andronikashvili TG, Sabelashvili SD, Urotadze SL. Chromatographic Separation of Gaseous Hydrocarbons on X Type Zeolite Containing Li Cations. Neftekhimiya. 1969;9(5):790-795.

33 Coe CG, Roberts DA, inventors. Selective Adsorption of Minor Constituents from Bulk Gas Streams by Contacting with Zeolitic Chabazite Adsorbents. 1988. US4732584-A.

34 Wilson SMW, Tezel FH. Equilibrium and Thermodynamic Analysis of CO_2 and CO Adsorption on ZSM-5 for Different SiO2/Al2O3 Ratios. (Submitted) Separation and Purification Technology. 2015.

35 Harlick PJE, Tezel FH. An Experimental Adsorbent Screening Study for CO_2 Removal from N_2. Microporous and Mesoporous Materials. 2004;76(1-3):71-79.

36 Golden TC, Sircar S. Gas Adsorption on Silicalite. Journal of Colloid and Interface Science. 1994;162(1):182-188.

Chapter IV: Separation of H_2, CO_2, and CO Using Adsorbents for the Reverse Water Gas Shift Reaction

Sean M.W. Wilson, F.H. Tezel,

Department of Chemical and Biological Engineering, University of Ottawa, Ottawa ON. Canada

4.1 ABSTRACT

The separation and recycle of CO_2 from a syngas mixture containing CO and H_2 using adsorbent technology is a potentially economical solution that can be used to improve the overall conversion of the reverse water gas shift (RWGS) process. In this study, three adsorbents; activated alumina AA-300, activated carbon BPL, and zeolite 4A were investigated for this separation. The results for gas adsorption isotherms for CO_2 and CO at 30^oC, and the adsorption breakthrough behaviour for an equimolar gas mixture of CO_2, CO, and H_2 are presented and discussed for each adsorbent.

The adsorption of CO_2 and CO was found to show Type I isotherms for all three samples, with CO_2 adsorption capacity being greater than that of CO. AA-300 was found to have the largest difference in adsorption capacity of CO_2 over CO followed by 4A then BPL at similar temperatures and pressures used for the breakthrough.

The breakthrough experiments showed the effective CO_2 separation from a gas mixture of CO_2, CO and H_2 for all three samples. The difference in adsorption capacity of CO_2 over CO translated into a sharper breakthrough behaviour which is desirable for adsorption separation, with AA-300 having the sharpest breakthrough over the other two samples indicating a smaller mass transfer zone compared to the other adsorbents.

Keywords: CO_2, CO, Reverse-Water-Gas-Shift (RWGS) Reaction, Separation

4.2 INTRODUCTION

The conversion of CO_2 to CO through the Reverse Water Gas Shift (RWGS) reaction can utilize CO_2 from a carbon capture project to produce a valuable syngas mixture of H_2 and CO. However, this syngas mixture contains unreacted CO_2 which is required to be separated before the syngas can be used as a chemical intermediate. An adsorption separation process, operating at moderate temperatures and pressures, which would be able to separate CO_2 from a mixture of CO_2, H_2, and CO, could recycle back the unreacted CO_2 to produce a CO_2 free syngas mixture. In this study, adsorbents such as activated alumina AA-300, activated carbon BPL, and zeolite 4A were analysed to determine the effectiveness of CO_2 removal from a raw syngas mixture produced by the RWGS process.

Increasing green-house gas (GHG) emissions and their impact on global warming has led to an increasing interest in alternative energy projects. This is particularly true with the fossil fuel power plants, with technologies being implemented to capture CO_2 after combustion. These projects look to sequestering CO_2 deep into the earth. However, projects that utilize the CO_2 may be reimbursed through the value of carbon as a useful commodity. There are several methods to utilize and transform CO_2 into useful chemicals which are reviewed in-depth in literature [1]. The RWGS reaction is one such method which converts CO_2 and H_2 into H_2O and CO (Equation 1).

$$CO_2 + H_2 \longleftrightarrow CO + H_2O \qquad [1]$$

This endothermic equilibrium reaction operates over a catalyst at high temperatures. Previous studies show that increasing the reaction temperature and/or the H_2/CO_2 ratio can increase the conversion of CO_2, with literature reporting CO_2 conversions of 80% at 800^{o}C with a 6 parts H_2 to CO_2 ratio on nickel catalysts [2]. However, increasing the H_2/CO ratio requires more H_2 to be produced from non-fossil fuel sources making the process less economically viable [3].

Another method to increase the overall conversion of the RWGS process is by separating out the unreacted CO_2 and recycling it back into the reactor. This will leave a syngas mixture stream that is CO_2 free and the overall conversion of the process will be increased. Conventional methods of gas separation such as cryogenic

distillation and absorption require high pressures and sub-zero temperatures which are energy intensive. A less energy intensive method would be the use of an adsorption process occurring at moderate temperature and pressures.

This adsorption process would require an adsorbent that would be able to adsorb CO_2 selectively from CO and H_2 and be easily regenerable in order to recycle the CO_2 back into the reactor. Three adsorbents were selected to be tested for this separation; one activated alumina, one activated carbon, and one zeolite. These three adsorbents were selected due to their performance observed in our earlier studies [4]. Due to H_2 adsorption being insignificant compared to CO_2 and CO, with these adsorbents, a temperature swing adsorption (TSA) cycle could be implemented using H_2 as a purge gas. This technology could recuperate lost heat from within the RWGS process, and regenerate the adsorbent, sending a pre heated combination of H_2 and CO_2 back into the reactor.

The scope of this study was to determine the adsorption behaviour of CO_2 and CO in their mixture with an activated alumina, an activated carbon and a zeolite. Multicomponent adsorption behaviour was investigated with an equimolar gas mixture of CO_2, CO, and H_2 fed to a packed adsorbent bed. Following the adsorption step a purge gas stream of H_2 was fed to a heated column to regenerate the adsorbent.

4.3 Materials and Methods

4.3.1 Materials

High purity CO_2, CO, and H_2 gases were obtained from Linde Canada Ltd at purities of 99.99%, 99.7%, and 99.99% respectively. The adsorbents that were tested include activated alumina AA-300 from Alcan (currently known as Axens Canada Specialty Aluminas Inc)(Brockville, Canada), activated carbon BPL from Calgon Carbon (Pennsylvania, United States), and zeolite 4A from Union Carbide (currently known as the Dow Chemical Company)(Danbury, United States). The adsorbents' properties are presented in **Table 1**.

Table 1 – Adsorbent properties for Alcan AA-300, Calgon Carbon BPL, and Union Carbide 4A.

Manufacturer	Name	Pellet Radius (cm)	Pellet Shape (shape factor)	Pore Radius (cm)
Alcan	AA-300	0.28	Sphere (1)	37.5×10^{-8}
Calgon Carbon	BPL	0.33	Cylindrical (0.91)	20×10^{-8}
Linde Union Carbide	4A	0.32	Cylindrical (0.91)	3.8×10^{-8}

4.3.2 Experimental Details

4.3.2.1 Gravimetric Analysis

Pure gas adsorption isotherms were determined using a gravimetric analysis done by a VTI Scientific Instruments GHP. The pure isotherms were performed on the gravimetric analyzer by regenerating the samples at 300°C under vacuum of around 10^{-8} atm. The samples were then evaluated at increasing pressures of up to 10 atm. Desorption experiments were then performed briefly by decreasing the pressure to determine hysteresis. Buoyancy correction was done using helium at similar pressure and temperatures. Isotherms were conducted at temperatures of 30°C for both CO and CO_2 for activated alumina AA-300, activated carbon BPL, and zeolite 4A.

4.3.2.2 Packed bed Adsorption Breakthrough

Adsorbent columns were packed and then degased before each experiment at 350°C with a helium purge for at least 24 hours. Feed gas flow rate and composition were controlled using three 100 sccm (±1.5 sccm) mass flow controllers which were connected to CO_2, CO, and H_2 gas cylinders. This gas stream would then enter a column filled with glass beads to adequately mix the gases. The gas mixture would then enter the packed bed adsorbent column whose operating conditions for adsorption are presented in Table 2. Five temperature probes were used to monitor the bed temperature with one probe located at the inlet and the outlet, and three located along the packed column. Column pressure was monitored with two pressure gauges located on the inlet and outlet, respectively. The column outlet gas composition was measured as a function of time using a gas chromatograph (GC) GOW-MAC 580 which was equipped with a thermal conductivity detector (TCD) and a Porapak Q column.

Table 2 – Column properties and operating conditions for adsorption breakthrough curves obtained in this study.

Parameter	Value
Column Properties	
Column length, L	32.5 cm
Inner column diameter, D_{in}	2.1 cm
Outer column diameter, D_{out}	2.3 cm
Volume of column, V_c	112.6 cm^3
Void Fraction, ε	0.4-0.45
Operating Conditions for Case Study	
Total feed volumetric flow rate, Q	60 sccm
Average column pressure, P	1.1 atm
Temperature, T	25^{O}C
Feed Concentration	
CO_2 feed concentration, y_{CO2}	0.33
CO feed concentration, y_{CO}	0.33
H_2 feed concentration, y_{H2}	0.33

After the complete breakthrough was achieved (ie. when the outlet composition from the column reached the inlet composition), the regeneration of the column would occur with a flow of 30 sccm of H_2 entering the column which would be kept an average of 100^{O}C by applying heating tape to the exterior of the column. Once there was no measureable CO_2 in the column during regeneration, the column would be brought down to 25^{O}C and adsorption would occur again. The adsorption regeneration process would be repeated until the system reached cyclic steady state. This was determined by observing no change in adsorptive capacity of the column from the previous runs.

Packed bed breakthrough experiments were conducted at 25^{O}C, at approximately 1.1 atm for all three adsorbents; AA-300, BPL, and 4A.

4.3.3 Modeling

4.3.3.1 ISOTHERM MODELING

In order to model the adsorption isotherm data points, Langmuir, Freundlich, and Toth model equations were used. These isotherm models are presented in Table 3. The model with the best fit for the coefficient of determination (R^2) was then used to reflect the isotherm for the calculation of the ideal breakthrough time, Rosen model, and Thomas model.

Table 3 –Langmuir, Freundlich, and Toth adsorption isotherm models.

Langmuir Model	Freundlich Model	Toth Model
$\frac{q_e}{q_s} = \frac{\beta P}{1+\beta P}$	$q_e = k\,P^{\,1/n}$	$\frac{q_e}{q_s} = \frac{\beta P}{(1+(\beta P)^t)^{1/t}}$

4.3.3.2 IDEAL BREAKTHROUGH TIME

With the adsorption capacity of the AA-300, BPL, and 4A known for pressures of 0 to 10 atm, the ideal breakthrough time (Δt_{BT}) can be calculated for a particular flow and concentration of the adsorbate. This ideal breakthrough time takes into consideration the saturation of the adsorbate in the bed as well as the interstitial velocity within the bed (Equation 2) [5].

$$\Delta t_{BT} = \left[\varepsilon + \rho_B \frac{\Delta q_e^{\,*}}{\Delta C_0}\right]\frac{L}{v_s} = \left[\varepsilon + \rho_B \frac{\Delta q_e^{\,*}}{\Delta C_0}\right]\frac{V_c}{Q} \qquad [2]$$

This calculation requires the total void fraction (ε), bulk density (ρ_B), the change in adsorption capacity of the adsorbent (Δq_e^*), change in positive feed step concentration (ΔC_0), superficial velocity (v_S), and the length of the bed (L).

4.3.3.3 ROSEN MODEL (RM)

The RM can be used to predict an individual component's breakthrough curve within an adsorbent bed by taking into consideration the internal pore diffusion rate within each individual pellet and the external film mass transfer resistance (Equation 3) [6] [7]. The RM assumes that there is no axial dispersion, isothermal adsorption, constant flow rate, and constant diffusion.

$$\frac{C}{C_0} = \frac{1}{2}\left[1 + erf\,\frac{{}^{3U}/_{2V} - 1}{2\left(\frac{1+5v}{5V}\right)^{1/2}}\right] \qquad [3]$$

Where, C is the concentration at the end of the column, C_0 is the feed concentration, U is the dimensionless contact time parameter (Equation 4), V is the dimensionless bed parameter (Equation 5), and v is the dimensionless film parameter (Equation 6).

$$U = \frac{2D_e(t - \frac{L}{v_i})}{{R_p}^2} \quad [4]$$

$$V = \frac{3D_e KL}{v_i {R_p}^2}\left(\frac{\varepsilon}{1-\varepsilon}\right) \quad [5]$$

$$v = \frac{D_e K}{k_c R_p} \quad [6]$$

In order to determine the *U*, *V*, and *v*, the intraparticle diffusion *(D_e)* was calculated using reciprocal sum of the Knudsen and Molecular diffusion [8], the external mass transfer coefficient (k_c) was calculated using the Ranz-Marshall equation [9], and the dimensionless Henry's law constant (*K*) was calculated from the isotherm. With the length of the bed, interstitial velocity (v_i), total void fraction, and the radius of the particle (R_P) are all properties and conditions for the bed.

4.3.3.4 THOMAS MODEL (TM)

The TM is another way of predicting the breakthrough behaviour of an individual component in a packed bed. It uses similar assumptions to the RM except that the external mass transfer is the limiting step for adsorption, and predicts the adsorption capacity with the Langmuir isotherm rather than the Henry's law constant. This allows for better prediction of breakthrough time, but worse at predicting the mass transfer uptake adsorption region. The TM is shown in Equation 7 [5].

$$\frac{C}{C_0} = \frac{\bar{J}(r^*\zeta, \tau)}{\bar{J}(r^*\zeta, \tau) + [1 - \bar{J}(\zeta, r^*\tau)]e^{(r^*-1)(\tau-\zeta)}} \quad [7]$$

Where, *J* is the average mass transfer which is dependent on dimensionless time (τ) (Equation 9), the number of transfer units (ζ) (Equation 10), and the equilibrium factor (r^*) which uses the β from Langmuir isotherm model (Equation 11). For τζ>3600, the adsorbent potential adsorption is significantly larger than the flow of the adsorbate, the Klinkenberg approximation applies to the TM which simplifies to Equation 8.

$$\frac{C}{C_0} = \frac{1}{1 + e^{(r^*-1)(\tau-\zeta)}} \quad [8]$$

$$\tau = \Delta(t - \frac{L}{v_i}) \quad [9]$$

$$\zeta = \Delta \frac{\rho_B}{\varepsilon} \frac{L}{v_i} \frac{q_e^*}{C_0} \quad [10]$$

$$r^* = (1 + \beta C_0) \quad [11]$$

These equations use Δ (Equation 12) and Ω (Equation 13) which take into consideration the shape and diffusion of the isotherm. For a positive concentration step on a Type I isotherm, which is the conditions in this study, $\overline{q_e}/q_e^*$= 0.5.

$$\Delta = \frac{k_c \alpha C_0}{\rho_B q_e^* \Omega \mathrm{T}} \quad [12]$$

$$\Omega = 1 + \frac{\overline{q_e}}{q_e^*}(r^* - 1) \quad [13]$$

The TM can also be fitted to the experimental breakthrough data. This is done my fitting two parameters, the external mass transfer coefficient and the adsorption capacity of the adsorbent [5]. The TM was fitted to the CO_2 cyclic steady state conditions for all three adsorbents.

4.4 Results & Discussion

4.4.1 Pure CO_2 and CO Adsorption Isotherms

For the separation of CO_2 from syngas obtained from the RWGS process, three adsorbents; activated alumina AA-300 from Alcan, activated carbon BPL from Calgon Carbon, and zeolite 4A from Linde Union Carbide were analysed. To characterize these adsorbents for this separation, pure single gas isotherms for CO_2 and CO were performed at 30^{0}C. These results are presented in Figure 1, Figure 2, and Figure 3 for AA-300, BPL, and 4A, respectively.

The adsorption of CO_2 and CO on activated alumina has been investigated before in the literature [10] [11] [12] and have reported similar adsorption capacities to the ones obtained with AA-300 in this study which are presented in Figure 1. AA-300 CO_2 adsorption capacity is greater than that of CO. Heat of adsorption values for CO_2 are also greater than CO which has been seen in literature [10] [11]. Both CO_2 and CO adsorption isotherms follow Type I isotherms from Brunauer classification of isotherms, also known as a favourable

isotherm for adsorption. The isotherm for CO_2 in shape is more rectangular then the CO isotherm which is more linear.

The fitted parameters of CO_2 and CO adsorption isotherms on activated alumina at 30^{o}C are presented in **Table 1**. The adsorption of CO_2 and CO fit better to the Toth and Freundlich model than they do for the Langmuir model as can be seen from Figure 1. This is due to the nature of the multi-sites that are available for adsorption on activated alumina [10] which is not considered in the Langmuir model.

AA-300 experiences hysteresis for CO_2 and CO adsorption which is visible on the desorption data points being greater than the adsorption data points on the isotherm. This hysteresis was observed in literature with the chemisorption of CO_2 and CO [11].

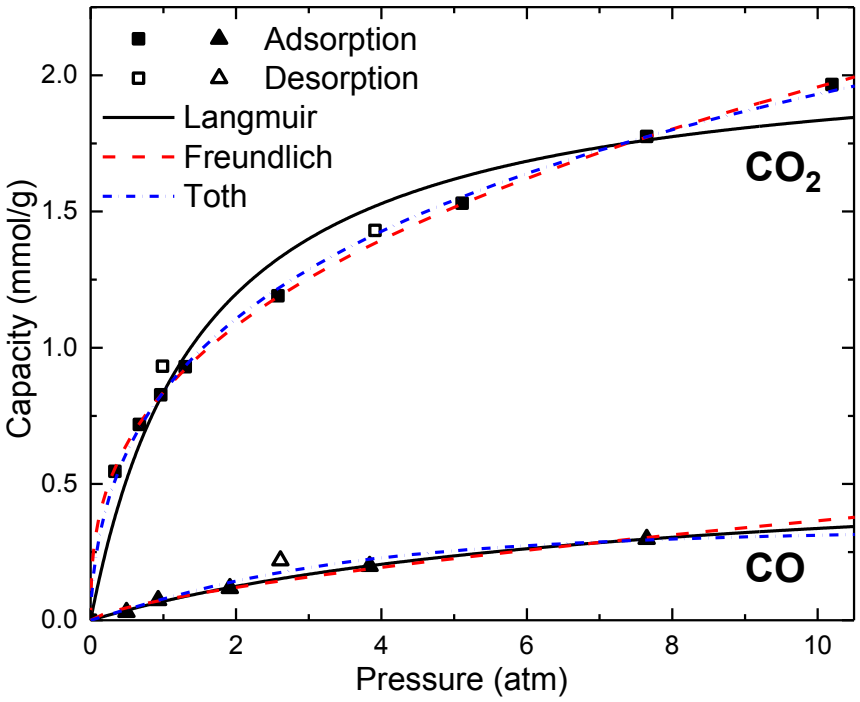

Figure 1 – CO_2 and CO pure adsorption isotherms at 30^{o}C for activated alumina AA-300 fitted to Langmuir, Freundlich, and Toth models.

Table 4 - The fitted parameters for the Langmuir, Freundlich, and Toth pure gas adsorption isotherms of CO_2 and CO for AA-300, BPL, and 4A.

		AA-300		BPL		4A	
		CO_2	CO	CO_2	CO	CO_2	CO
Langmuir	**q_m (mmol/g)**	2.114	0.588	7.242	2.882	2.242	1.435
	β (Atm^{-1})	0.653	0.134	4.56×10^{-4}	0.130	1.470	0.172
Freundlich	**k (mmol/g•atm)**	0.836	0.0746	1.957	0.366	1.292	0.233
	a	2.708	1.449	2.077	1.467	4.135	1.595
Toth	**q_m (mmol/g)**	11.342	0.347	19.41	5.770	2.320	4.775
	β (Atm^{-1})	4.751	0.234	0.413	0.0839	1.700	0.0943
	t	0.209	1.809	0.380	0.603	0.875	0.436

The adsorption of CO_2 is greater than that of CO on the activated carbon BPL as well which can be seen by the pure gas adsorption isotherm at 30^0C presented in Figure 2. This difference in adsorption capacity was noticed in literature with CO_2 heats of adsorption also being greater than that of CO [13] [14] . The adsorption isotherms of both CO_2 and CO follow a Type I isotherm behaviour from Brunauer classification for both gases being relatively more linear than isotherms for other adosrbents which is common for activated carbons due to their dispersed pore size distribution.

The adsorption of CO_2 and CO on BPL fit a Langmuir and Freundlich isotherm model as well as the Toth model. These fitted parameters are presented in Table 4.

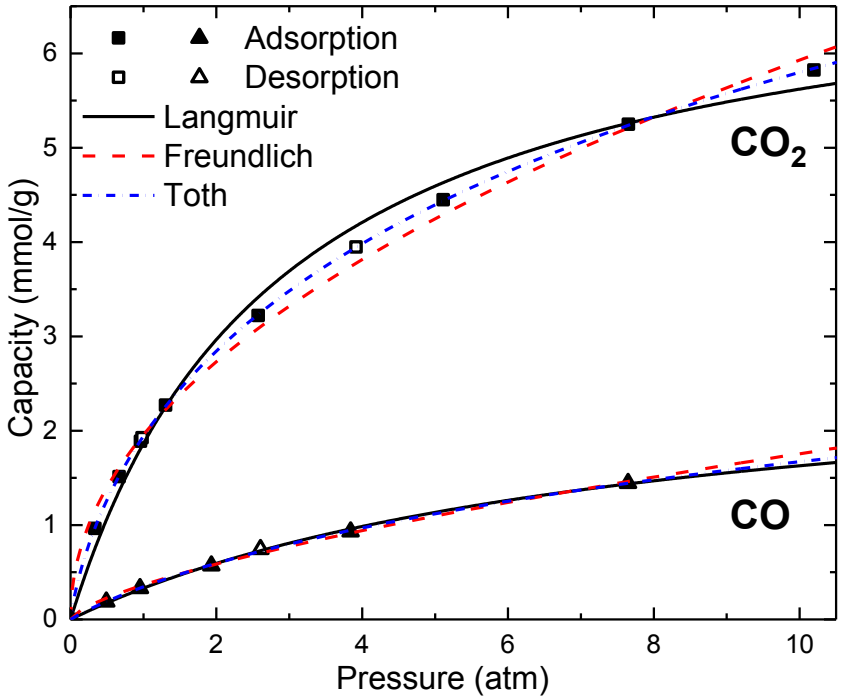

Figure 2 - CO_2 and CO pure adsorption isotherms at 30^{O}C for activated carbon BPL fitted to Langmuir, Freundlich, and Toth models.

The adsorption capacity of CO_2 is greater than the adsorption capacity of CO on zeolite 4A which can be seen in Figure 3 from the pure gas adsorption isotherms for CO_2 and CO at 30^{O}C. This concurs with literature with zeolites having higher capacities and heats of adsorption for CO_2 than for CO [15] [16] [17] [18]. The adsorption isotherms of both CO_2 and CO follow a Type I behaviour from Brunauer classification of isotherms with the CO_2 isotherm being more rectangular in shape then the CO isotherm.

The Langmuir isotherm model as well as the Toth model fit the CO_2 isotherm behaviour quite well for zeolite 4A but Freundlich does not. This is due to the sharp Henry's law behaviour at low pressures which is not accounted for in the Freundlich model. However, for CO adsorption, all three isotherm models fit the isotherms behaviour. The fitted parameters for the Langmuir, Freundlich, and Toth model are presented in Table 4.

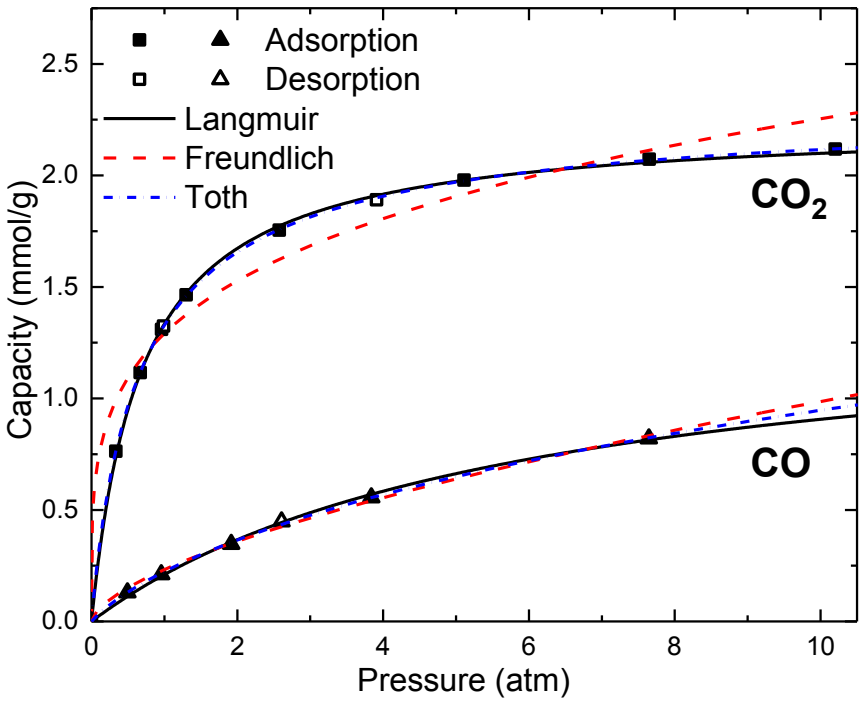

Figure 3 - CO_2 and CO pure adsorption isotherms at 30^{O}C for zeolite 4A fitted to Langmuir, Freundlich, and Toth models.

For all three adsorbent samples studied, the adsorption capacity of CO_2 is larger than that of CO. This is apparent in Figure 4 which shows the adsorption capacity ratio of CO_2/CO over different pressures at 30^{O}C for the three adsorbents looked at in this study. The adsorbent with the biggest difference in adsorption capacity for CO_2 over CO is AA-300 which adsorbs significantly more CO_2 than CO at all pressures. BPL and 4A have similar adsorption capacity ratios to each other. One noticeable trend is that this adsorption capacity ratio is larger at lower pressures and it decreases as pressure increases. This trend shows that CO_2 adsorption is significantly more preferred than CO at lower pressures.

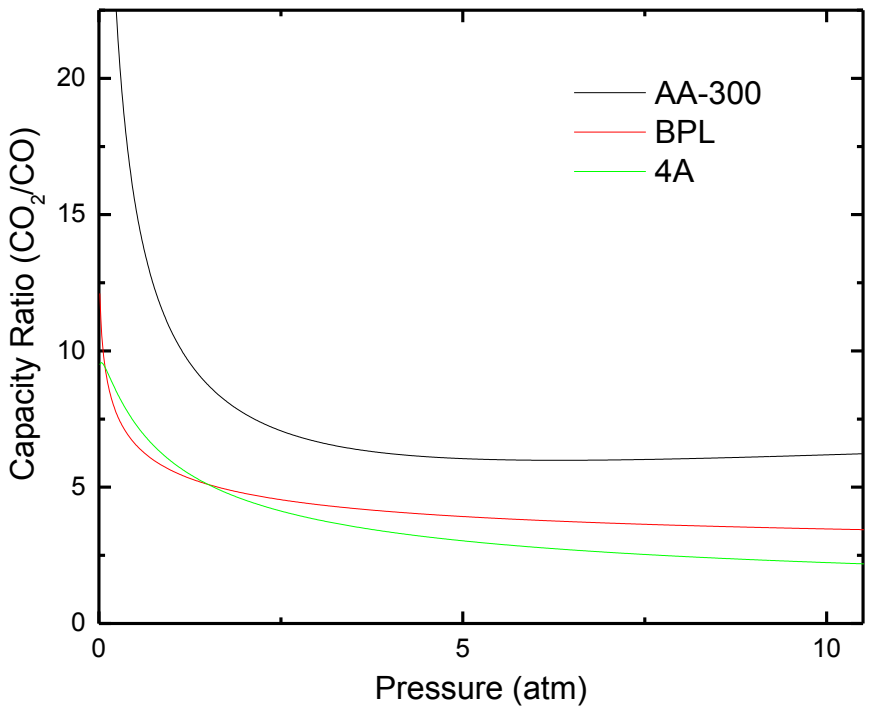

Figure 4 – Adsorption capacity ratio of CO_2 over CO for 4A, BPL, and AA-300 at 30°C.

Under the case study conditions given in Table 2 for the breakthrough experiments, Table 5 shows AA-300, BPL, and 4A adsorption capacities of CO_2 and CO for the columns respective partial pressures calculated from the isotherms, the ratio of the adsorption capacity of CO_2 over CO, and the ideal breakthrough time of CO_2 calculated from Equation 2. BPL with the largest CO_2 capacity is also predicted to have the longest ideal breakthrough time followed by 4A, then AA-300. The capacity ratio of CO_2/CO indicates that CO_2 adsorption is preferential to CO adsorption which can also be indicative of a steeper CO_2 breakthrough, with AA-300 having the largest capacity ratio followed by 4A, and BPL.

Table 5 – At breakthrough condition presented in Table 2, CO and CO_2 calculated adsorption capacities from isotherms, capacity ratios, and ideal CO_2 breakthrough times calculated using Equation 2 for AA-300, BPL, and 4A.

Adsorbent	CO_2 Capacity (mmol/g)	CO Capacity (mmol/g)	Capacity Ratio (CO_2/CO)	Ideal CO_2 Breakthrough Time (s)
AA-300	0.54	0.03	18.0	3600
BPL	1.03	0.15	7.0	4550
4A	0.81	0.10	7.8	4090

4.4.2 Breakthrough Curves

Figure 5 shows the breakthrough curve of a positive concentration step of 20/20/20 sccm of $H_2/CO_2/CO$ at the inlet of a packed bed adsorbent column filled with AA-300 at 1.1 atm total pressure and at isothermal operation at 25^0C. This mixture was prepared according to a RWGS reactor conversion of 50% for an equimolar flow of CO_2 and H_2 being fed into the reactor. The adsorption of H_2 on AA-300 is negligible; so that it is not adsorbed and breaks through the backed bed right away. This confirms our assumption of negligible H_2 adsorption compared to CO_2 and CO. This leaves an existing stream of H_2 that is higher than the feed concentration. At 300 s the concentration front for CO begins to break through the column packed with AA-300 and approaches near equimolar flow of CO/H_2. This is an ideal syngas composition for further processing. This indicates that CO and H_2 do not adsorb as strongly and as preferentially on AA-300 as CO_2. This flow of CO and H_2 exiting the column continues until 3450 s until finally, the concentration front movement of CO_2 begins to break through the column. This front proceeds very sharply due to the compressive nature of the concentration front but ends up tailing as it approaches equilibrium. This tailing is due to departure from ideality of the concentration front which is affected by axial dispersion, intraparticle mass transfer resistances, and non isothermality. In this study, the exiting temperature of the gas never fluctuated more than 0.5^0C indicating that axial dispersion and intraparticle mass transfer resistance were the main factors of the tailing.

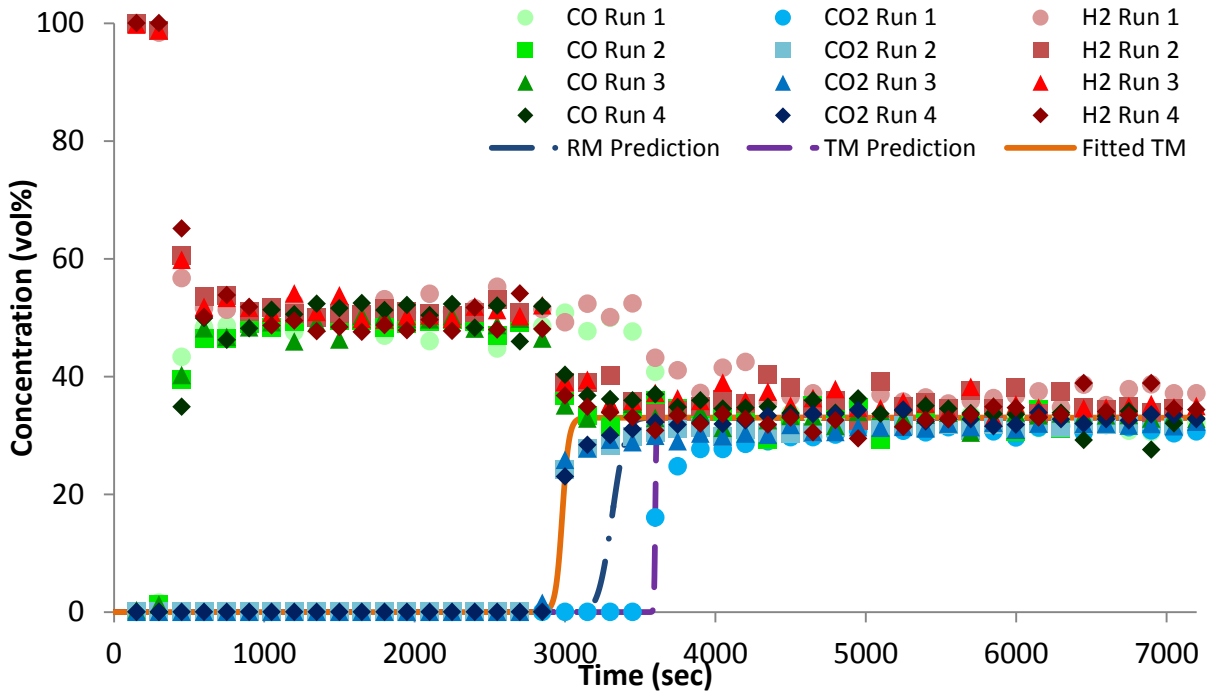

Figure 5 – Breakthrough curves (exit CO_2, CO, and H_2 concentrations as a function of time) for a positive equimolar concentration step of 60 sccm total flow at the inlet for a column packed with activated alumina AA-300. The Rosen Model and Thomas Model were used to predict the CO_2 breakthrough behaviour with the Thomas Model being fitted to the CO_2 breakthrough for cyclic steady state conditions.

After the adsorption was complete, desorption took place by inducing a 30 sccm flow of H_2 at the inlet and heating the exterior of the column to an average of 100^0C. The change in outlet concentration of H_2, CO, and CO_2 gases under these conditions as a function of time are presented in Figure 6. Within the first 150 s the CO is removed from the column, indicating that very little CO was adsorbed during the adsorption step. From 150 s until 750 s the majority of the flow was composed of CO_2 with no CO and lesser amounts of H_2 present. The diffuse wave shape of the CO_2 breakthrough curve is due to a negative concentration step associated with a favourable isotherm. At 750 s, the effluent concentration of H_2 increases and the CO_2 concentration decreases over time until there was no more measurable CO_2 concentration at 7200 s.

After the first regeneration, adsorption step was repeated by a positive concentration step with the CO_2 breaking through earlier than before as can be seen in Figure 5. This difference in adsorption capacity

decreased the adsorption capacity of AA-300 from 0.59 mmol/g to 0.47 mmol/g from the first run to the second, respectively. This data is presented in Table 6. This decrease is due to the chemisorption of CO_2 and CO that is not able to regenerate at temperatures of 100^{o}C. However, the majority of the adsorbate is regenerated and reaches cyclic steady state after the first run which was observed in runs 2 to 4 in Figure 5.

The adsorption capacity of CO_2 predicted from the isotherm at 30^{o}C was 0.53 mmol/g for AA-300 which is less than what was calculated from the first breakthrough curve at 25^{o}C at 0.59 mmol/g. This difference in adsorption capacity is due to the temperature of adsorption; with lower temperatures having higher capacities (exothermic adsorption). After the first run, due to chemisorption of CO_2, regeneration of the column at 100^{o}C does not fully regenerate the column in-between adsorption runs.

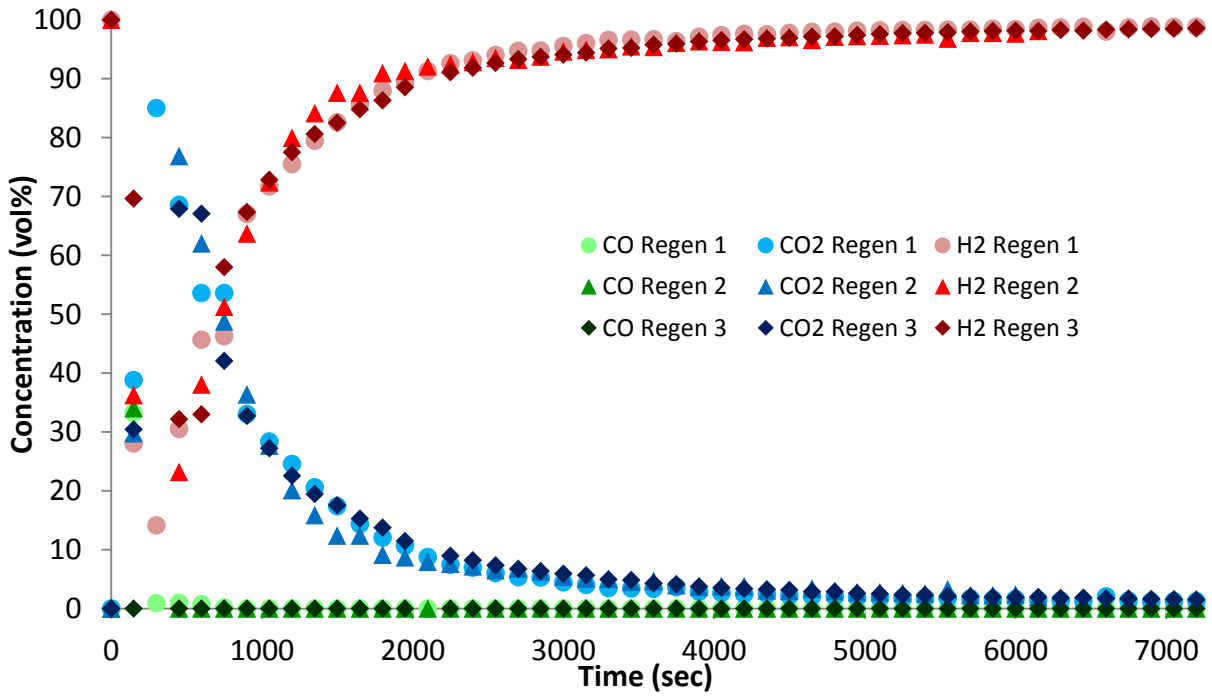

Figure 6 - Breakthrough curves (exit CO_2, CO, and H_2 concentrations as a function of time) for a negative concentration step of 30 sccm of H_2 at the inlet with an average of 100^{o}C applied to the exterior of the column for a column packed with activated alumina AA-300.

The breakthrough behaviour of CO_2 during the adsorption step was predicted using the TM and RM with adsorbent parameters shown in **Table 1**, column parameters shown in Table 2, and the average tortuosity of 4 provided from literature [8]. The RM and TM closely approximate the breakthrough of CO_2 for the first adsorption run with the RM predicting a more broad mass transfer zone and the TM predicting a sharper mass transfer zone as can be observed in Figure 5. Both of these predictions however, do not take into consideration the tailing of the mass transfer zone [8]. The TM was then fit to the cyclic steady state data by changing the adsorption capacity and mass transfer coefficient and shows a good correlation with the breakthrough behaviour of CO_2 during the uptake step. Although it does not predict the tailing of the breakthrough curve as can be seen in Figure 5.

Table 6 – CO_2 adsorption capacities calculated from the isotherm at 30^{0}C and from breakthrough runs 1 through 4 at 25^{0}C for AA-300.

	Isotherm (30^{0}C)	Run #1 (25^{0}C)	Run #2 (25^{0}C)	Run #3 (25^{0}C)	Run #4 (25^{0}C)
Capacity (mmol/g)	0.53	0.59	0.47	0.48	0.48

The breakthrough curve of a positive concentration step of CO_2, CO, and H_2 on BPL was also performed with the column properties and operating conditions mentioned in Table 2, and the adsorption breakthrough curves are presented in Figure 7. At the beginning of this experiment, H_2 does not interact and breaks through the packed adsorption bed first with insignificant adsorption compared to CO_2 and CO. This leaves a pure stream of H_2 until 1080s, where the concentration front movement of CO begins to break through the column. The CO that was adsorbed up until 1080s then is displaced by the CO_2 as it adsorbs down the column as the concentration front of the CO_2 from inlet to the outlet of the column. At 4590 s, CO_2 concentration front begins to break through the column and reaches equilibrium with minimum tailing. This breakthrough data shows that H_2 has the smallest interaction with BPL with it being the first component to breakthrough as expected. CO_2 has the strongest interaction with BPL, with adsorption of CO_2 continuing past 3510s. As observed for AA-300, there is a long period of time at that the outlet composition from the column is an equimolar mixture of CO and H_2 that can be used as syngas. The reason H_2 and CO compositions to be higher than the feed composition is the fact that H_2 is desorbed by CO adsorption and CO is desorbed into the gas phase by CO_2 adsorption.

The regeneration took place after adsorption with a negative concentration step of 30 sccm of H_2 and heating the exterior of the column to 100^0C. Regeneration of BPL had a similar profile to AA-300, however, unlike AA-300, this regeneration was sufficient to fully regenerate the BPL which can be seen in **Table 1** from the adsorbent capacity staying the same for all three runs. The adsorption capacities of BPL from the breakthrough runs are slightly higher than that of the isotherm. This is due to the exothermic nature of adsorption with adsorption capacities being higher at lower temperatures.

The positive concentration step of CO_2 breakthrough curve was predicted using the TM and the RM with the adsorbent parameters shown in **Table 1**, column parameters shown in Table 2, and the average tortuosity of 35 provided from literature [8]. The RM and TM closely approximated the breakthrough behaviour of BPL but due to the approximation coming from the isotherm, the RM and TM breakthrough slightly before the experimental data. The RM was found to have a very accurate prediction of the broadening of the breakthrough curve with the TM predicting a sharper breakthrough with closer breakthrough time to the experimental data. The TM was then fitted to the experimental data and models the adsorption behaviour quite well.

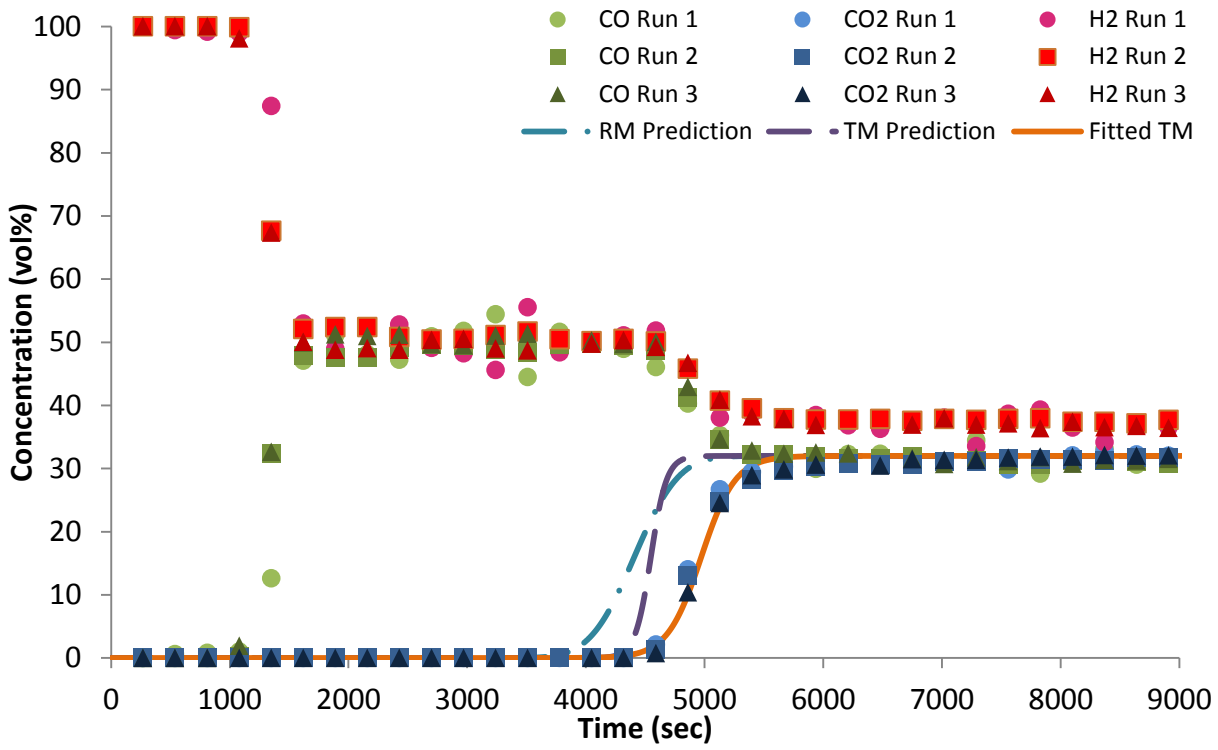

Figure 7- Breakthrough curves (exit CO_2, CO, and H_2 concentrations as a function of time) for a positive equimolar concentration step of 60 sccm total flow at the inlet for a column packed with activated carbon BPL. The Rosen Model and Thomas Model were used to predict the CO_2 breakthrough behaviour with the Thomas Model being fitted to the CO_2 breakthrough for the cyclic steady state conditions.

Table 7 - CO_2 adsorption capacities calculated from the isotherm at 30^{0}C and from breakthrough runs 1 through 4 at 25^{0}C for BPL.

	Isotherm (30^{0}C)	Run #1 (25^{0}C)	Run #2 (25^{0}C)	Run #3 (25^{0}C)
Capacity (mmol/g)	1.01	1.14	1.16	1.15

Figure 8 shows the breakthrough curve of a positive concentration step of 20 sccm of H_2, 20 sccm of CO_2, and 20 sccm of CO at the inlet of a packed bed column filled with 4A at 1.1 atm and at isothermal operation at 25^{0}C for column properties and operating conditions mentioned in Table 2. H_2 does not interact with the 4A adsorbent which was also the case observed with AA-300 and BPL, and a pure gas stream of H_2 exits the

column from 0s to around 1050 s due to the extraction of H_2 from the adsorbed phase by CO and CO_2 adsorption. At this point, the concentration front movement of CO begins to break through the adsorbent column. From around 1050 s to 4350 s, CO is displaced by CO_2 within the 4A and exits the column in above feed concentration, leaving an effluent that is composed of equimolar mixture of H_2 and CO which is ideal for syngas. At 4350 s, the concentration front of CO_2 breaks through the column with only a slight amount of tailing. This data concurs with literature with similar breakthrough curve behaviour on an activated carbon at 30^{O}C and 2.5 atm with ternary gas mixtures [13].

After adsorption was complete, desorption took place with similar conditions to AA-300 and BPL. This desorption, like BPL, was able to fully regenerate the sample which can be seen in Table 8, with the adsorbent capacity of runs 1 through 4 being consistent. The adsorption run CO_2 capacity is higher than the capacity of the isotherm. This is due to the temperature of the isotherm being higher than the breakthrough run but might also be affected by competitive adsorption.

Using the RM and TM model, the positive concentration step of CO_2 breakthough was predicted using adsorbent parameters shown in **Table 1**, column parameters shown in Table 2, and the average tortuosity of zeolites of 3.1 provided from literature [8]. The RM closely approximates the breakthrough shape of 4A with not very good approximation of the breakthrough time. The TM is predicting a very sharp breakthrough. This difference is due to the RM using the intraparticle diffusion (mass transfer limiting) and the external mass transfer coefficient where TM looking only at the external mass transfer resistance. This is compounded by the Langmuir model's β parameter which is significantly higher than that for AA-300 and BPL making the adsorption prediction worse. Both the RM and TM under predict the breakthrough time which is due to the adsorption capacity being calculated from the isotherm which is at 30^{O}C. The TM was also fitted to the CO_2 breakthrough experimental data by varying the adsorption capacity and mass transfer coefficient which models the adsorption behaviour quite well.

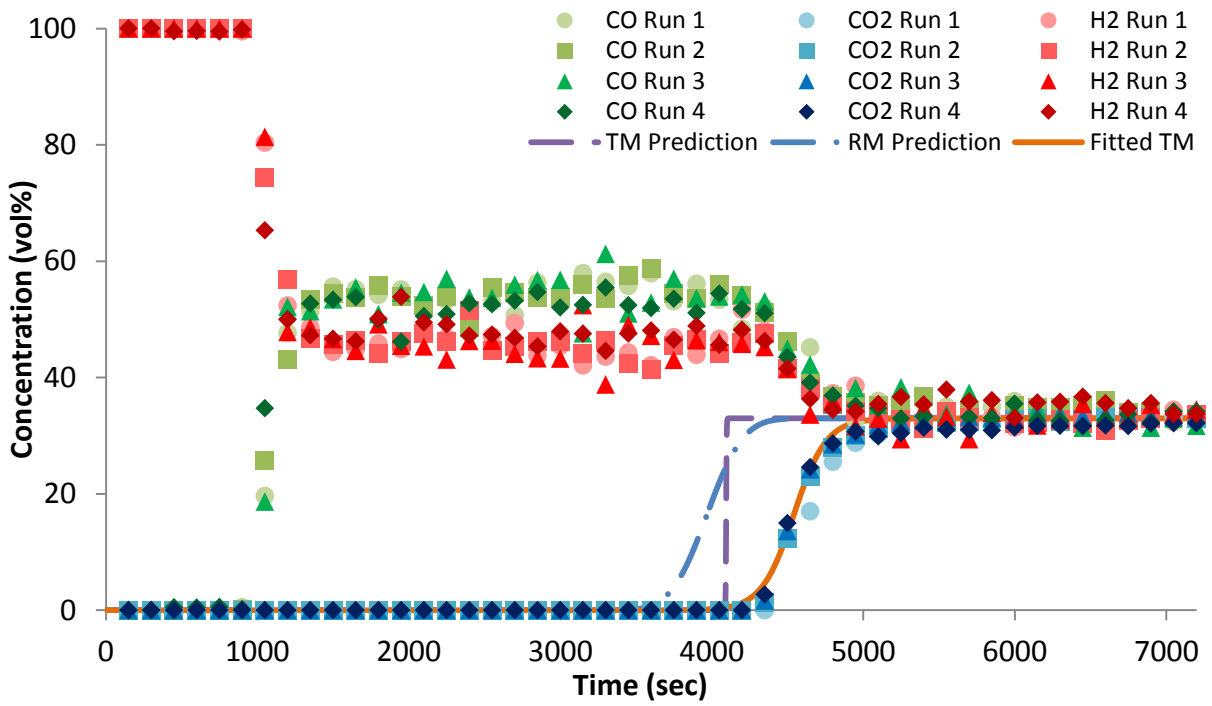

Figure 8 - Breakthrough curve (exit CO_2, CO, and H_2 concentration as a function of time) for a positive equimolar concentration step of 60 sccm of total flow at the inlet for a column packed with zeolite 4A. The Rosen Model and Thomas Model were used to predict the CO_2 breakthrough behaviour with the Thomas Model being fitted to the CO_2 breakthrough at cyclic steady state.

Table 8 - CO_2 adsorption capacities calculated from the isotherm at 30°C and from breakthrough runs 1 through 4 at 25°C for 4A.

	Isotherm (30°C)	Run #1 (25°C)	Run #2 (25°C)	Run #3 (25°C)	Run #4 (25°C)
Capacity (mmol/g)	0.80	1.08	1.06	1.05	1.08

The shape and width of the breakthrough curve is indicative of the mass transfer region occurring in the system. It is crucially important for an efficient separation using adsorbents to have a small mass transfer zone which is observed with a sharp breakthrough front [8]. In this study, AA-300 had the sharpest breakthrough which lasted for 450 s from 2850 s to 3300 s of cyclic steady state for this adsorbent as can be seen from Figure 5, and also the highest adsorption capacity ratio of CO_2/CO of 18. This forms a trend with 4A having an adsorption capacity ratio of 7.8 and the next sharpest CO_2 breakthrough which lasted for 750 s

from 4200 s to 4950 s (see Figure 8). Finally, with BPL having the lowest CO_2/CO capacity ratio of 7, it also had the most broadened CO_2 breakthrough which lasted 1350 s from 4320 s to 5670 s (see Figure 7) which is indicative of a large mass transfer region.

4.5 CONCLUSIONS

In the present study, the adsorption behaviour of CO_2/CO/H_2 was investigated for the RWGS process with activated alumina AA-300, activated carbon BPL, and zeolite 4A. For all three adsorbents, there were three main concentration regions leaving the adsorbent column. A pure H_2 stream would first exit the adsorbent bed due to minimal interaction of H_2 with all three adsorbents. CO would then breakthrough after some time, with CO in the column being displaced by CO_2, to create an equimolar mixture of CO and H_2 gases (syngas stream). Finally, CO_2 would breakthrough after a significant amount of time and eventually the concentration of the exiting gas stream would be the same as the inlet concentration. At this point, regeneration would take place by purging the column with H_2 and heating the column to an average of 100^{0}C. For BPL and 4A, this regeneration would be sufficient but for AA-300, the column did not fully regenerate after the first regeneration cycle but did reach cyclic steady state after the second run.

These three adsorbents were all modelled with the RM and TM for the CO_2 breakthrough with the RM giving a better prediction of the breakthrough shape. Each of these adsorbents effectively separated CO_2 from a simulated syngas mixture. However, AA-300 with its high adsorbent capacity ratio calculated from the pure gas adsorption isotherms of CO_2 and CO, translated into having the sharpest concentration front movement and the smallest mass transfer region which is desirable for a separation.

4.6 NOMENCLATURE

C	Concentration (mmol/cm^3)
D_e	Effective diffusivity (cm^2/s)
D_{in}	Inner Column Diameter (cm)
D_{out}	Outer Column Diameter (cm)
k	Freundlich parameter (mmol g^{-1} atm^{-1})

k_c	External film mass transfer coefficient (cm/s)
K	Henrys law constant (dimensionless)
L	Column Length (cm)
n	Freundlich parameter (dimensionless)
P	Pressure (atm)
Q	Standard Volumetric Flow Rate (sccm)
q_e	Equilibrium adsorption capacity (mmol/g)
q_s	Monolayer or saturated adsorption capacity (mmol/g)
r^*	Equilibrium factor (dimensionless)
R^2	Coefficient of Determination (dimensionless)
R_p	Radius of particle (cm)
t	Toth parameter (dimensionless)
T	Temperature (^{0}C)
v_i	Interstitial velocity (cm/s)
V_c	Volume of Column (cm^3)
y	Gas feed concentration (dimensionless)
α	Thomas parameter (cm^{-1})
β	Langmuir parameter (atm^{-1})
Δ	Thomas Model parameter (s^{-1})
ΔH_{ads}	Heat of Adsorption at zero loading (kJ/mol)
ε	Overall Void Fraction (dimensionless)
ζ	Number of transfer units (dimensionless)
ρ_B	Bulk density (g/cm^3)
Ŧ	Tortuosity (dimensionless)
Ω	Thomas Model parameter (dimensionless)

4.7 List of Abbreviations

GC	Gas Chromatography
GHG	Green House Gas
RM	Rosen Model
RWGS	Reverse Water Gas Shift
TCD	Thermal Conductivity Detector
TM	Thomas Model

TSA Temperature Swing Adsorption

4.8 BIBLIOGRAPHY

1 Mikkelsen, M., Jorgensen, M., and Krebs, F. C. The Teraton Challenge: A Review of Fixation and Transformation of Carbon Dioxde. *Energy & Environmental Science*, 3, 1 (2010), 43-81.

2 Kaiser, P., Unde, R. B., Kern, C., and Jess, A. Production of Liquid Hydrocarbons with CO_2 as Carbon Source based on Reverse Water-Gas Shift and Fischer-Tropsch Synthesis. *Chemie Ingernieur Technik*, 85, 4 (2013), 489-499.

3 Centi, G. and Perathoner, S. Opportunities and Prospects in the Chemical Recycling of Carbon Dioxide to Fuels. *Catalysis Today*, 148, 3-4 (2009), 191-205.

4 Wilson, S. M. W., Kennedy, D. A., and Tezel, F. H. Adsorbent Screening for CO_2/CO Separation. *(Submitted) Microporous and Mesoporous Materials* (2015).

5 Knaebel, K. S. A How To Guide for Adsorber Design (1995), 1-27.

6 Rosen, J. B. Kinetics of a Fixed Bed System for Solid Diffusion into Sherical Particles. *Chemical Physics*, 20, 1 (1952), 387-394.

7 Rosen, J. B. General Numerical Solution for Solid Diffsuion in Fixed Beds. *Industrial & Engineering Chemistry*, 46, 8 (1954), 1590-1594.

8 Yang, R. T. *Gas Separation by Adsorption Processes*. Butterworth-Heinemann, 1987.

9 Ranz, W. E. and Marshall, W. J. Evaporation from Drops Part II. *Chemical Engineering Progress*, 48, 1 (1952), 141.

10 Manchado, M. C., Guil, J. M., P., Masia A., Paniego, A. R., and Menayo, J. M. Adsorption of H_2, O_2, CO, and CO_2 on a Gamma-Alumina: Volumetric and Calorimetric Studies. *Langmuir*, 10, 3 (1994), 685-691.

11 Mao, C. F. and Vannice, M. A. High Surface Area Alpha-Alumina. I. Adsorption Properties and Heats of Adsorption of Carbon Monoxide, Carbon Dioxide, and Ethylene. *Applied Catalyst. A, General*, 111, 2 (1994), 151-173.

12 Dewaele, O. and Froment, G.F. TAP Study of the Sorption of CO and CO_2 on Gamma-Al_2O_3. *Applied Catalysis A: General*, 185, 2 (1999), 203-210.

13 Grande, C. A., Lopes, F. V. S., Ribeiro, A. M., Loureiro, J. M., and Rodrigues, A. E. Adsorption of Off-Gases from Steam Methane Reforming (H_2, CO_2, CH_4, CO, and N_2) on Activated Carbon. *Separation Science and Technology*, 43, 6 (2008), 1338-1364.

14 Triebe, R. W. and Tezel, F. H. Adsorption of Nitrogen, Carbon Monoxide, Carbon Dioxide and Nitric Oxide on Molecular Sieves. *Gas Separation & Purification*, 9, 4 (1995), 223-230.

15 Park, Y., Moon, D. K., Kim, Y. H., Ahn, H., and Lee, C. H. Adsorption Isotherms of CO_2, CO, N_2, CH_4, Ar, and H_2 on Activated Carbon and Zeolite LiX up to 1.0MPa. *Adsorption*, 20, 4 (2014), 631-647.

16 Belmabkhout, Y., Pirngruber, G., Jolimaitre, E., and Methivier, A. A Complete Experimental Approach for Synthetic Gas Separation Studies Using Static Gravimetric and Column Breakthrough Experiments. *Adsorption*, 13, 3-4 (2007), 341-349.

17 Sievers, W. and Mersmann, A. Single and Multicomponent Adsorption Equilibria of Carbon Dioxide, Nitrogen, Carbon Monoxide and Methane in Hydrogen Purification Processes. *Chemical Engineering Technology*, 17, 5 (1994), 325-337.

18 Golden, T. C. and Sircar, S. Gas Adsorption on Silicalite. *Journal of Colloid and Interface Science*, 162, 1 (1994), 182-188.

Chapter V: Conclusions and Recommendations

5.1 CONCLUSIONS

Adsorbents have been studied in this thesis to determine their CO_2 and CO adsorption properties, as well as investigating multicomponent H_2, CO_2, and CO adsorption behaviour. Three main objectives were complete in this thesis; the equilibrium and thermodynamic analysis on the effect of SiO_2/Al_2O_3 ratios on ZSM-5, the screening of promising adsorbents for the separation of CO_2 from CO for applications in syngas, and the practical separation of CO_2, CO, and H_2 for the chosen three adsorbents for the improvement of the reverse water gas shift reaction.

The SiO_2/Al_2O_3 ratio in ZSM-5 had multiple effects on the adsorption of CO_2 and CO. This included that as the SiO_2/Al_2O_3 ratio within the ZSM-5 decreased, there were more cations present within the zeolite structure, and in turn, higher adsorption capacity at low loading of CO_2 and CO were found within the ZSM-5 samples. However, with more cations present within the ZSM-5, ZSM-5 had a decrease in the surface area and at high loadings; ZSM-5 with lower SiO_2/Al_2O_3 ratios had lower CO_2 capacities than samples with higher areas. The SiO_2/Al_2O_3 ratio in the ZSM-5 also impacted the heat of adsorption which was determined using vant Hoff plots. This data showed that the effect of SiO_2/Al_2O_3 ratio had only a small impact on the heat of adsorption. However, the CO_2 heat of adsorption was greater than CO for all four ZSM-5 samples. Out of these four ZSM-5 samples, there was no clear trend on SiO_2/Al_2O_3 ratio on the adsorption capacity ratio of CO_2/CO. ZSM-5 (280) however, had the highest adsorption capacity ratio over the largest range of pressures and temperatures according to the surface plots calculated from the TD-Toth equations.

20 zeolites, 2 activated aluminas, 3 activated carbons, and 2 silica gels were categorically screened in order to determine which of these adsorbents would be the best for practical use in industrial syngas production for two types of separation; bulk separation, and purification. Out of these 27 adsorbents studied, high density silica gel from Strem Chemicals and H-Y were found to be the most promising adsorbents for a bulk separation using a PSA cycle. H-Y had high adsorption capacity for CO_2, a high adsorption capacity ratio, and a

linear isotherm that would allow for large loading capacities over wide pressure swing. High density silica gel from Strem Chemicals had similar adsorption capacity ratios and isotherm shape but did not have as high a CO_2 adsorption capacity as H-Y. However, high density silica gel is less expensive than H-Y and could have economic benefits for the separation. For a purification separation, Na^+ FAU zeolite and activated alumina AA-300 were the most promising for use in a VPSA cycle at below ambient pressures. Na^+ FAU zeolite had the sharpest CO_2 adsorption in the Henry's Law region, highest CO_2 adsorption capacity, and reasonably high adsorption capacity ratio at low pressures. AA-300 adsorption capacity was not as high as high as Na^+ FAU zeolites but had very strong adsorption of CO_2, and a significantly higher adsorption capacity ratio. This with AA-300 cheaper price tag makes it also a desirable adsorbent for this syngas separation.

Three adsorbents, activated alumina AA-300, activated carbon BPL, and zeolite 4A, were then investigated in depth for the syngas separation produced from the RWGS reaction. This process requires the CO_2 bulk separation from a gas mixture containing CO_2, CO, and H_2 which would then be recycled back into the RWGS reactor after it is separated. Pure gas adsorption isotherms were performed and compared to breakthrough data at 1.1 atm total pressure at equimolar total flow of 60 sccm to determine which of these three adsorbents would be most promising for this separation. All three adsorbents effectively separated CO_2 from a syngas mixture but AA-300 had the best performance, with the steepest breakthrough which would give the best recovery and purity for the final products. Out of AA-300, BPL, and 4A, AA-300 is the most viable adsorbent for this separation.

5.2 RECOMMENDATIONS

Four main recommendations can come from this thesis in order to get a better understanding of this separation and expand the practical importance for industry. To expand the practical importance of this separation, other gas components of syngas, including CH_4, N_2 and other minor constituents should be experimented upon in order to replicate industrial circumstances. This would require more pure gas adsorption studies as well as determining multicomponent effects. In order to test out the conclusions of the screening study, two groups of experiments need to be carried out; VPSA cycle of Na-X (13X) and AA-300 for

the purification of syngas from CO_2, and the PSA cycle of H-Y and high density silica gel for the bulk separation of CO_2 from syngas. These experiments will require breakthrough experimentation to determine the adsorption cyclic behaviours. Finally, testing of novel new age adsorbents should be conducted to determine promising adsorbents for this separation in the future once these adsorbents become more commercially available. These adsorbents include metal organic frameworks, graphene, aerogels, nanotube, and many others.